PERFORMANCE OF SAND GRANULATED RUBBER MIXTURE FOR SOIL STABILIZATION USING DISCRETE ELEMENT METHOD (DEM)

A Thesis Submitted to the
Graduate School of Engineering and Sciences of
İzmir Institute of Technology
in Partial Fulfillment of the Requirements for the Degree of

MASTER OF SCIENCE

in Civil Engineering

by

Kuralay KADEKESHOVA

June 2022

İZMİR

ACKNOWLEDGMENTS

This research has been completed in Izmir Institute of Technology during the period September 2021 to 2022 with the help from many people.

First and foremost, I offer my sincerest gratitude to my supervisor Prof. Dr. Nurhan ECEMIŞ who supported me throughout my thesis with her knowledge and experience. Her guidance, encouragement and supervision are gratefully acknowledged.

My heartfelt thanks go to my friends Ali HAMID KHLAIF, Shukrona MAKHMADOVA, Hacer AKBUDAK and Jetmir SELAMI for their support and contribution to my work. They were always on my side and I highly value their friendship, support and help.

I wish to acknowledge the funding I have received throughout my research.

Finally, my heartfelt thanks go to my family and friends for their support during the last few years. Especially my parent, Gulshara, brother and sister-in-law, Askar and Mereke, and sister, Saida, receive my deepest gratitude and love for their dedication, neverending support and understanding. This thesis is dedicated to them.

ABSTRACT

PERFORMANCE OF SAND GRANULATED RUBBER MIXTURE FOR SOIL STABILIZATION USING DISCRETE ELEMENT METHOD (DEM)

The results of a detailed analysis of the capability of numerical approach Discrete Element Method (DEM) to replicate a physical model of a sheet pile foundation in dry soil under static loads are presented in this study. Accordingly, the DEM software Particle Flow Code 2-Dimensional (ITASCA, 2019) is used to model experimental tests.

Numerical model of direct shear test on clean sand and sand mixed with 10% granulated rubber has been done to calibrate the micromechanical parameters of the granular materials, such as sand and rubber particles. The particle sizes, density, interparticle friction coefficient, and contact stiffness of the discrete elements were determined and used in DEM simulations of sheet pile foundation.

A total of four DEM models of the sheet pile foundation with different sand-rubber mixture backfill area were tested and analyzed in PFC2D. The loading process speed, contact stiffnesses, and porosity of the system had a significant impact on the deformation parameters of the sheet pile and lateral pressure distribution of the sand-rubber mix backfill.

In this study two measurement methods were investigated. First, the measuring particles of the sheet pile particles were used, whereas the second, the measuring circles were placed behind the sheet pile foundation. The measurement circles proposed by (ITASCA, 2019) were suitable for the DEM model.

Numerical outcomes showed a relative good match with the physical model. Finally, the ability of the PFC2D code as a discrete element approach in modelling of cohesionless granular material and sheet pile foundation is confirmed in this work.

ÖZET

KUM GRANULER LASTİK KARIŞIMININ ZEMİN STABİLİZASYONUNDAKİ PERFORMANSININ AYRIK ELEMANLAR YÖNTEMİ (DEM) İLE ARAŞTIRILMASI

Bu çalışmada, sayısal yaklaşım Ayrık Eleman Yönteminin (DEM) statik yükler altında kuru toprakta bir levha kazık temelinin fiziksel bir modelini çoğaltma kabiliyetinin ayrıntılı bir analizinin sonuçları sunulmuştur. Buna göre, deneysel testleri modellemek için DEM yazılımı Parçacık Akış Kodu 2 Boyutlu (ITASCA, 2019) kullanılır.

Kum ve kauçuk parçacıkları gibi granül malzemelerin mikromekanik parametrelerini kalibre etmek için% 10 granül kauçuk ile karıştırılmış temiz kum ve kum üzerinde doğrudan kesme testinin sayısal modeli yapılmıştır. Sac kazık temelinin DEM simülasyonlarında ayrık elemanların partikül boyutları, yoğunluğu, parçacıklar arası sürtünme katsayısı ve temas sertliği belirlenmiş ve kullanılmıştır.

PFC2D'DE farklı kum-kauçuk karışımı dolgu alanına sahip sac kazık temelinin toplam dört DEM modeli test edilmiş ve analiz edilmiştir.Sistemin yükleme işlem hızı, temas sertlikleri ve gözenekliliği, sac kazığın deformasyon parametreleri ve kum-kauçuğun yanal basınç dağılımı üzerinde önemli bir etkiye sahipti dolguyu karıştırın.

Bu çalışmada iki ölçüm yöntemi araştırılmıştır. İlk olarak, tabaka kazık parçacıklarının ölçüm parçacıkları kullanılmış, ikincisi ise ölçüm çemberleri tabaka kazık temelinin arkasına yerleştirilmiştir. (ITASCA, 2019) tarafından önerilen ölçüm çevreleri DEM modeli için uygundu.

Sayısal sonuçlar fiziksel modelle göreceli olarak iyi bir eşleşme gösterdi. Son olarak, PFC2D kodunun, kohezyonsuz granül malzeme ve tabaka kazık temelinin modellenmesinde ayrı bir eleman yaklaşımı olarak kabiliyeti bu çalışmada doğrulanmıştır.

TABLE OF CONTENTS

LIST OF FIGURES

Figures **Page**

Figures **Page**

Figures **Page**

Figures **Page**

Figures **Page**

LIST OF TABLES

Tables **Page**

CHAPTER 1

INTRODUCTION

1.1 General

Resource conservation issues remain relevant for all developing countries, where 450 million tons of industrial waste is generated annually. A systematic approach to the use of recyclable materials in civil engineering will not only contribute to solving environmental problems, but with the proper approach can bring significant economic benefits to the state as the main customer.

The list of wastes used in civil engineering is quite extensive, and the construction industry can accept quite large volumes of secondary resources. Thus, primary natural raw materials can be gradually replaced by secondary ones, thereby using many millions of cubic meters of wastes. The use of large–tonnage waste of rubber chips in construction is a world practice, which, unfortunately, is poorly applied in modern countries.

The global average generation of scrap tires is estimated to be 1.5 billion entire tires (Mashiri et al., 2015), which contributes to the massive volume of tire currently discovered in landfills and stockpiles. More than 300,000 tons of waste tires are disposed in Turkey each year, and this number is expected to rise in accordance with the country's population growth (Demir T., 2020).

According to the European Union (EU), the majority of old tıre trash is neither stored nor disposed of in a legal manner (Lo Presti, D., 2013). For different reasons, the failure to regulate this solid waste produces dozens of new problems (Chang N. B., 2008, Cao W., 2007, Zhang S. L., 2009), such as human health problems (infectious illness, respiratory diseases) and environmental damage (pollution of water, soil, air, fires, etc.) are among the issues mentioned in (Onay O., 2015, Lee S. J., 2008).

Recycling of waste car tires has become a major problem all over the world; many of these wastes are located in landfills, as shown in Figure 1.1. It might be difficult to find suitable storage facilities with sufficient capacity, particularly in rapidly growing cities.

Therefore, it is necessary to consider possible removal methods within a plan to reduce the amount of solid waste that will arrive at landfills.

Figure 1.1. Tire landfill
(Source: www.ecosight.com/tire-waste-and-recycling)

The development of tire recycling processes and their use in different industry sectors was one of the alternatives to this issue.

Laboratory tests have reported that the tire chips, alone or in combination with the soil, have exceptional properties and can be utilised as an improving material.Waste tires have specific properties that can be used in civil engineering applications. In this sense it should be considered a special material. Some of the characteristic features of waste rubber materials are: low density low earth pressure, good insulating properties, good drainage capability, good long-term durability, and high compressibility. These characteristics will open up the possibilities of using the material in an innovative way. It was discovered that using such material in road and highway constructions improved the engineering

characteristics of the foundation, slopes, base, subbase, or embankment materials significantly (Ashmawy A., 2006).

Waste Tires are a potential material in geotechnical engineering applications. Because of its low unit weight and excellent strength, tire chips can be utilised as a fill material in construction purposes. The addition of rubber tire chips to soil minimizes soil deformation while also improving the strength of the backfill.

1.2 Problem Statement and Scope of the Study

The Discrete Element Model was developed by (Cundall, P.A., and Strack, 1979) to model the mechanical behavior of (DEM) granular assemblies. For each time interval, the movement of all particles, commonly discs in 2D and spheres in 3D, is determined. The main advantage of using DEM modeling in comparison with other numerical approaches is to study material mechanical behavior at both the micro and macro scales. DEM simulation can be used to establish a virtual laboratory.

The results of the experiments presented in this study, as well as observations of individual studies described in the literature, show that it is difficult to simulate the real behavior of the soil. Because the distribution of soil particles by size, particle shape and randomness of the packing, among many other factors, lead to inhomogeneity of the granular medium.

The goal of this study is to understand more about how clean sand and a sand-rubber mixture behave in backfill when vertical loads are applied. Numerical DEM models of sheet pile foundations with sand-rubber mixture backfilling were conducted as part of this research. All numeric simulations have been performed in PFC2D software.

We focused on the following aspects in our study:

- The soil properties determined from laboratory tests need to be replicated in the PFC2D model
- The soil microproperties calibration using direct shear tests in the PFC2D environment
- The calibration of the numerical models of pile foundations with sand-rubber mixture backfilling

- Model monitoring methods
- Comparison DEM model results with the laboratory experiment results.

Several laboratory tests were conducted at Izmir Institute of Technology's Geotechnical Laboratory for this study (Khlaif, 2021). The following experimental tests were performed as part of this study objective:

1. Laboratory tests to determine the soil parameters
   - Moisture Content test;
   - hydrometer test;
   - sieve analysis;
   - specific gravity tests;
   - soil compaction test.
2. Direct shear tests under 20kg, 50kg, and 100kg normal weight
3. Physical sheet pile model tests.

The numeric tests in PFC2D:

1. DEM simulation of the direct shear test
2. Numeric simulation of the slope model to validate the peak friction angle (φ) of the soil assembly
3. DEM sheet pile model tests.

1.3 Organization of the Thesis

This thesis attempts to numerically simulate sheet pile model testing in dry clean sand and with granulated rubber mix. It uses the discrete element approach to simulate direct shear and sheet pile model testing. The commercially available application Particle Flow Code in Two Dimensions – PFC2D was used to conduct all numerical analyses described in this thesis (Itasca, 2019).

The thesis is divided into seven chapters:

✓ **Chapter 1:** This chapter describes the research, which briefly explains the topic, research objectives, scope, and structure of the thesis.

✓ **Chapter 2:** This chapter provides an overview of the various ways of dealing with sheet pile model difficulties. The literature on recent research projects, numerical models for granulated rubber-sand mixtures, and sheet pile model results with soil characteristics is compiled.

✓ **Chapter 3:** This chapter consists of the principles of distinct element method, theoretical considerations, and usage of DEM software. The most significant components of the PFC2D software for model generation are detailed. This chapter covers Itasca's basic analysis option, which allows us to replicate dry conditions from sheet pile foundation experiments in the laboratory.

✓ **Chapter 4:** This chapter involves the calibration of the physical properties of the DEM model using direct shear tests in the PFC2D environment. It was therefore feasible to match the DEM direct shear test results with the laboratory test result by selecting the optimal set of parameters. At the end, the verification of peak friction angle has been done.

✓ **Chapter 5:** This chapter presents the numerical calibration of the DEM model using PFC2D. The experimental model of a sheet pile foundation is simulated in PFC2D in the first part, including calibrations of boundary conditions, packing configuration, particle size, and applied load speed. In the second part, methods for monitoring and storing model results are chosen. At the end of this chapter, a comparison between the DEM model results and the laboratory experiment results is given. Finally, the DEM model results were compared to the results of laboratory experiments.

✓ **Chapter 6:** This chapter provides the main results and summarised conclusions. In addition, recommendations for future studies are presented.

CHAPTER 2

LITERATURE SURVEY

2.1 Introduction

In this chapter, literature on current research that dealt with scrap tires is summarized.

The literature on the main subjects is the primary focus:

- Soil Stabilization;
- Tire waste as a soil enhancement material;
- Tire scraps applications in specific geotechnical problems;
- Earth retaining structures;

Furthermore, the discrete element methods' implementations are discussed. Previous numerically produced models of earth retaining structures and soil stabilization are offered as examples.

2.2 Tire Scrap as a Soil Enhancement Material

To avoid huge stockpiles and waste disposal operations, governments in several countries have established tight laws and restrictions regarding waste tires. Therefore, there was the chance to study appropriate strategies and alternative solutions for reusing waste tires. Forrest (2014) reported a global assessment of the usage of End of Life Tires (ELT), with 3-15% recycled rubber, 5-23% re-used rubber, 20-30% rubber sent to landfills and stored, and 25-60% total rubber for energy recovery. Numerous studies on the application of fine and coarse tire chips to enhance sandy soil have been accomplished by many researchers.

Hong et al. (2015) investigated the shear strength and liquefaction properties of a sand-tire mix using many sets of undrained cyclic triaxial tests. They observed that the size of the tire chips had a significant influence on the liquefaction behavior of the sand-tire

mixture, with large-sized tire chips having higher liquefaction resistance and higher undrained shear strength. Singh and Vinot (2011) investigated the influence of waste tires on the strength parameters of two soils in an experimental investigation on specimens. On a specimen of the clayey silt soil, the percentage of tire chips ranged from 5% to 20%. While on the sample of the fine sand soil, it was from 10% to 50%. According to the findings, a tire chips percentage of 13% and 30% by weight are ideal for the strength of two soil mixes, respectively.

Various studies on DEM simulations of sand and rubber chips mix were performed in order to determine the strength parameters of the mixture and investigate the relations between micro and macro properties of the mixture.

The work by Gong et al. (2019) compares discrete element method (DEM) simulations of railway ballast mixed with various amounts of tire-derived aggregate (TDA) to laboratory direct shear tests. Clumps were employed in this study to reflect the complex geometry of ballast and TDA. Figure 2.1 depicts the four clump kinds that were employed in this investigation. TDA was included into the ballast at volume values ranging from 0% to 10%.

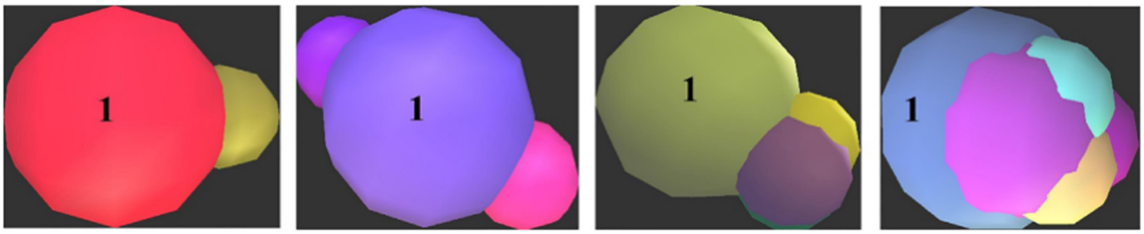

Figure 2.1. Particles of ballast and rubber

(Source: Gong et al., 2019)

The TDA greatly reduced the peak shear stress and the dilatation impact of the ballast-TDA combination, according to both the laboratory and DEM experiments. Additionally, the ballast-TDA mix's cohesion strength and internal friction angle reduced, according to figure 2.2. Large contact forces (F >250 N) were less common with TDA, which reduced ballast destruction in the ballast-TDA combination. Ballast breakage was greatly reduced with a 10% TDA content.

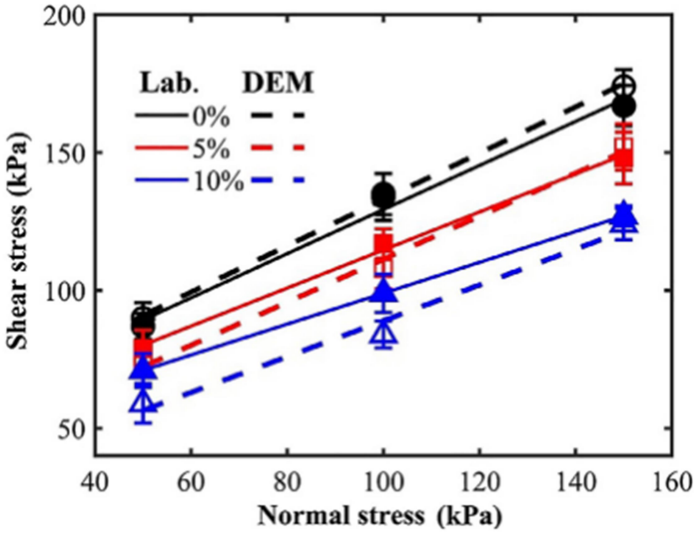

Figure 2.2. Normal and shear stresses development

(Source: Gong et al., 2019)

In the study by Zhang et al. (2020), numerical simulations employing the DEM were used to examine the macro- and micro-mechanical characteristics of rigid-grain and soft-chip mixes (GCMs). Additionally, a number of numerical triaxial tests were conducted on GCMs with volumetric chip contents of 0%, 10%, 20%, and 30%, *P* (Figure 2.3). Tire was modelled as deformable agglomerates (clusters) in PFC3D.

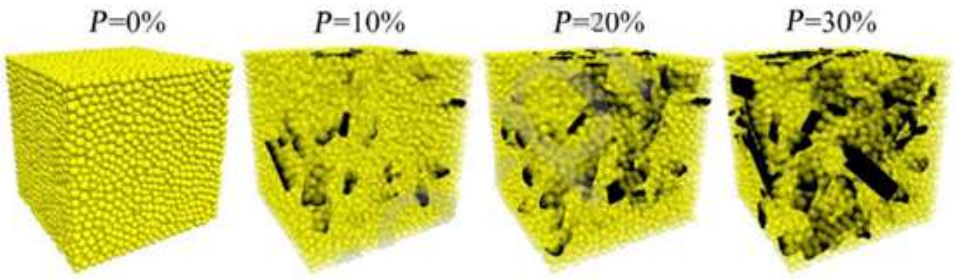

Figure 2.3. Prepared samples with different tire contents

(Source: Zhang et al., 2020)

The results of DEM triaxial test are presented in figure 2.4 (a) and (b). The simulation results showed that raising P causes an increase in sample toughness, deviatoric peak stress, and associated shear strain. Greater volume contraction and less dilatation are

both influenced by higher P. Increasing P causes a considerable increase in the friction angles in both the peak and residual states.

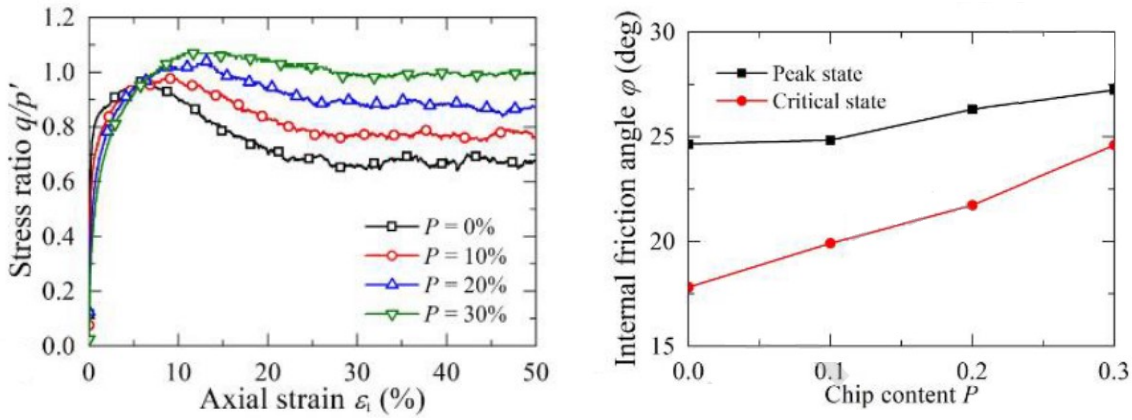

(a) (b)

Figure 2.4. Simulation results: (a) stress ratio, (b) internal friction angle

(Source: Zhang et al., 2020)

Laboratory experiments and numeric simulation were performed by (Valdes and Evan, 2008) to study the sand-rubber mixture with similar size of grains. The DEM model performed using PFC2D software. The samples of the sand with different rubber content (Fr = 1 rubber particles only, Fr = 0.6 rubber content is 60%) were subjected to a load of 1D and isotropic conditions. The role of the type of load on the deformation properties of the mixture was investigated throughout the research. The application of compressible particles for filtration control was also examined, as well as the selection of appropriate parameters for discrete element modelling of a sand–rubber mixture. As a result, the load-deformation response of sand–rubber depends on the amount of rubber in the mixture and the type of loading.

Due to interlocking effects and side friction caused by the rigid boundaries, specimens loaded in 1D compression demonstrate considerable residual stresses after unloading in both rubber contents. The appropriate selection of the properties for the rubber fraction was complicated due to the stiffness difference between sand and rubber grains. As a result, alternative approaches for DEM modelling of the sand-rubber mix were developed. All simulations were modelled using the Hertz–Mindlin contact model (Mindlin and

Deresiewicz, 1953). The 2D DEM model was able to reflect loading-unloading hysteresis, but the residual strain was not predicted well, as we could also see in Figure 2.5 and Figure 2.6.

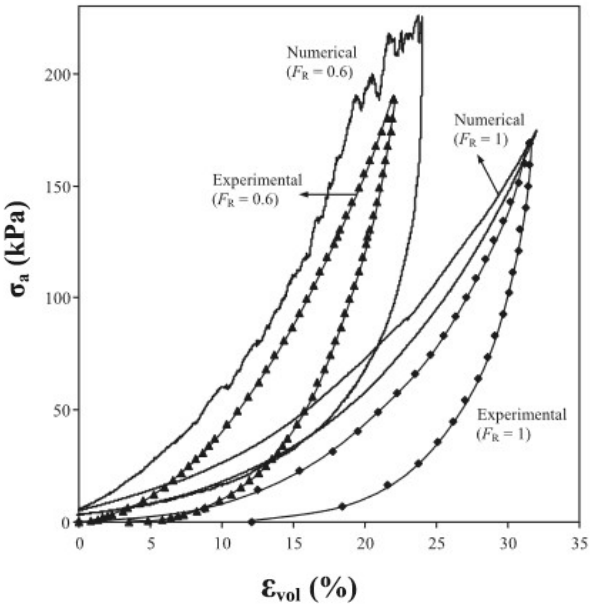

Figure 2.5. The results of experimental and numeric 1D loading tests.

(Source: Valdes and Evan, 2008)

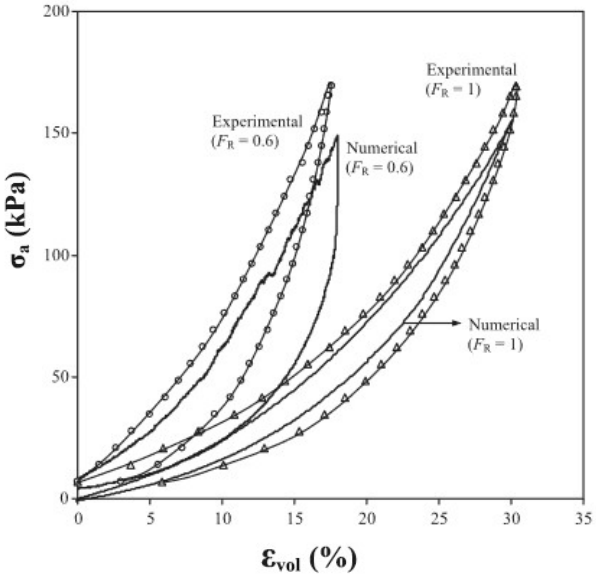

Figure 2.6. The results of experimental and numeric isotropic loading tests.

(Source: Valdes and Evan, 2008)

New approach for numeric modelling of the sand-tire mixture was provided by (Asadi et al., 2018). Figure 2.7 illustrates the deformability of tire when it is in contact with sand grain, where contact surface increase with load increasing. This method encompasses the particle's shape and deformability. Simulated triaxial compression experiments were used to examine the effect of tire content and confining pressure (80kPa and 100kPa) on the stress–strain response of the mixture. The test was performed in 3D using the open-source program YADE.

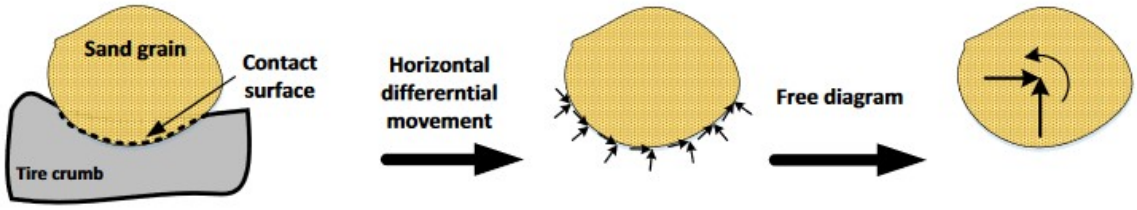

Figure 2.7. Sand to tire contact.
(Source: Asadi et al., 2018)

Figure 2.8 shows the shapes of considered sand and tire grains. Sand particles were represented by rigid agglomerates, whereas tire grains were represented as bounded spheres that could move relative each other. Therefore, the soft-rigid contact model is considered in this study.

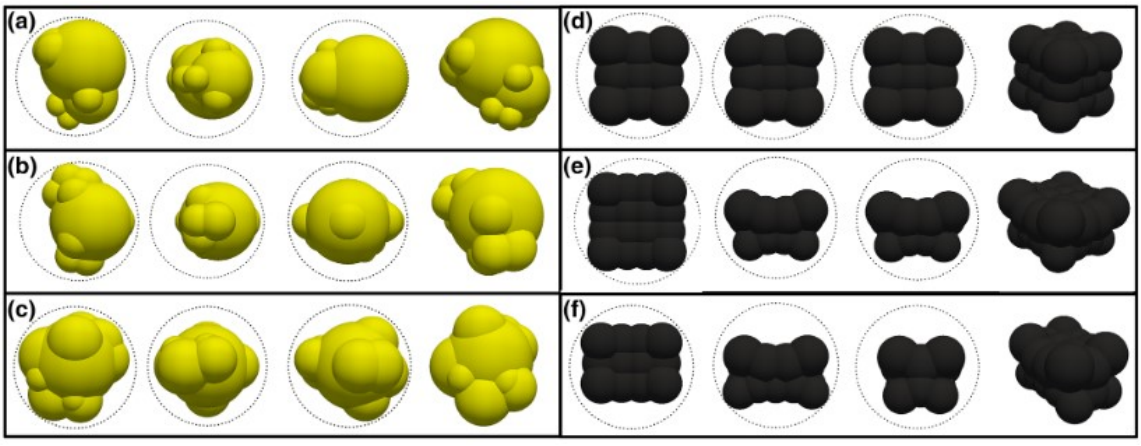

Figure 2.8. Sand and tire grains: a–c sand grains and d–f tire grains
(Source: Asadi et al., 2018)

The samples used in numeric triaxial tests are represented in Figure 2.9

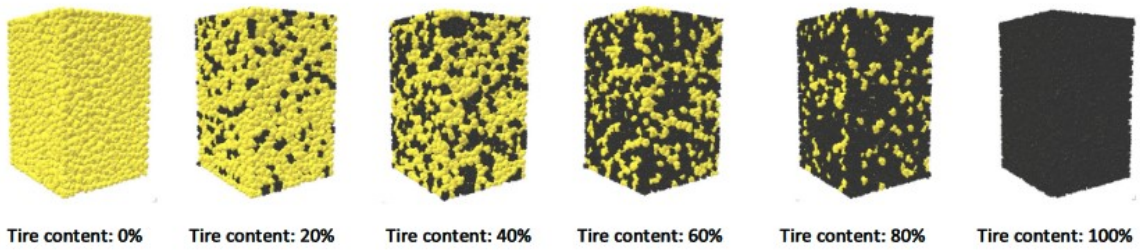

Figure 2.9. Prepared samples with various tire contents

(Source: Asadi et al., 2018)

Figure 2.10 illustrates the development of the deviatoric stress against axial strain for a sample at the confining pressure of 80 kPa. The results of the numerical simulation showed a decrease in the sample strength and stiffness with an increase in the tire content. The sample with the rubber's 80% and 100% content demonstrated nearly linear behavior up to 16% of axial strain. Dilative tendency of the sand was reduced by tire additives, whereas high tire content resulted in pure contractive tendency, as observed in Figure 2.9(b). The boundary between rubber-like and sand-like behavior is determined as a sample with 40% tire content.

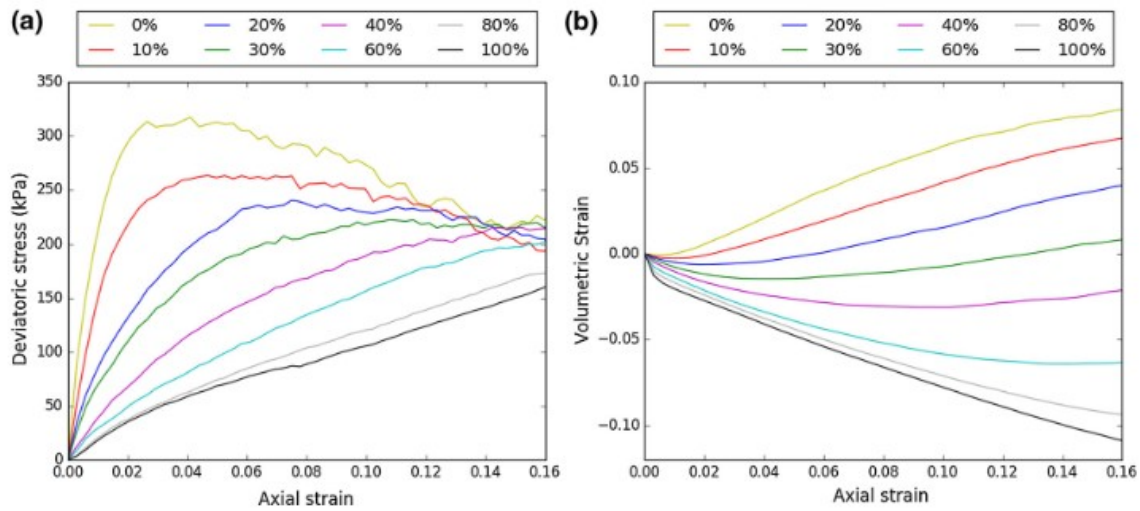

Figure 2.10. The results of the simulations; (a) stress against axial strain and (b) volumetric strain against axial strain

(Source: Asadi et al., 2018)

Eidgahee and Hosseininia (2013) studied the influence of mixing ratio on the engineering properties of the mixtures. The linear unbound contact model was implemented in all simulations. The specimens of sand-rubber mixture with different rubber content were analyzed using the DEM model of the biaxial test. The rubber content varied from 0 to 50%.

Figure 2.11 presented the results of the DEM simulations of the biaxial test at confining stress of 200kPa. Rubber additives improved the shear strength of sand by up to 50%, according to the results of a sample biaxially tested under confining pressure of 200kPa.

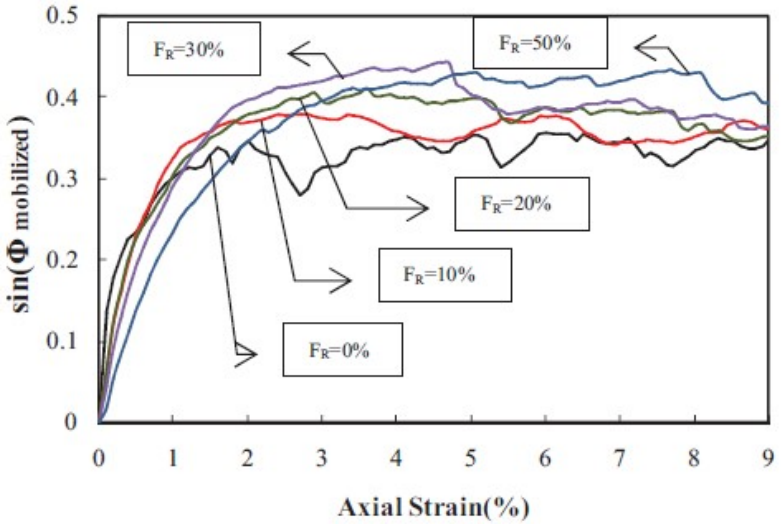

Figure 2.11. Shear strength development against axial strain
(Source: Eidgahee and Hosseininia, 2013)

It should also be mentioned that in a combination containing 50% rubber, the granular material's compressibility has risen. That was the reason for the shear strength reduction. As illustrated in Figure 2.12, increasing the rubber content caused the samples to compress at first and then expand as the axial deformation increased.

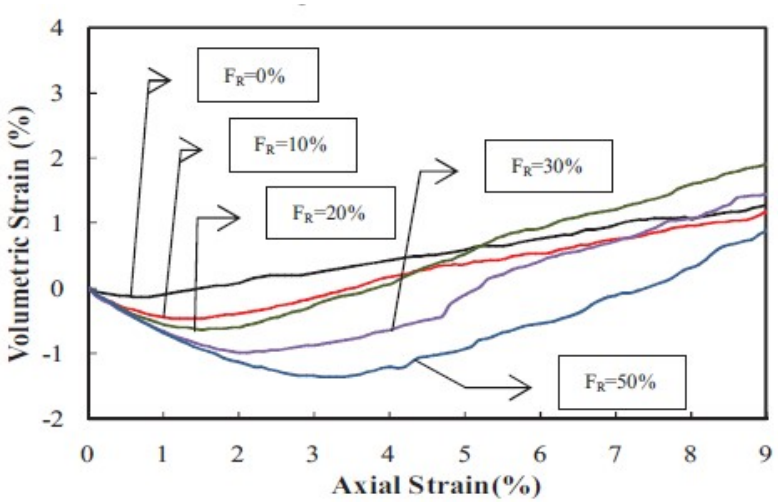

Figure 2.12. Volumetric strain against axial strain

(Source: Eidgahee and Hosseininia, 2013)

In the paper of (Takano et al., 2014), laboratory experiments and numeric tests were performed to study the shear behavior of sand-rubber mixture. 3-D simulation of the direct shear test was done using the DEM code called SDEC. Additionally, the material behavior in the shear box was investigated using X-ray CT scanning. CASE 1 and CASE 2 represent only sand and only tire chips samples, respectively. CASE 3 and CASE 4 samples contain 50% and 20% of tire chips. Figure 2.13 represents the laboratory and numeric results of the direct shear for all cases.

According to the laboratory and numeric tests:

- Shear stress curve of the samples with tire additives monotonically increased and had no peak (CASE 2, CASE 3 and CASE4)
- The tire chips content reduced the dilatancy effect of the sand
- Tire chips have the ability to prevent soil failure by minimizing shear strain distribution
- Afterward, realistic behavior was examined by employing X-ray CT and DEM modeling.

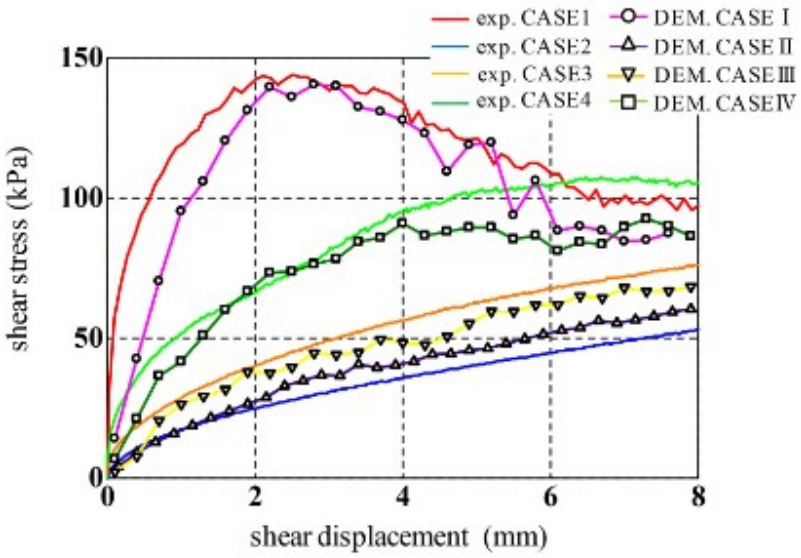

Figure 2.13. Comparison of the direct shear test results with laboratory tests results (Source: Takano et al., 2014)

2.3 Tire Scraps Applications in Specific Geotechnical Problems

The use of rubber in civil engineering has been studied for the past 30 years (Oikonomou and Mavridou, 2009). However, some sources suggest that it was first employed in the nineteenth century with the invention of vehicles (Shu and Huang, 2014).

The condition of used tires affects the application areas. To handle some geotechnical issues, new forms of waste tires (shredded, crumb, and chips) are formed during tire recycling.

Scrap tires can be used:

- As for parking places for ships and breakwaters on sea coasts
- As pavement subgrade reinforcement (Umar et al., 2015)
- Playgrounds
- Erosion control by connecting with each other
- They are used as crash barriers on highways.

Whereas recycled (shredded) used tires are used in civil construction:

- As a light-weighted filler material to reduce consolidation in the ground layer and increase overall stability (Zomberg, 2004),
- As thermal insulation to reduce the depth of freezing of base,
- As a drainage layer,
- To reduce lateral pressures in support structures (Bosscherp, 1997).

A few ASTM standards on the correct utilization of recycled waste tires have previously been produced. ASTM D6270-98, titled "Standard Practice for Use of Scrap Tires in Civil Engineering Applications," is the most suited for geotechnical applications.

Vignali et al. (2016) used a DEM approach to investigate the application of crumb rubber as a modifier or addition in asphalt concretes. Two alternative methods were used to study the effect of rubber powder within the bituminous mastic. The first one is a rheological technique that includes macro-scale investigation in a laboratory setting as well as DEM simulation. Multiple Stress Creep Recovery tests are the second. The dynamic shear rheometer was simulated in 3D DEM environment, as illustrated in figure 2.14. The results demonstrated that rubber enhances the rheological properties of the polymer modified bitumen and behaves as a filler.

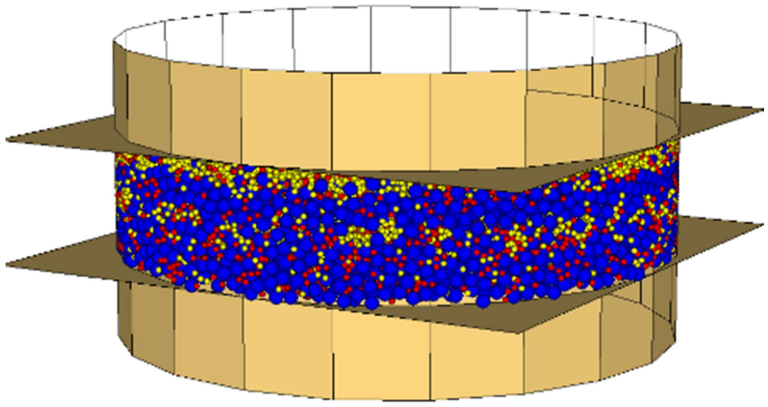

Figure 2.14. DEM simulation: bitumen particles are blue, limestone filler particles are yellow and crumb rubber particles are red

(Source: Vignali et al., 2016)

Gotteland et al. (2008) studied the possibility of employing sand-tire chips mixture as fill material in cellular structures (gabion method) for civil engineering applications. The study proposed a new advancement employing gabion technology to create the front surface, core, and perhaps the back surface of a reinforced structure, as shown in Figure 2.15.

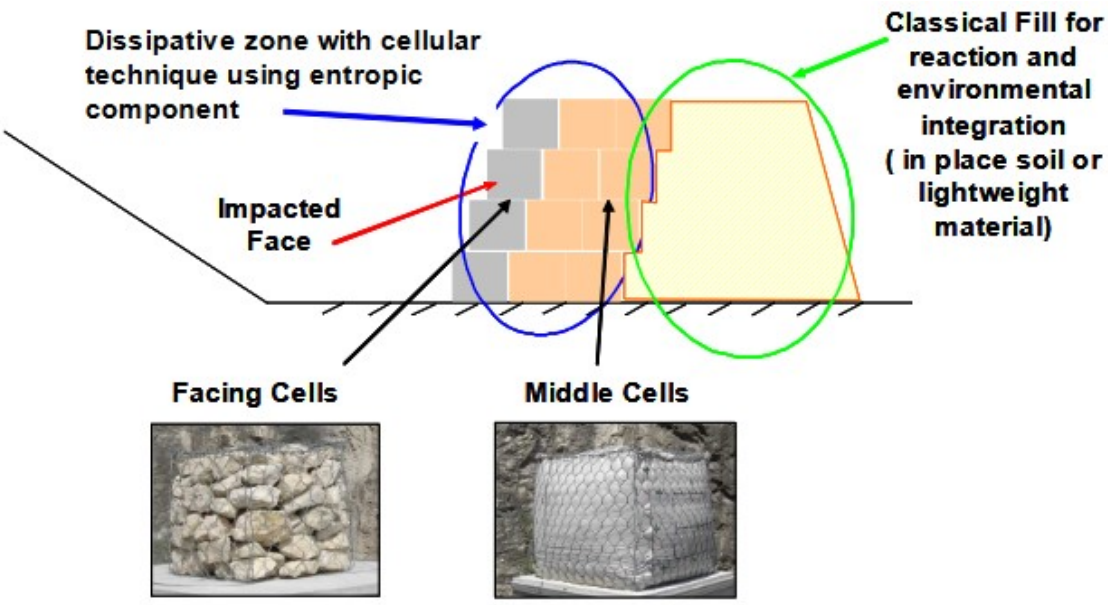

Figure 2.15. Schematic view of cellular structures
(Source: Gotteland et al., 2008)

The mechanical behavior of the gabion cells filled with sand-tire mixtures was analyzed. 3D DEM simulation of the triaxial test was conducted on the samples of sand with various tire chips mixing ratio to determine strength parameters, angle of friction and cohesion. Numeric results were compared with laboratory tests results. The strength of the mixture increased until the tire mixing ratio reached a value of 34%.

The impact tests were carried out by dropping a 250kg spherical rock from a height of 5.5m onto a 0.5m cubic cell filled with various materials (gravel, sand, and a tire-sand combination). According to the obtained data from Figure 2.16(b), the impact time length clearly illustrates that adding tires to the sand modifies the cell's behavior. The suggested type-sand mixture behaved as an energy absorber rather than a dissipater of energy.

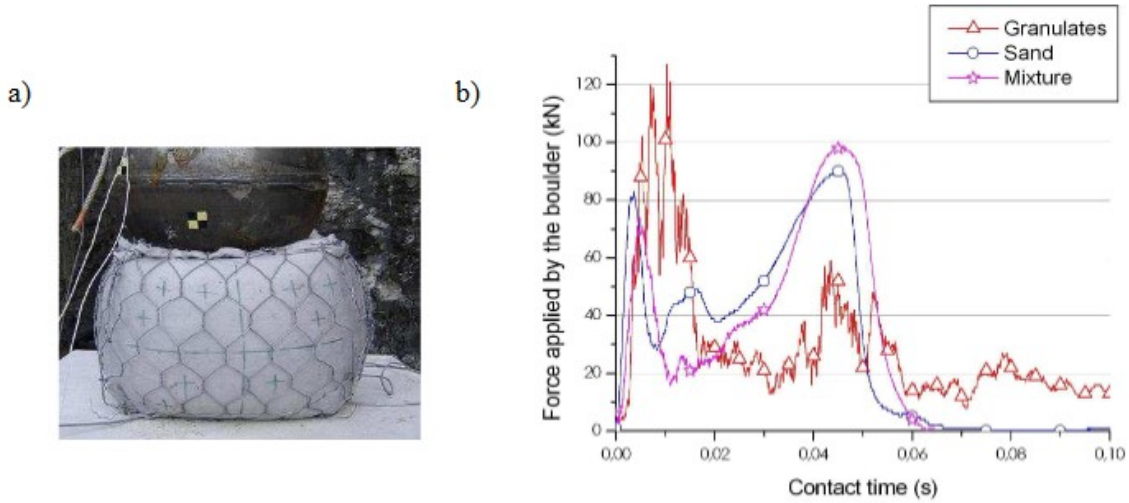

Figure 2.16. Impact tests: (a) Sand cell with a height of 500mm; (b) recorded data of the test (Source: Gotteland et al., 2008)

Resilience, strength, durability, and high frictional resistance are some of the characteristics of waste or scrap tires that improve highway embankment performance (Liu, 2000).

2.4 Earth Retaining Structures

For a better knowledge of the mechanical behavior of road dry stone retaining walls, Quezada et al. (2016) conducted the numeric study. A small-scale sample with steel blocks operating as concentrated loads on the backfill surface and clay bricks for the wall was modelled in three dimensional 3DEC (ITASCA code), as shown in Figure 2.17. The average force levels obtained throughout the experiments was in good match with the concentrated force values leading to failure in the DEM models. However, the relative inaccuracy reached 8% when the loading was extremely close to the retaining wall. For each distance d of 2 cm, 3 cm, and 4 cm between the steel block and the retaining wall, Figure 2.18 compares the values of force at failure for experimental testing and numerical simulations.

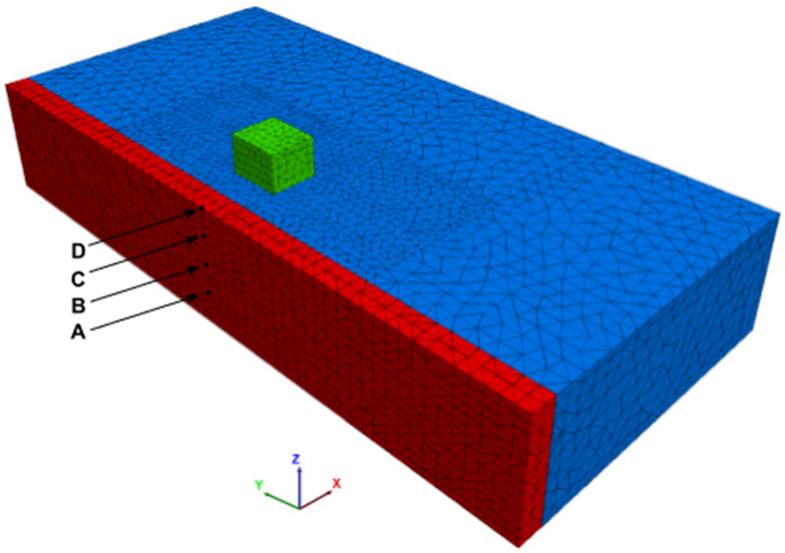

Figure 2.17. Numeric model setup. A, B, C, D are measurement points
(Source: Quezada et al., 2016)

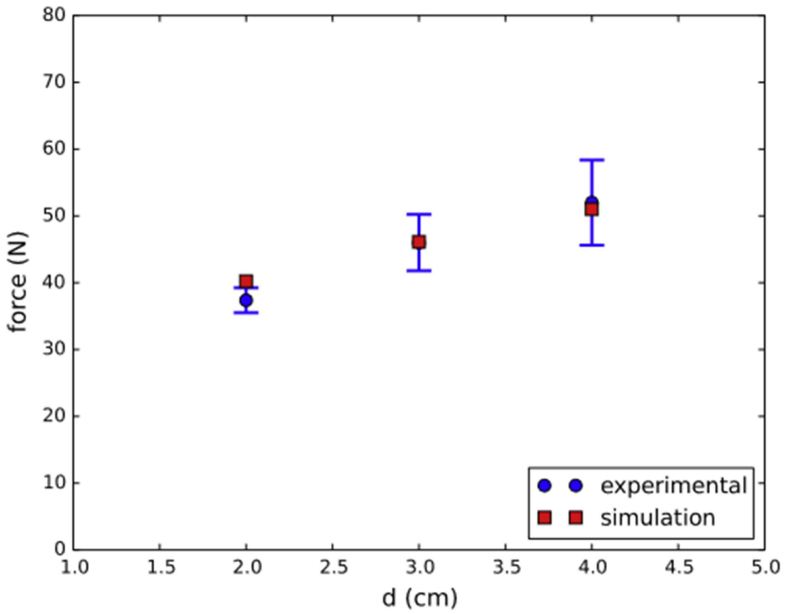

Figure 2.18. Comparison of the forces at failure for each distance d in numerical models and experimental testing
(Source: Quezada et al., 2016)

Oetomo et al. (2015) used DEM approach to investigate plane strain failure of the dry-stone retaining walls (DSRW). They simulated three actual full scale model using PFC2D package. The results were compared to full-scale experimental results. Hydrostatic load and backfill were applied to the walls in the experiments (Figure 2.19). The crucial backfill heights discovered in the simulations were likewise within the Yield Design Method's range. The Yield Design Methodology provides some insight into the validity of using the DEM technique to correctly simulate slope DSRW behavior.

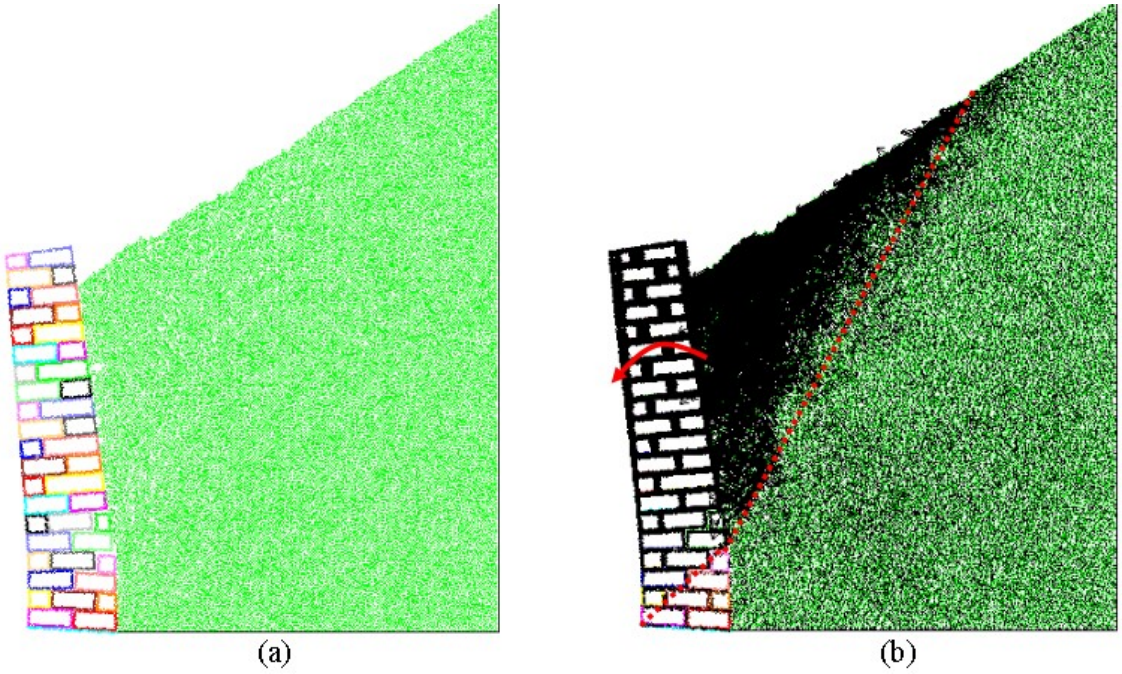

Figure 2.19. Toppling failure: (a) general view, (b) velocity field of the particles (Source: Oetomo et al., 2015).

Nadukuru and Michalowski (2012) investigated the soil-retaining wall interaction and force chain in a numeric model. The retaining wall was simulated as segmented rigid walls using 3-Dimensional DEM model. Three modes of retaining wall movements were considered: (1) rotation about the base, (2) rotation about the top, and (3) horizontal translation. All modes of wall movement in DEM simulations showed similar stress distribution on a retaining wall as in physical experiments. After backfill generation, the distribution of stress on the wall was approximately linear. Whereas the stress distribution

became distinctly nonlinear for the wall translation mode and rotation about the top. These simulations were able to mimic the experimental tests.

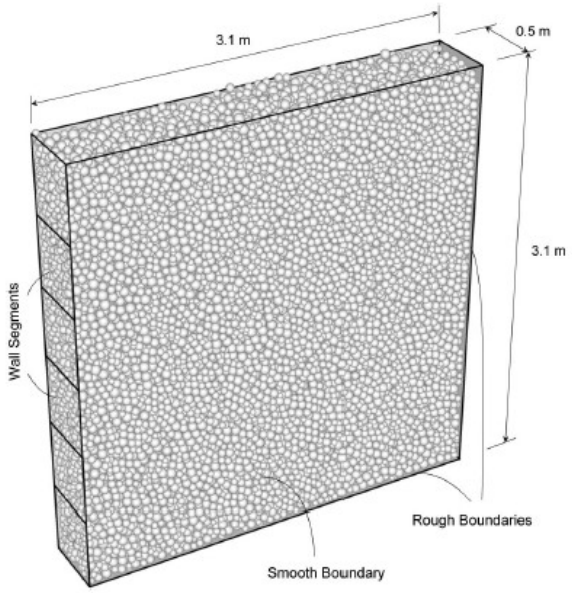

Figure 2.20. DEM model of a retaining wall and sand particles
(Source: Nadukuru and Michalowski, 2012).

A similar study has been conducted by Yang and Deng, (2019). The discrete element method was used to mimic the behavior of cohesionless soil with narrow width behind a rigid retaining wall as the wall translation moved from the soils using 2-dimensional Particle Flow Code (PFC2D) software. Figure 2.21 presents the DEM model of generated soil particles and retaining wall. The influences of backfill width, soil interparticle friction, and system friction angle are examined during simulation studies on the active earth pressure distribution.

According to the results, the active failure form of the narrow-width backfill was a trapezoid with an upper rectangle and a lower triangle. The value of the internal friction angle of the soils is connected to the inclination angle of the triangular failure wedge. With the width of the backfill narrowing, the lateral active earth pressure reduced significantly.

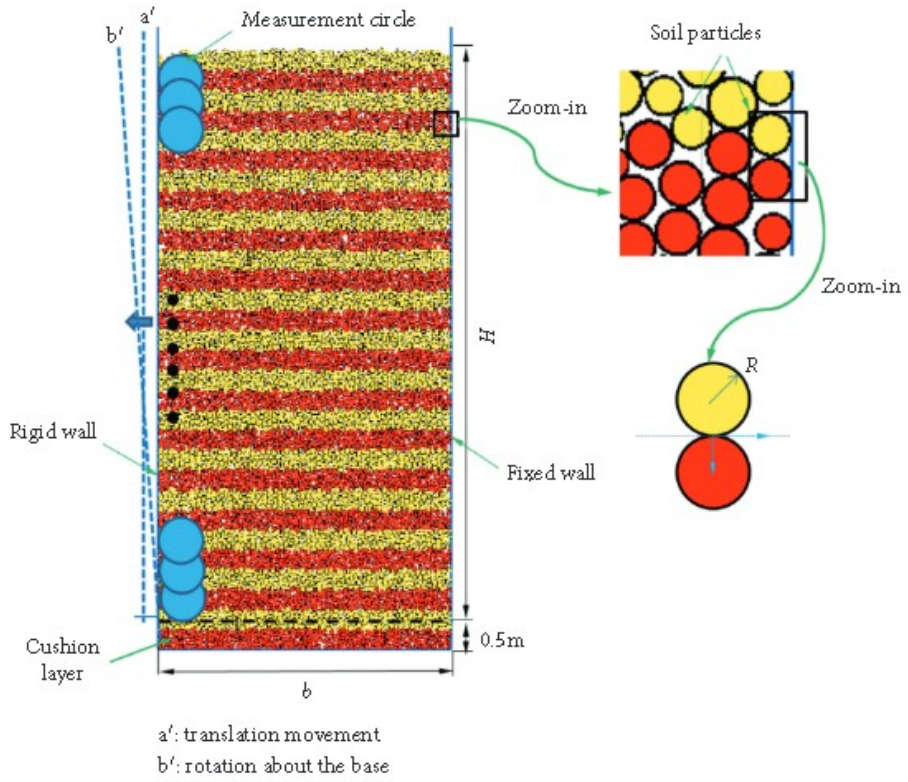

Figure 2.21. Simulated model of the soil particles behind retaining wall

(Source: Yang, and Deng, 2019)

2.6 Numerical Models of Soil Stabilization

Another researcher Indraratna et al. (2019) coupled DEM-FEM modelling in approach to simulate ballast deformation. They offered new ways to increase track stability and longevity by incorporating plastic inclusions (e.g., geogrids) and energy-absorbing materials (e.g., rubber materials). Moreover, the study presented the results of laboratory experiments, mathematical and numerical modeling. The behavior of geogrids and tire cells were calibrated using FEM (Finite Element Modelling) and DEM (Discrete Element) modelling compared with laboratory test results.

Figure 2.22 shows a 3D FEM modeling of a track embankment reinforced with recycled tires. Ballast, capping, and subgrade are modeled as linearly elastic-perfectly plastic materials using the Mohr-Coulomb failure criterion in the FEM simulation. Scrap tires are modelled as cylinders of the same thickness as those used in the laboratory.

Between 15 and 65 kPa was the optimum range of confining pressures for minimising ballast breakage. The confining pressure in this study was less than 25kPa.

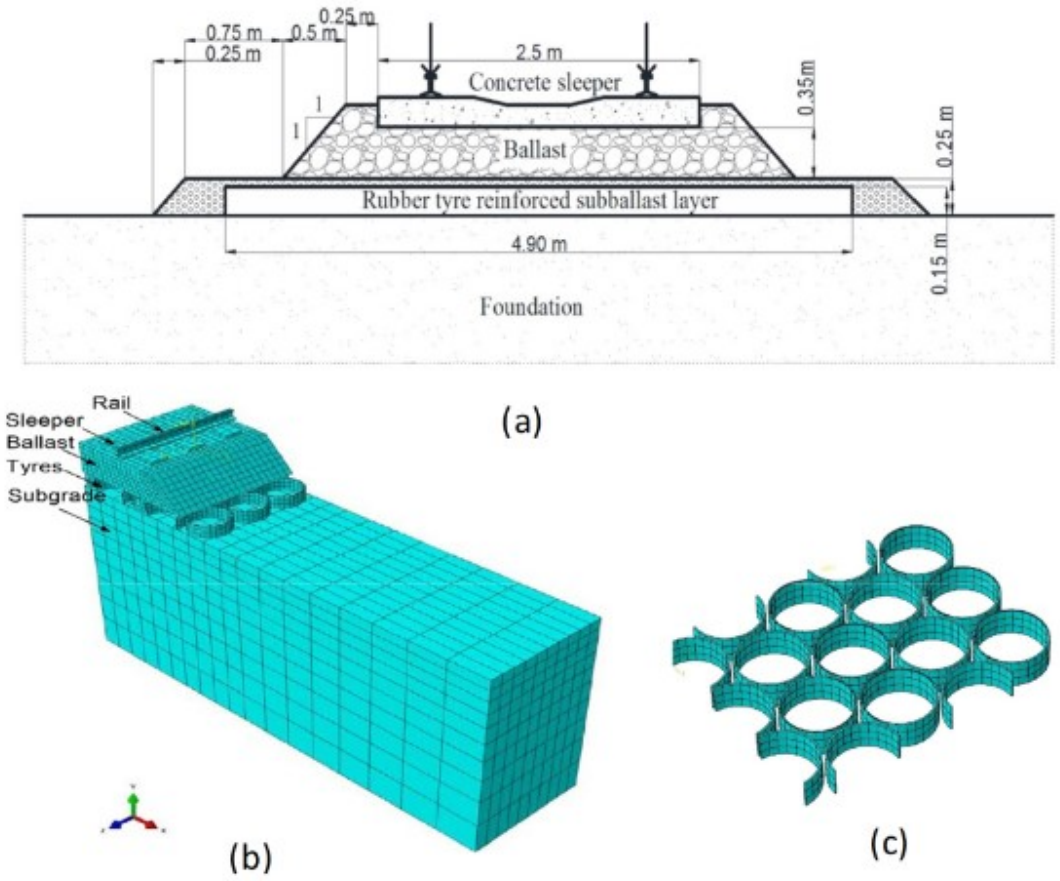

Figure 2.22. 3D FEM simulation of rubber tire-reinforced capping layer: (a) schematic view of the ballasted track embankment; (b) FEM mesh of track embankment; (c) FEM mesh of rubber tires

(Source: Indraratna et al., 2019)

The proportions of horizontal displacement that occur in a sub-ballast layer with and without recycled tires are shown in Figure 2.23(a) and (b). The lateral displacement of the subballst layer reinforced with rubber tires was 10mm. Reinforced subballast layer displayed flexible mattress response under additional confinement, which allowed for a lower and more uniform stress to be delivered to the underlying subgrade, resulting in less

lateral deformation. This composite system enhanced the capping layer's stiffness and demonstrated energy dissipation potential.

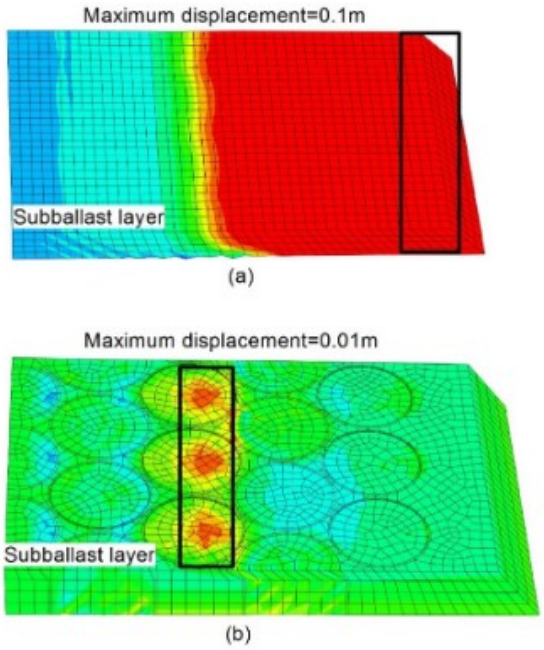

Figure 2.23. Lateral displacement distribution in a sub-ballast layer (a) with and (b) without recycled tires

(Source: Indraratna et al., 2019)

A coupled DEM-FEM simulation of ballasted track embankment under cyclic loading was developed in order to investigate the load-deformation response of ballast. Ballast aggregates were modelled as bonded rigid particles (clumps) using DEM approaches, whereas the FEM method is used to model the subballast layer of 150mm thickness. At the ballast-capping interface, the finite element nodal displacements were used as boundary conditions for the discrete elements, and the forces acting from the discrete elements were used as force boundary conditions for the finite element. The physical load-deformation behavior of ballast subjected to cyclic loads could be captured using a coupled DEM-FEM model (Figure 2.24).

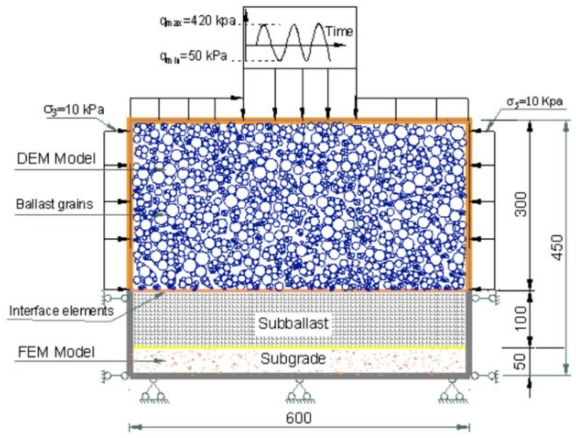

Figure 2.24. Coupled DEM-FEM model of ballast (Source: Indraratna et al., 2019)

Numeric study of geogrid use in soil enchantment has been performed using DEM PFC2D software (Wang et al. 2014).

The geogrid was modelled as bonded twenty particles in one row with a length of 200mm as in the laboratory test. In order to match the physical parameters, geogrid parameters were calibrated in a numeric tensile test. The calibration procedure was done using a numeric direct shear test under confining stresses of 50, 100 and 200kPa. The sand-geogrid load transfer at a microscopic scale was investigated using numeric compound tensile tests. The calibration test results are represented in Figure 2.25 (a) and (b).

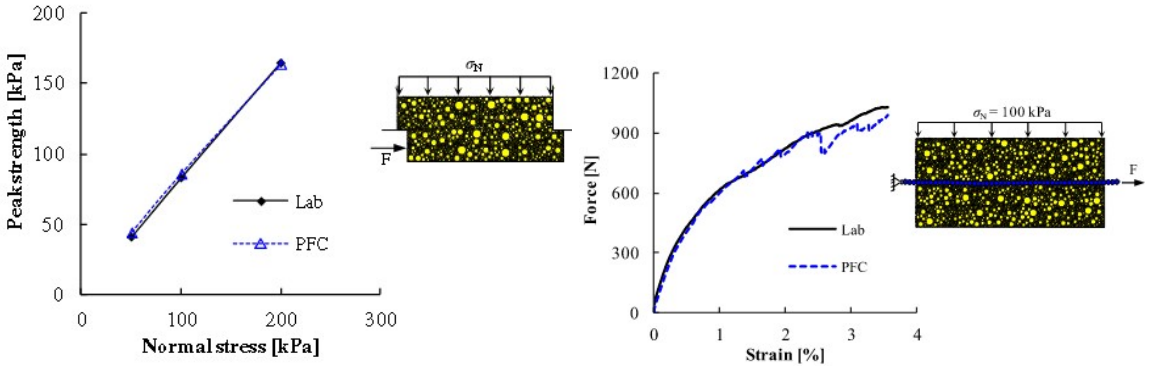

(a) (b)

Figure 2.25. Calibration results of the (a) direct shear test and (b) compound tensile test (Source: Wang et al., 2014).

The geogrids and load transfer were affected by variations in parallel bond forces on the geogrid. The load was gradually transmitted from the geogrid to the sand, according to the measurements from Figure 2.26 (a)-(d). According to the findings, the PFC2D DEM model can be used to demonstrate the geogrid-sand load transfer.

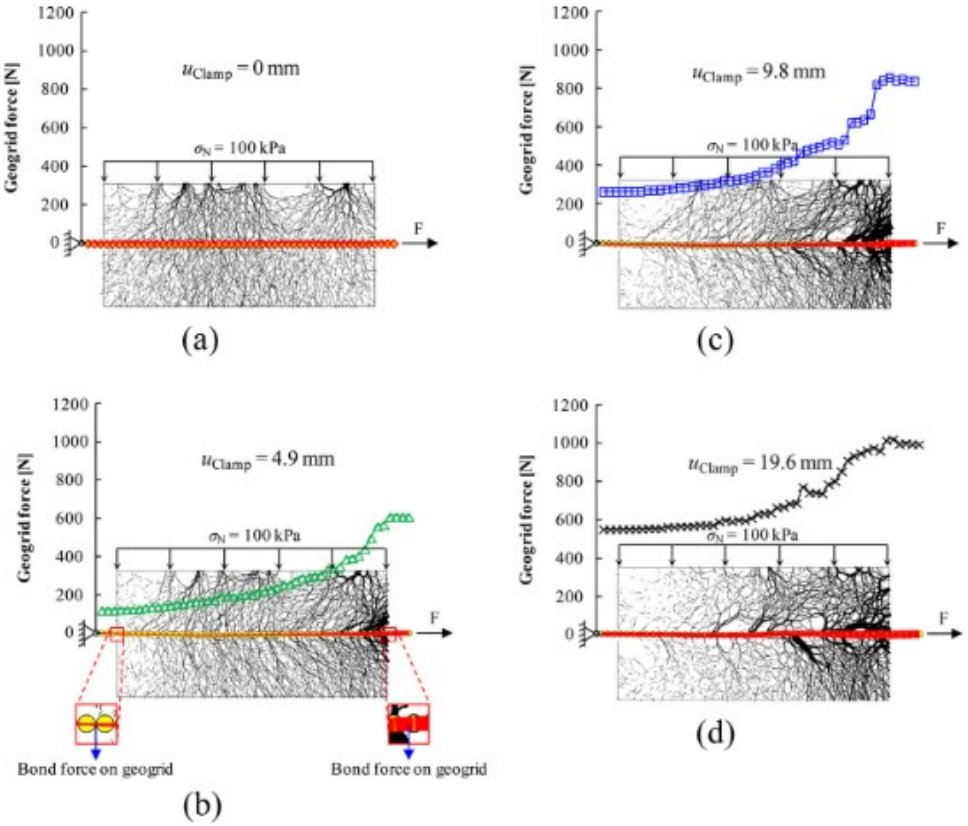

Figure 2.26. Load transfer in the specimen at different stages of clamp displacements (Source: Wang et al., 2014).

2.7 Conclusion

According to the accomplished studies of many researches the application of fine and course tire chips could be used to enhance soil properties. Recycled tire additives to sand reduce the specific gravity and dry density while increasing the shear strength of the soil. Hence, the sand-tire mixture can be effectively used as a backfill material. Using scrap materials can help reduce construction costs, solve disposal issues, and contribute to a

greener and more sustainable use of disposal materials. Rubber tires come in a variety of shapes and sizes. They can be used in a variety of civil and non-civil engineering applications, including the production of rubber composites, as a fuel, as an aggregate or additive in cement products, in road construction, as lightweight fill for embankments, and as backfill material for retaining walls.

DEM simulations that are used to model granular materials, as well as sand-tire mixture, could mimic the physical behavior of the materials. The previous investigations provided crucial information on the interaction of sand and tire particles. The literature review shows that, the DEM simulation of sand and granulated rubber backfill was simplified. Consequently, nobody studied the micro interaction between the soil and the sheet pile foundation under static vertical load. Presented work was performed to investigate the force-displacement response of the sheet foundation subjected to the applied pressure.

CHAPTER 3

DEM METHOD IN PFC2D SOFTWARE

3.1 Introduction

This chapter describes the numerical Distinct Element Method (DEM) implemented in this study. First, a general description of the DEM is given. Next, a walk-through explains the fundamental principles and theory of the DEM method.

The DEM software PFC2D used in this study is also mentioned. The description consists of applying PFC2D in this thesis, the basic mechanics of the software, and methods that develop a particle generation algorithm. Finally, the information about the DEM simulations is given.

3.2 Distinct Element Method

The discrete element method (DEM) has been established as the most effective numerical tool for modeling particle phenomena in various scientific and engineering challenges (Cundall 1971 and 1974). Individual (non-overlapped) physical particles are represented as rigid components that interact exclusively along with their interfaces in the DEM's original model. The movement of particles occurs independently of each other while interacting only at exact contact points.

At present, the discrete element method is gaining more and more popularity and is used to solve geomechanic problems. Its essence lies in the fact that the reagent medium is replaced by a significant packing of discrete particles, between which specific interaction laws are defined (Cundall, P.A., and Strack, 1979). Shapes are also distinguished by a free multidimensional parameter, which must be chosen from additional considerations. This method is a fundamental alternative to classical methods based on traditional concepts of continuum mechanics.

As is well known, the discrete element method's advantages lay in the fact that there are no additional difficulties in solving large deformations and rotations problems. In

addition, it is possible to describe the presence of side effects and physically nonlinear effects without fundamental complications (Aksenov et al., 2014).

Indeed, setting the initial packing of particles and the laws of interaction between particles is not the same as setting the governing equations for the deformation of the medium. The constitutive equations contain information about the behavior of the elementary volumes of the medium. Within the limits of an elementary volume, the distribution of stresses and strains can be considered constant, and the distribution of velocities and displacements can be considered linear in coordinates (we will exclude gradient models.) Thus, having the governing equations, we clearly imagine the macro properties of the medium we are dealing with. Therefore, DEM simulations provide the so-called micro-macro-transition (Pöschel et al., 2001), enabling microscopic knowledge of macroscopic particles.

In addition, we have access to the entire arsenal of tools that have been developed in continuum mechanics over the past 200 years. It includes tools for analyzing the type of equations, determining the velocities of various types of waves, theorems on limit loads, stability criteria, and much more. In other words, even before solving a specific problem, we already know the main features of the solution in advance. This greatly facilitates both the search for adequate problem statements and the interpretation of the solutions obtained.

There are no such possibilities when utilizing the discrete technique. The ultimate objective of "creating a bridge" is to combine the benefits of discrete element approaches and continuum mechanics methods.

3.3 Principles and Theory of Discrete Element Method

Cundall (1978) provided the principles on which the method of the distinct element is based, and the nature of the fictitious material that can be modeled using this method.

The equilibrium contact forces and displacement of the stressed node of the discs during the movement of individual particles are obtained by a series of computations in the distinct method. The propagation of disturbances occurring at the borders and characterizing the dynamic process is the results of these motions. The physical parameters of the discrete media determine the speed of propagation.

The distinct element approach is based on the idea that the specified time step might be sufficiently small that disturbances from each disc propagate only to its nearest neighbours during that time step. The velocities and accelerations are assumed to be constant while using a time step. The forces that develop on each disc at any time are solely defined by its interaction with the discs it comes into contact with. The discs are calculated using Newton's second law in the distinct element method, while the contacts are calculated using a force-displacement law. The motion of a particle caused by external forces is described by Newton's second law. Whereas contact forces are determined by displacements using the force-displacement law.

3.4 DEM application in geotechnics

O'Sullivan (2015) updated the information on the number of DEM-related publications by provided by Zhu et al. (2007) from 1985 to 2005. Figure 3.1 shows the results of this analysis from 1985 to 2014. It represents that since 1996, there has been a continuous almost linear growth in the number of articles related to discrete elements modeling.

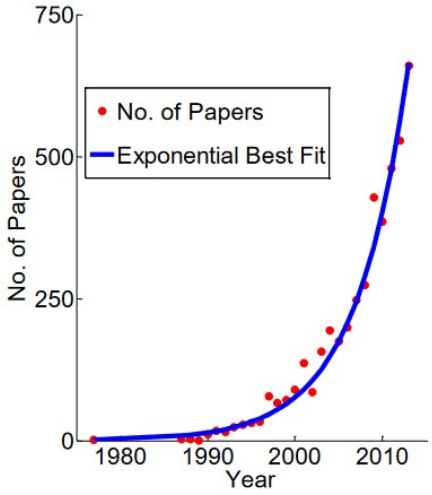

Figure 3.1. The annual volume of publications on discrete element modelling obtained using the (Zhu et al., 2007) approach.
(Source: O'Sullivan, 2015)

Almost every year, as shown in Figure 3.2, the number of articles reporting two-dimensional (2D) DEM simulations outweighed the number of publications describing three-dimensional (3D) simulations. The reduced computing costs are the primary reason for the widespread use of 2D DEM modelling.

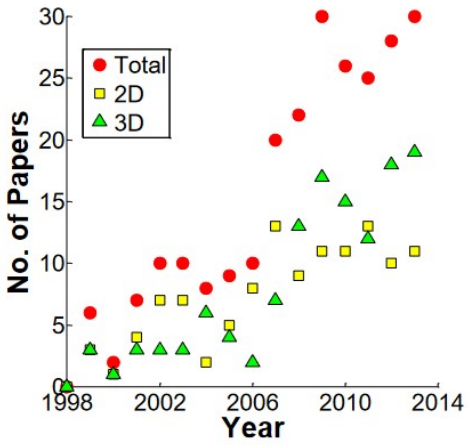

Figure 3.2. The annual rate of DEM publications in geomechanics literature (Source: O'Sullivan, 2015)

DEM simulations are used to model granular unbounded materials as well as cemented sand/rock mass as bonded material (Potyondy and Cundall 2004). Many mechanical response properties specific to granular materials may be captured with DEM.

According to the reviewed literature stress-dependent/frictional strength may be captured using DEM (Cui and O'Sullivan, 2006). As example, the corn internal friction angle and the friction angle in PFC2D were determined using a direct shear test (Coetzee, C. J., 2009). The effects of the inclination angle and the number of prefabricated fractures were examined using simulations of rock-like materials with a hole. (Cao et al., 2014). The development of crushing in a simulated granular material exposed to a direct shear test was the subject of another study (Lobo-Guerrero and Vallejo, 2005). The shear strength, dilatancy effect, and development of microcracks on the structural surface of argillaceous limestone were investigated using the Particle Flow Code in Two Dimensions (PFC2D) (Wenmin et al., 2016).

3.5 Particle Flow code in Two Dimensions

There is a large range of DEM-based software. In this thesis, all DEM simulations have been implemented using Particle Flow Code in 2D (PFC2D). This section covers both theoretical and practical parts of using PFC2D, focusing on issues that are closely connected to the study performed in this thesis.

3.5.1 Development of DEM Modelling

The modeling of geoengineering mechanical processes requires unique considerations and a design concept. In a discipline like geomechanics, where data isn't always easily accessible, (Starfield and Cundall, 1988) proposes a modeling technique that is suitable for a data-limited system. To better understand the problem, the numerical "sample" must be appropriately created and tested on several samples. More calibration stages may be performed to employ numerical models, where existing conditions are simulated, and model parameters are modified to match actual values. More calibration stages may be performed to use numerical models, where existing circumstances are simulated, and model parameters are adjusted to match observed findings. After that, the calibrated model may be applied in additional numerical experiments.

Since some of the questions will be related to situations in which little data is available, Itasca software offers a recommended modeling technique, which is presented in Table 3.1.

Table 3.1. Recommended Steps for Numerical Analysis in Geomechanics
(Source: Itasca, 2019)

Step 1	Define the objectives for the model analysis.
Step 2	Create a conceptual picture of the physical system.
Step 3	Construct and run simple idealized models.
Step 4	Assemble problem-specific data.
Step 5	Prepare a series of detailed model runs.
Step 6	Perform the model calculations.
Step 7	Present results for interpretation.

There are three main steps in the modeling algorithm (Itasca, 2019), as shown in Figure 3.3:

- ❖ Model Setup;
- ❖ Calculation and;
- ❖ Solution analysis.

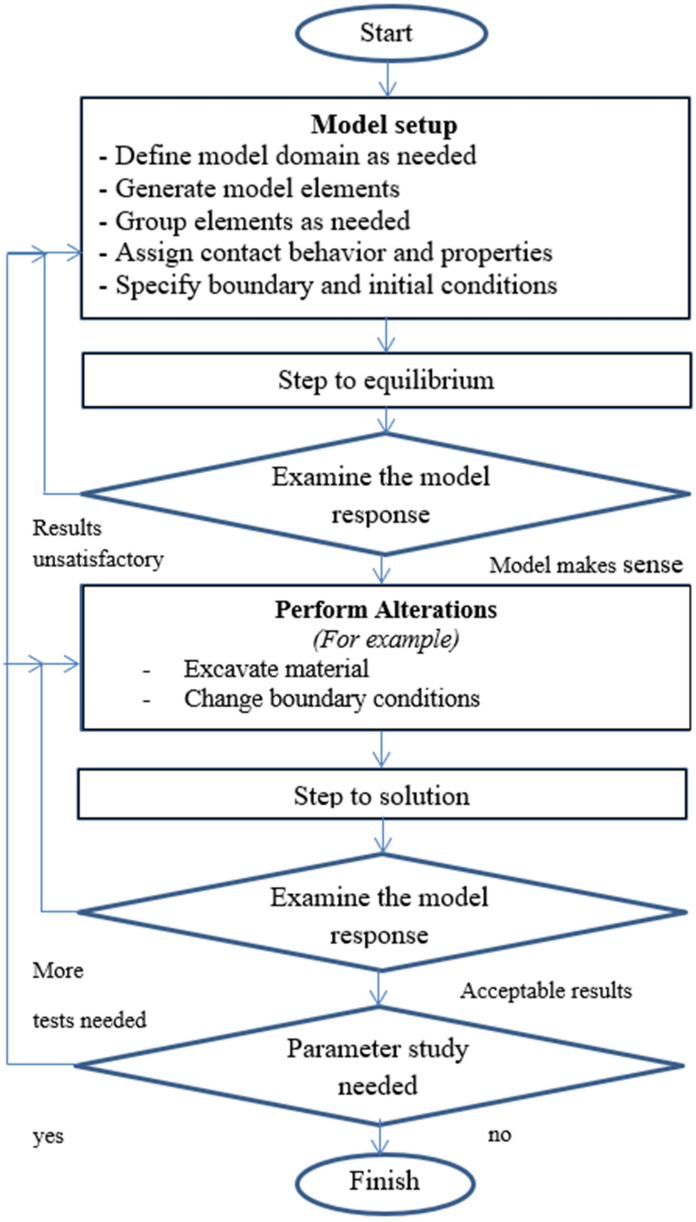

Figure 3.3. General solution procedure: the modeling methodology as a workflow within the software

(Source: Itasca, 2019)

Setting up the model is the initial step in the workflow, and it is divided into four primary components of the problem:

1. The model domain;
2. Fundamental model elements (assembly of particles);
3. Contact and material properties;
4. Initial and boundary conditions.

The position and distribution of the particles establish the model's geometry. The domain, walls, and circular particles, typically known as balls, are the major components of the model. The model domain and walls are used to specify boundary conditions and to help in the generation of particle assemblies. The contact and material properties, in turn, determine the type of response the model will exhibit when disturbed.

3.5.2 Particle assembly generation

The initial particle assembly generation is important in the DEM modeling process. Indeed, the number of methods to pack particles into a linked network is enormous, as are the properties of the packaging generated.

When there are only a few particles in the system, the placements may be decided manually. In bigger systems, the particles can be put by designating a greater number or by distributing balls inside a specific volume to reach a particular porosity. Given the user's input, a random size and position are generated for each ball to be distributed.

Though since nature is not regular, we usually use the second type in geomechanics. In this work particle distribution (ball distribute) approach has been used to generate assembly for direct shear tests and model simulations in PFC2D. To build multilayered soil, a population of particles (with specified packing and radius) is created layer by layer inside a particular region. In PFC2D, the porosity, n, is defined as:

$$n = 1 - \frac{A_p}{A} \tag{3.1}$$

where, A_p - the total area of the particles, A – total area. It is important to keep in mind the drawbacks of applying two-dimensional modeling of the granular materials to simulate three-dimensional physical processes (Calvetti, 2003, and Bagi, 2005).

3.5.3 Contact models

The physical behavior at a contact is described by a contact model. The forces that occur at contacts allow particles to interact with each other (ball-ball type) - Figure 3.4(a), and with walls (ball-facet type) – Figure 3.4(b).

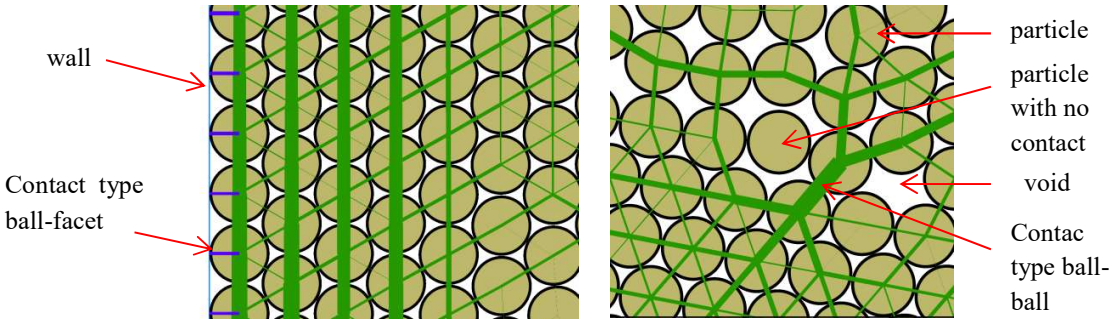

Figure 3.4. Contact model in PFC2D for (a) walls, and (b) particles.

Each contact model is composed of three main components: (1) a contact stiffness model; (2) a slip and separation model; (3) a bonding model.

The linear unbonded contact model was implemented to the soil material to create a granular material such as sand (Cundall, 1979). Linear elastic (no-tension) frictional behaviour is provided by the linear component. Linear springs with constant normal and tangential stiffnesses, k_n and k_s, provide the linear force.

Contact forces and relative displacement directly depend on contact stiffness in both normal and shear directions.

Total contact force for the linear model, according to the force-displacement law:

$$F_c = F_l + F_d \tag{3.2}$$

where F_l is the linear force and F_d is the dashpot force.

The magnitude of the contact force in the normal direction is calculated by:

$$F_n = k_n g_s \tag{3.3}$$

where k_n – normal stiffness at the contact, g_s – contact displacement.

The shear contact force is given by:

$$\Delta F_s = -k_s \Delta g_s \tag{3.4}$$

where k_s –shear stiffness at the contact, Δg_s – increment of contact displacement.

Hence, the shear contact force can be determined by adding the old shear force with the shear force increment:

$$F_s^t = F_s^{t-1} - k_s \Delta g_s \le \mu F_n \tag{3.5}$$

where μ – friction coefficient.

A linear parallel bonded contact model is established to improve the sheet pile simulation. Parallel to the linear component, the parallel-bond component creates an elastic contact between the parts. Both force and moment can be transmitted between the parts using parallel bonds. Total contact force has been obtained by adding parallel-bond force, as compared to the linear stiffness model alone, due to the inclusion of bonded.

Total contact force for the linear parallel bonded model, according to the force-displacement law:

$$F_c = F_l + F_d + \overline{F} \tag{3.6}$$

where F_l is the linear force and F_d is the dashpot force, $\bar{F}$ is the parallel-bond force.

The normal and shear contact forces have been defined similarly, but with additional multiplication by the area of the bond cross-section:

$$\overline{F_n} = \overline{k}_n \overline{A} g_s \tag{3.7}$$

$$\Delta \overline{F}_s = -\overline{k}_s \overline{A} \Delta g_s \tag{3.8}$$

where A - the area of the bond cross-section.

3.5.4 Boundary conditions

Application of the correct boundary conditions is very important in DEM modeling. Additionally, a balance between computational limitations and practical solutions has to be maintained.

During simulation of the triaxial testing, the use of conventional periodic boundaries was ineffective (Sitharam et al., 2005, Powrie et al., 2005). This type of the boundary conditions exhibited non-physical behavior. According to (Lu and Frost 2010), 3D simulations of the triaxial tests performed better than 2D simulations.

In the case of simulating a latex membrane, layers of particles are used to produce a cylinder surface that replaces the rigid-wall cylindrical boundary. (Cui et al., 2007, Wu, K., 2021) used stress-controlled borders, which have been demonstrated considerably different peak and post-peak soil properties than servo-controlled walls (Cheung et al., 2008).

Although, the servo-controlled approach was still employed in several following works (Jeong et al., 2021, Wenmin et al., 2016, Shi D., 2015, Lobo-Guerrero and Vallejo, 2005).

The boundary conditions can be represented using wall mechanism; however in PFC2D they do not follow Newton's laws of motion. They can stay motionless, as a fixed container or the user can apply their own kinematics to them (ITASCA, 2019). For example, the user can impose a velocity and rotational velocity to the walls, as seen in (Jeong et al., 2021).

In this study walls were used as the model container boundaries that have no freedom and with fixed positions. Servo-controlled boundaries were used to simulate confining stress in simulation of the direct shear test.

3.5.5 Numerical time-step

The computation cycle in PFC2D is a time-stepping algorithm that involves applying the law of motion to each particle multiple times. A suitable timestep has to be determined to reliably modify the model state for the numerical integration of Newton's laws.

Excessively long timestep may result instability in the DEM system. Choosing a timestep that is too small, on the other hand, might result in extremely extended simulation periods. The minimum timestep must not be greater than a critical value, also known as critical timestep. The critical timestep of the system considered the motion of a single point mass is given by (Bathe and Wilson, 1976):

$$t_{crit} = \frac{T}{\pi} \tag{3.9}$$

$$t_{crit} = \sqrt{m / k} \tag{3.10}$$

where T is the period of the system, m – single point mass and k is the stiffness of each of the springs.

Since the critical time step is related to the particle size, smaller sand particles may result in a quite small timestep. Under quasi-static conditions in geotechnical tests, (Thornton, C. 2000) proposed an approach to speed up DEM simulation times. The main purpose of the time scaling procedure was to raise particle density until the Rayleigh wave time step and the minimum contact time step was equal. Afterward the advantage of the approach proposed by O'Sullivan, and Bray (2004) is that the critical time step is calculated directly using Rayleigh's theorem.

The mass and velocity of the balls are scaled in this method to rapidly achieve an equilibrium configuration. The new mass of the particle with scaled timestep is determined by:

$$m_{new} = k \cdot \Delta t^2 \tag{3.11}$$

The scaled velocity of the particle is:

$$v_{new} = v \cdot m_i / m_{new} \tag{3.12}$$

Timestep scaling procedure has been implemented during DEM simulation in PFC2D environment.

3.5.6 Tools for storing and extracting results

Information about the system is stored and written to files after a specified number of time steps in the simulation.

A specified set of variables at a certain timestep, such as the model's contact network, may be extracted directly from the stored files. History logic allows storing and then plotting the variables against other recorded variables.

An alternative way to store and create the histories of the variables is to use FISH programming language in PFC2D. User-defined variables and functions may be plotted and saved in results files.

The files with the extension ‘sav’ store the most basic information. Furthermore, these saved files may be restored for further modeling without recalculating the previous stages whenever a new modification has to be examined.

CHAPTER 4

CALIBRATION OF PHYSICAL PROPERTIES OF THE DEM MODEL USING DIRECT SHEAR TESTS

4.1 Introduction

Micromechanical phenomena of the DEM model must be clarified before a thorough calibration of the soil parameters. This chapter describes the calibration of the granular material parameters used in the numerical simulations by comparing the physical and simulated direct shear test results with the DEM model. The set of micro-parameters characterizing granular material that required calibration were Young's modulus, the ratio of particle normal to shear stiffness and the particle friction coefficient. To match laboratory results of granular material, numerical tests that simulate the laboratory test have been performed. Input soil parameters have been varied until the behavior of the numerical sample matches that of the physical sample. An inverse modeling procedure was used.

The first part of this chapter presents information about the calibration procedure. Since there are two types of soil, such as (1) dry sand material and (2) sand-rubber mixture, two contact models have been implemented in the Particle Flow Code in 2D (PFC-2D, Itasca, 2019). In the second part, the comparison of experimental and numerical test results is presented. A good match was observed between the experimental data and the two-dimensional DEM analysis. Finally, a set of parameters is constructed for the subsequent DEM modeling.

4.2 DEM Model Calibration Procedure

The laboratory testing program consists of two main stages: (1) Determination of sand and rubber mixture's basic index and mechanical properties; and (2) Experimental model with sheet pile foundation. All above-described laboratory experiments were conducted at the Geotechnical Laboratory at Izmir Institute of Technology (Khlaif, 2021). Afterward, a numerical model of the direct shear test has been done in the PFC2D

environment. The analogous DEM model has the same dimensions as the real device. The tests were conducted under identical conditions.

Sand grains were modeled in this study. Because only cohesionless granular materials were considered, the particle size, density, interparticle friction coefficient, and contact stiffness were examined. The trial-and-error approach was used. The microscopic soil parameters that were estimated from the calibration are given below:

1. n: the material porosity;
2. E_c: Young's modulus at each particle-particle contact;
3. k_n/k_s: the ratio of the particles normal to shear stiffness;
4. μ: the particle friction coefficient.

These parameters allowed us to replicate the macroscopic response of the granular materials. After verifying experimentally and numerically determined peak friction angle (φ), additional tests were done using the DEM method. The direct shear test procedure by the DEM is consisted of:

1. Model generation (Geometry, boundary, etc.)
2. Calculating and controlling stress states
3. Monitoring the test during the shearing process
4. Analysis of the numerical test.

4.2.1 Model Generation for DEM Direct Shear Test

The soil specimen which was used in the laboratory is represented as the circular particle in PFC-2D. The numerical simulations used in the direct shear test are featured by the random distribution of balls of uniform size (discs with unit thickness). To obtain meaningful test results, a sufficient number of particles has to be more than a thousand elements, which was suggested by many researchers (e.g., Kruyt, 1993). Dry sand and sand-rubber mixture samples have been simulated and tested.

For the numeric model of the dry sand, the assembly of 3142 balls of 0.49 mm radius has been created in the particle generation approach. The system of ball assembly was modelled as elastic with interface friction. Uniform sized balls were used with avarage particle diameter d_{50} = 0.14mm, from sieve analysis results in Figure 4.1. All particles

were featured with the following properties: dry solid density, Young's modulus, the ratio of particle normal to shear stiffness, and friction coefficient. Dry solid density (d) was considered for soil solids (d=2.67) and granulated rubber (d=1.12) from specific gravity tests (Khlaif, 2021). Linear contact model was used to represent particle-particle interaction. Porosity is a critical component influencing the assembly's initial stress state. In direct shear testing, the initial porosity estimation of the granular material in the direct shear test was set as 0.12. The porosity of 0.122 was computed from several tests in PFC2D as the limit value for the direct shear test.

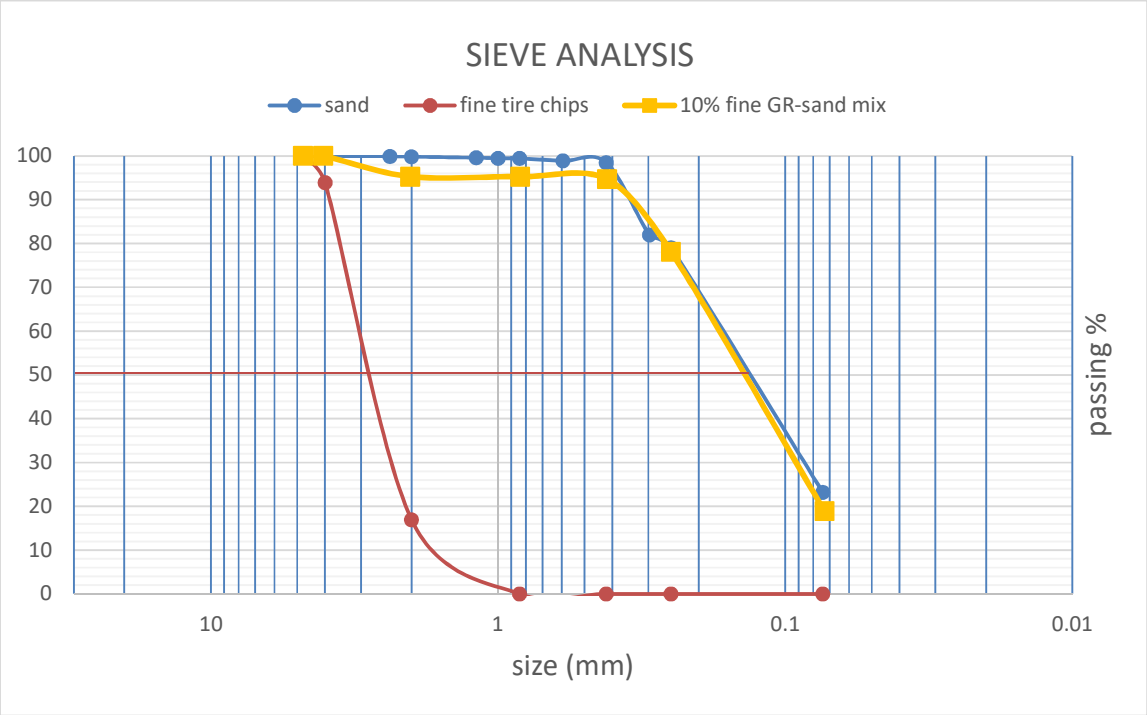

Figure 4.1. Sieve analysis results.

(Source: Khlaif, 2021)

Dimensions of the shear box are agreed as 45mm in height and 60mm in width. The shear box was constructed of eight rigid frictionless walls. The model is shown in Figure 4.2(a). Clean sand sample used in the laboratory is illustrated in Figure 4.2(b).

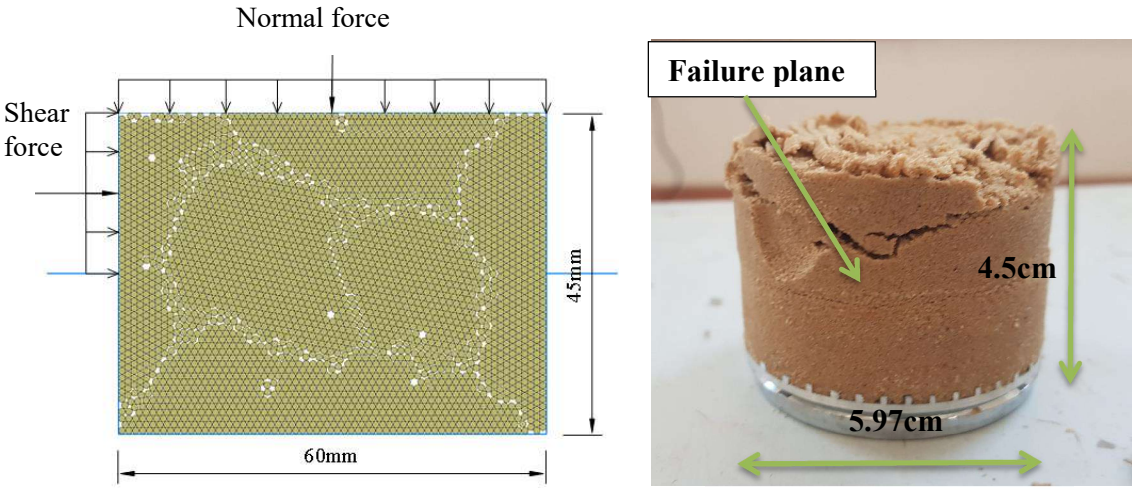

(a) (b)

Figure 4.2. a) The DEM model used in the direct shear test simulations; b) Clean sand sample used in the laboratory

(Source: Khlaif, 2021)

Elasticity modulus (E) estimation has been determined from the experimental direct shear test, according to the developed method by Noonan and Nixon (1972):

$$E = \frac{T}{k\delta} \tag{4.1}$$

where k is a constant depending on Poisson's ratio and the geometry of the test configuration, the values are plotted in Figure 4.3. And T is the shear load on the sample per unit width.

The presented analysis utilizes the theory of linear elasticity to evaluate the elasticity parameters of materials. The obtained value of the E has been calibrated in the numeric model in PFC2D. Effective elasticity modulus in the numeric 2D model is generally greater than the material's Young's modulus (Cundall, 1979).

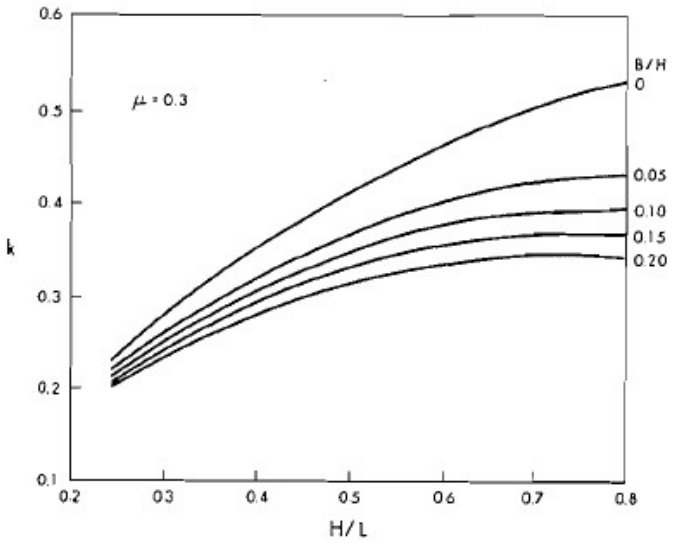

Figure 4.3. k values for μ (Poisson's ratio).
(Source: Noonan and Nixon, 1972)

The analogous procedures were used for the sand-rubber mixture. Figure 4.4 (a) shows the assembly of 2831 balls of the sand particles with a 0.49 mm radius and 38 balls of rubber chips particles with a 1.4 mm radius (Figure 4.1). The volumetric ratio between sand and rubber is chosen to be 10%, which is implemented using the volume-fraction command in PFCD (Eidgahee and Hosseininia, 2013):

$$F_R = \frac{W_R}{W_R + W_S} \times 100 \tag{4.2}$$

where W_R and W_S are rubber and sand dry weight, respectively. The dry soil density was assigned as 2670kg/m^3, and rubber chip density was given as 1120kg/m^3.

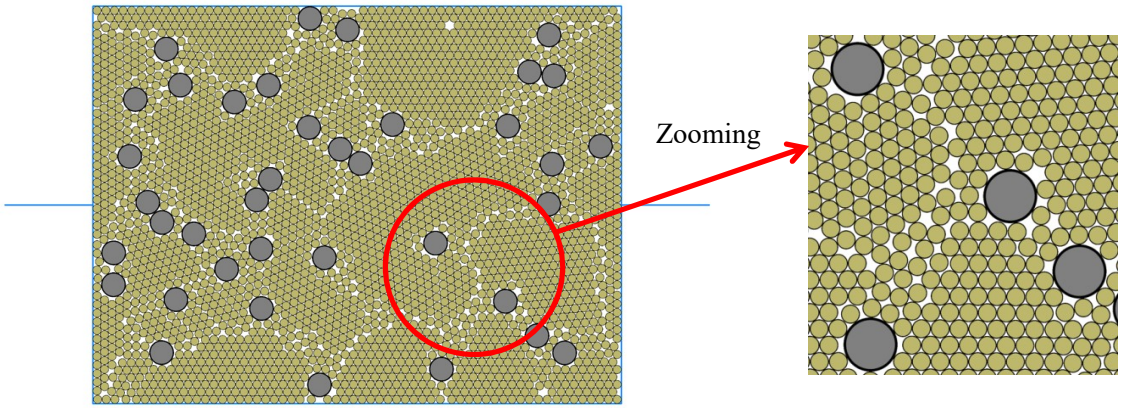

(a) (b)

Figure 4.4. a) The sand-rubber mixture specimen used in DEM model of the direct shear test; b) Rubber particles with adjacent soil particles

If the combination is to be produced for additional soft-rigid materials, suitable parameters must be considered. The soil parameters obtained from the test for the clean sand are used for the further sand-rubber mixture sample shear test. Additional contact was established between sand and rubber chips.

The values of shear modulus and friction of granulated rubber, which were reported by Valdes and Evans (2008), Liang et al., (2004) and Schallamach, A. (1958) presented in Figure 4.5, have been slightly modified during the test. The whole load-deformation behavior must be captured in a 2D model.

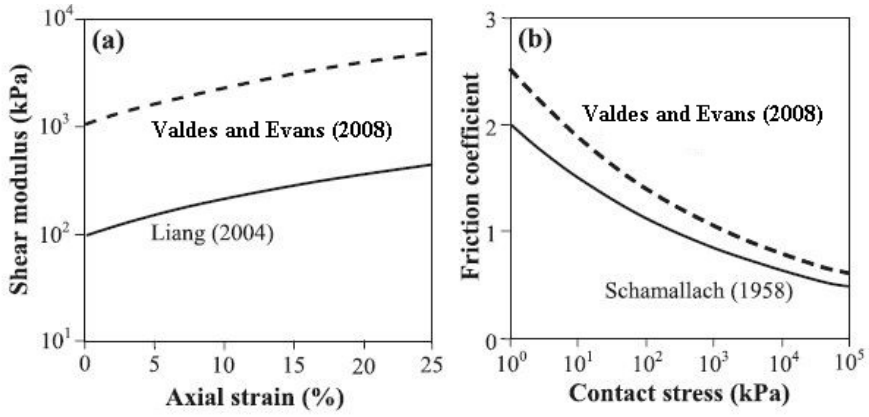

(a) (b)

Figure 4.5. Parameters implemented in DEM model. a) Shear modulus versus axial strain; b) friction coefficient versus contact stress. (Source: Valdes and Evans, 2008)

4.2.2 Calculating and Controlling Stress States in the Model

A set of the direct shear tests at the constant vertical loads of 20kg, 50kg, and 100kg has been conducted in the DEM analysis. At the first stage of the test, a sample was simulated with the interparticle friction (μ) of 0.01. Sample initial properties were attributed at this state. The particles were randomly generated within the shear box to provide initial assembly. After assembly generation, the soil sample was subjected to isotropic compression.

During the simulation of isotropic compression, the normal load is introduced to the system to maintain the target stress level until a quasi-equilibrium state is reached. The normal load was implemented using the numerical servo-control mechanism, as described in ITASCA, 2019. At the isotropic compression state, to prepare a loose assembly model was simulated with the interparticle friction of 0.7 for dry sand and 1.5 for rubber, which were calibrated during the test. Isotopically compressed specimens were prepared for the following shearing process.

Since the boundaries had no friction with containing particles, the primary stress and strain orientations correspond with the coordinate axes x and y. Hence, the significant strains were estimated from the wall displacements. At the same time, the principal stresses were derived by summarizing the contact forces acting from all the neighboring balls to the specified wall and dividing by the wall length and balls thickness. The horizontal forces have been considered horizontal force reaction of the opposite wall force-contact.

4.2.3 Monitoring the Analysis during the Shearing Process

Throughout the shearing process of the model, compressing load is kept constant at the requested values of 20 kg, 50 kg, and 100 kg. The servo-wall mechanism has been set by specifying the target contact force on the top platen. FISH logic (ITASCA, 2019) was used to determine horizontal force and displacement at the decided walls. The Fish Code is given in Appendix A. History logic is used to monitor the process and obtain results.

4.3 Comparison of the model and real test results

A series of shear experiments were carried out with varying particle stiffness and friction coefficient values. The shear simulations revealed that particle stiffness and friction coefficient affected the internal friction angle, particularly at low stiffness levels.

4.3.1 Verification of the Elasticity Modulus

The horizontal force-horizontal displacement curve and stress-strain curve were obtained from DEM direct shear test and later compared with the laboratory test results. Figures from 4.6 to 4.8 show the comparison of stress-strain curves of clean sand. Figures 4.9 to 4.11 compare the stress-strain curves of the granulated rubber-sand mixture. As shown in the figures, the experimental data and the two-dimensional DEM results were found to be quite similar. More remarkable similarities are observed in the tests under 100 kg normal force for dry sand and sand-granulated rubber mixture specimens.

Figure 4.6 compares the stress-strain curves of sand that were obtained from the laboratory direct shear test and DEM model under a normal force of 100 kg. The DEM stress-strain curve peaks at the axial strain of 7.5%, whereas the laboratory experiment curve is at 10%. Until 7.5% axial strain, the shear stress-strain curve matches well with the laboratory experiment. The maximum shear stress for the DEM test of the clean sand was 254.6kPa at the 7.5% axial stress. Shear stress is higher for the laboratory results than for DEM between 7.5% - 12.5% axial strains.

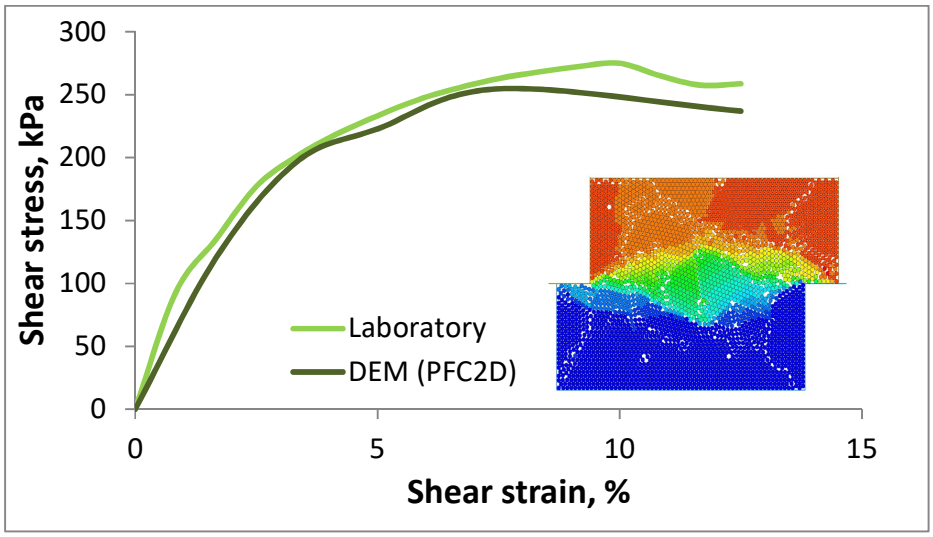

Figure 4.6. The comparison of stress-strain curves of clean sand that were obtained from the laboratory direct shear test and DEM model under a normal force of 100 kg.

For 50kg normal load, Figure 4.7 compares the stress-strain curves of a laboratory direct shear test and DEM test for a clean sand sample as well as displacement distribution within the soil particles. The peak shear stress of the clean sand sample of the DEM model was 131.6 kPa at 3.8 % axial strain, which is earlier than in the laboratory test (6.67 %). However, the sample continued to lose strength until the end of the simulation.

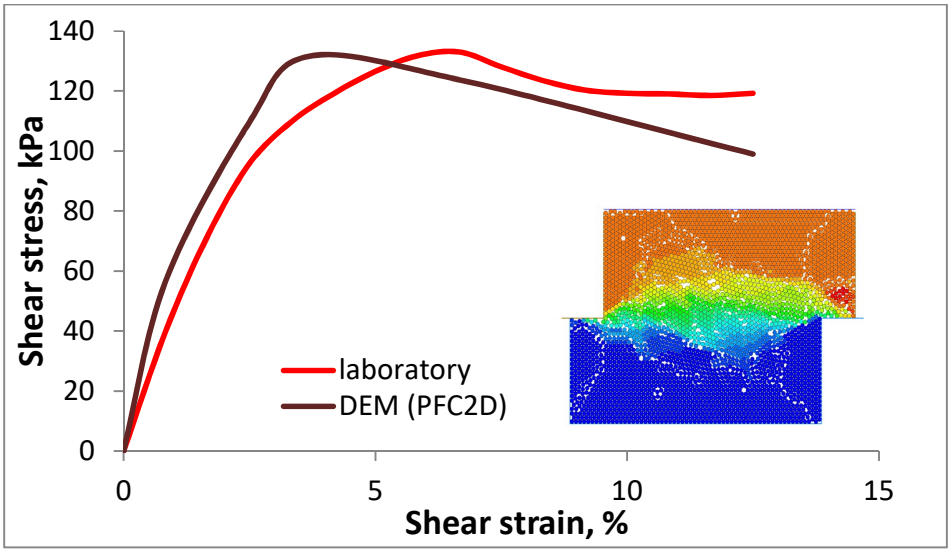

Figure 4.7. The comparison of stress-strain curves obtained from the laboratory direct shear test and DEM model under a normal force of 50 kg.

Figure 4.8 shows the test results for 20kg normal load, shown in produces stress-strain curves of a laboratory Direct shear test and DEM test for clean sand sample as well as displacement distribution within the soil particles.

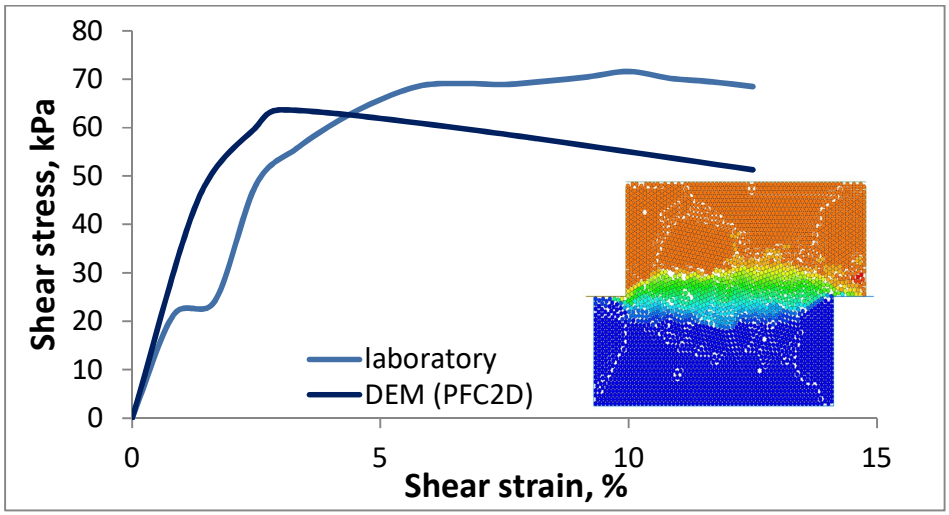

Figure 4.8. The comparison of stress-strain curves that were obtained from the laboratory direct shear test and DEM model under normal force of 20 kg

The peak shear stress of the clean sand sample of the DEM model was 63.7 kPa at 3% axial strain, which was earlier than in the laboratory test (10%). Consequently, after the peak shear stress, the model starts to lose its strength until the end of the simulation.

Figure 4.9 shows the DEM and laboratory test results for 100 kg normal load of sand mixed with 10% granulated rubber.

The stress-strain curve of the DEM model at the 100kg normal load has its peak at the axial strain 5.5 % whereas the laboratory experiment curve is at 9.1 %. Shear stress good matches the curve from laboratory experiment until 5.5 % axial strain. The maximum shear stress for the DEM test of the clean sand was 244.04 kPa at the 5.5 % axial stress. The 10 % granulated rubber mixture sample gains its strength until 5.5 % axial strain, then loses the strength. The 10% sand-rubber mixture demonstrates a weaker response than the numeric clean sand sample.

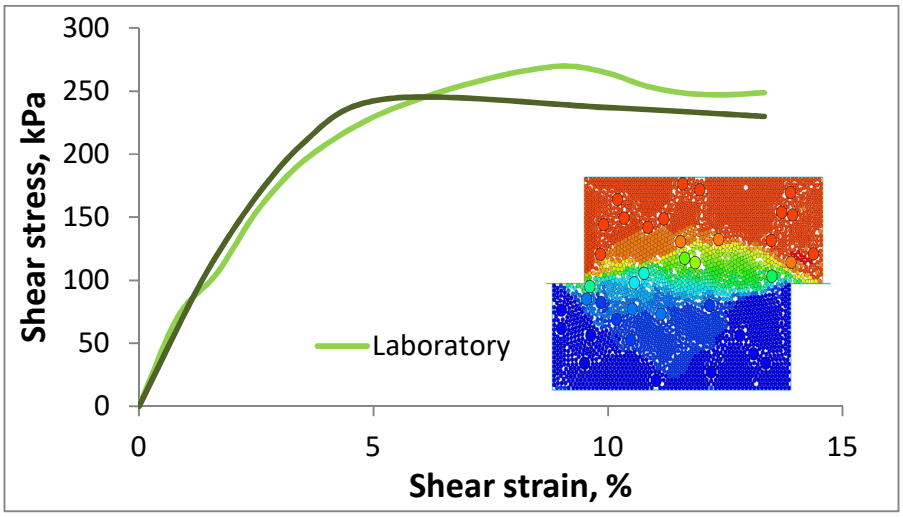

Figure 4.9. Stress-strain curves of a laboratory direct shear test and DEM test for sand-rubber mixture under the normal force of 100 kg.

For 50kg applied normal load, Figure 4.10 represents stress-strain curves of a laboratory direct shear test and DEM test for sand mixed with 10% granulated rubber sample and displacement distribution within the soil particles. The peak shear stress of the 10 % granulated rubber mixture sample of the DEM model was 125.43 kPa at 3.7 % axial strain, which is earlier than in the laboratory test (8.33 %). At the end of the test, the sample shear stress reaches 117kPa, whether the laboratory test sample shear stress is 140kPa.

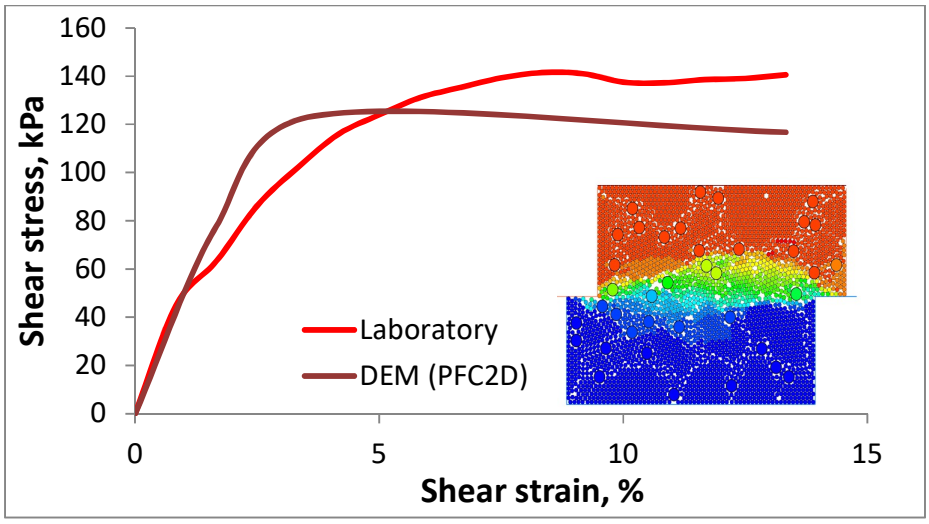

Figure 4.10. Stress-strain curves of a laboratory Direct shear test and DEM test for sand-rubber mixture under normal force of 50 kg.

For 20kg applied normal load, shown in Figure 4.11 produces stress-strain curves of a laboratory Direct shear test and DEM test for sand mixed with 10% granulated rubber sample and displacement distribution within the soil particles. The peak shear stress of the sand mixed with 10% granulated rubber sample of the DEM model was 67.2 kPa at 3.7 % axial strain, which was earlier than in laboratory test (6.67 %). The shear stress at the 13.33% axial strain in DEM simulation has been measured at 50.22kPa, however in laboratory test the shear stress is 67kPa.

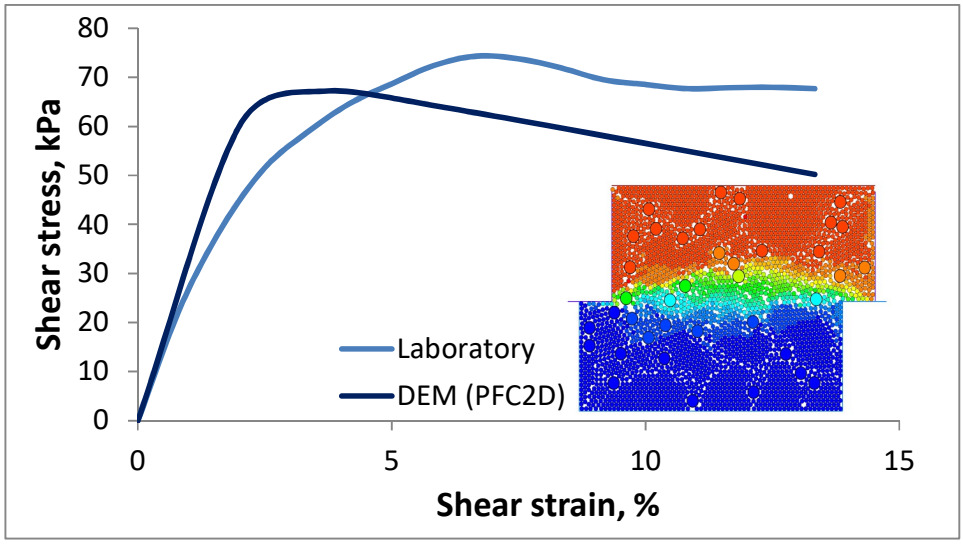

Figure 4.11. Stress-strain curves of a laboratory direct shear test and DEM test for sand-rubber mixture under normal force of 20 kg.

4.3.2 Verification of the Peak Friction Angle

For further tests, micro-properties have to be verified with physical properties. The friction angle of the material assembly was determined from the direct shear test, and an additional test was conducted.

The material's internal friction angle, φ, was influenced by particle stiffness and friction coefficient.

The internal friction angle increases once the particle stiffness rises (Asaf et al. 2005). Corriveau et al. (1996) also used a linear spring-dashpot model and the contact model of Walton and Braun (1986) to investigate the influence of particle friction on the

internal friction angle numerically. In the lower range of μ, their findings revealed that the particle friction coefficient highly influenced the internal friction angle.

The numerical model was compared to the Mohr-Coulomb friction angle determined from the laboratory direct shear test of the sand and sand-granulated rubber mixture for vertical loads of 20 kg, 50 kg, and 100 kg. Figure 4.12 and figure 4.13 depict an outstanding fit between experimental and numerical results.

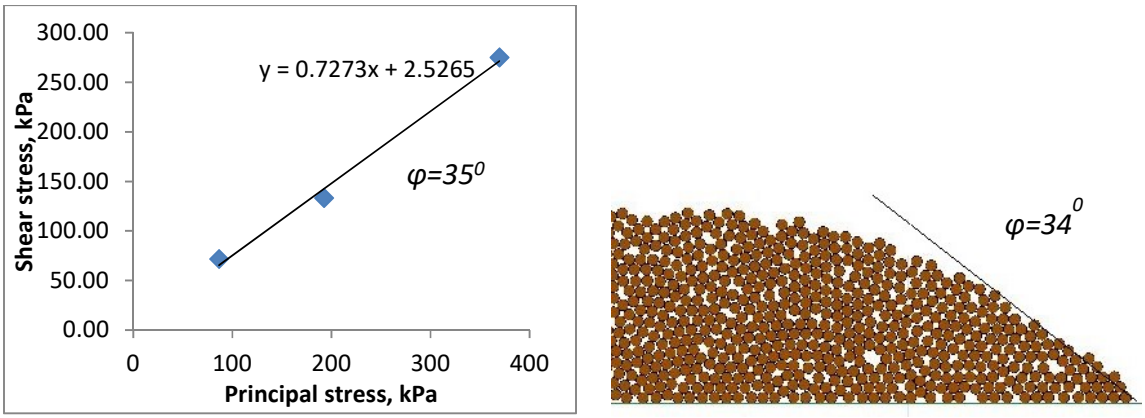

(a) (b)

Figure 4.12. Friction angle from (a) laboratory and (b) DEM simulation of direct shear test for clean sand

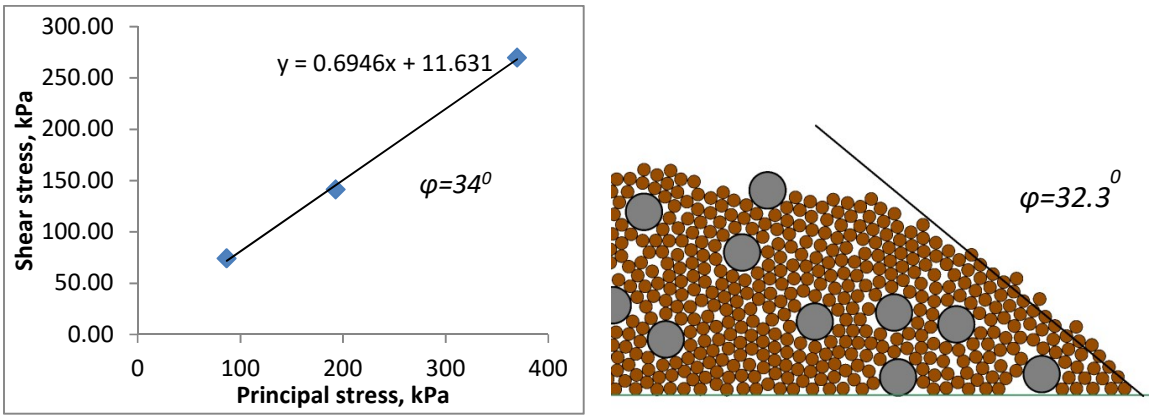

(a) (b)

Figure 4.13. Friction angle from (a) laboratory and (b) DEM simulation of direct shear test for sand-granulated rubber mixture

4.4 Conclusion

A direct shear test and experimental model test were carried out for calibration of a 2D distinct element model (DEM). The results of laboratory tests were used for the subsequent soil modeling in the PFC2D environment.

The optimal set of parameters to match the laboratory results was obtained through a trial and error method. Furthermore, the calibration step revealed that different parameter combinations might result in appropriate discrete material behavior. As a result, no unique set of values best matched the laboratory data. From the verification study, Table 4.1 lists the parameters that were used in the DEM model simulations.

Table 4.1. Input parameters for simulations

	Sand particles	Rubber particles
Diameter of the disk (mm)	0.49	2.8
Density, ρ (kg/m^3)	2670	1120
Normal stiffness, k_n (N/m)	$8 \cdot 10^5$	$6 \cdot 10^4$
Tangent stiffness, k_s (N/m)	$4 \cdot 10^5$	$3 \cdot 10^4$
Friction coefficient, μ	0.7	1.5
$\alpha = k_n / k_s$	2	2

During a direct shear test on clean sand, the peak value of shear stress and its related displacement increased as the constant normal load increased. At both clean sand and sand-rubber samples under 50 and 20kg, the system of particles first compressed until the maximum shear stress was reached, and then expanded, which leads to a decrease in shear strength. The dilatancy effect becomes less noticeable, and the peak value of shear resistance declines, which implies a degradation of shearing capacity.

The dilatancy effect was more obvious in the direct shear test at the normal force of 50kg and 20kg, where shear stress differences between the shear results of laboratory and DEM tests increased. The use of larger sand and rubber particles is one of the primary reasons of this phenomenon.

Rubber additives reduce the shear strength of sand, according to the results of a simulated sand-rubber mixture under 100kg and 50kg normal force. The direct shear test results on 10 % granulated rubber sand mixture sample demonstrated the shear strength increase under 20kg normal force. The dilatancy effect was indeed observed at the direct shear test of the sand-rubber mixture, where the decrease in shear strength was detected once the peak value was attained.

CHAPTER 5

CALIBRATION OF DEM MODEL USING PHYSICAL EXPERIMENT

5.1 Introduction

The DEM calibration of the drained direct shear test developed in the previous chapter required testing on the DEM model. The main purpose of this chapter is to represent how to use the DEM model to simulate a sheet pile foundation in dry soil with static loading. This chapter details the calibration of the numeric model parameters. The analysis presented in this chapter determined the boundary conditions, packing parameters, and appropriate grain sizes for the sheet pile foundation and soil. Furthermore, the 'up-scaled' particles were used in this stage of the DEM modeling. The DEM model study enables us to compare physical and numeric models using the new calibration method. The physical model test was created using PFC2D software.

5.2 Calibration of Experimental Model

Calibration procedure steps are given below:

- Numerical Model Setup,
- Loading process,
- Monitoring the test, and
- DEM model results analysis

5.2.1 Numerical Model Setup

Khlaif, 2021 performed small-scale model tests ting is used to represent a physical model of a sheet pile foundation which that is embedded in dry soil under static loading.

The testing procedure consists of the following steps given below:

1. Soil preparation (160mm depth for foundation and 500mm for the backfill);
2. Pressure transducer installation on the sheet pile at the specified depths(170mm and 340mm below the surface);
3. The sheet pile driving into foundation soil and its fixation;
4. Linear transducer installation at the sheet pile head;
5. Leveling the soil surface and installing the loading plate onto the surface to the center of the backfill;
6. Connecting the LABVIEW program;
7. Beginning of the manual load application through the hydraulic jack;
8. Test monitoring and data collection.

Dry model configuration is schematically illustrated in Figure 5.1.

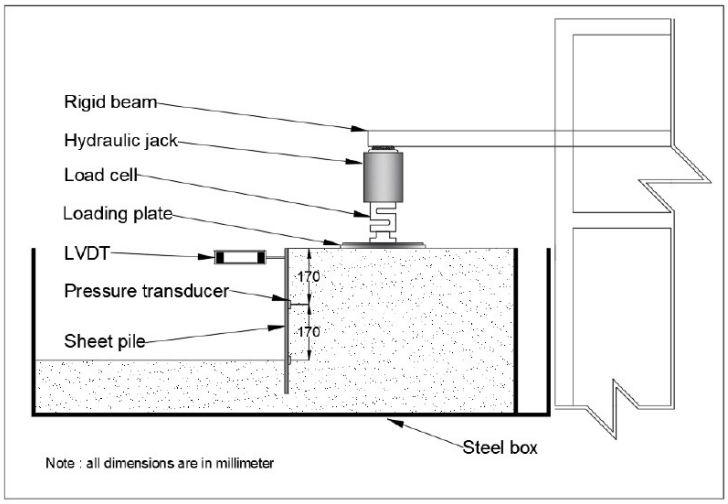

Figure 5.1. Schematic view of the dry model configuration.
(Source: Khlaif, 2021)

A numerical DEM model of the physical problem is generated using parameters from laboratory experiments. The dimensions of the box in PFC2D were fixed to be 1.46m x 0.5m, the same as in the laboratory.

The soil was modelled using rigid discs with specified size. The boundary conditions of the DEM model were simulated by using walls. The microparameters

obtained from the DEM direct shear test are used to determine the normal and tangent stiffnesses of the walls. Additionally, the walls were designed as frictionless.

Modeling relatively small particles increases computation time significantly, whereas modeling too large particles fails to replicate the physical behavior of the soil. The soil particles were "up-scaled" during calibration tests to allow faster calculations. As a result of the calibration, the maximum diameter that could be used in the DEM model was five times larger than the size obtained from the DEM direct shear test. Balls with a diameter of 4.9mm were used to generate the soil assembly.

The sample preparation stage is an important part of the DEM simulations. The procedure of the sample generation explained in Chapter 3 is implemented. Hence, the preparation procedure is employed by the air pluviation method proposed by (Thay et al., 2012). The dry soil is layered into the model chamber with a predetermined constant thickness (t = 150-160mm) in this procedure.

In order to generate a homogeneous specimen with desired density in DEM, a multilayering method proposed by Jiang et al. (2003) was used (Figure 5.2). Several experiments with different the particles fall heights and porosities were conducted to achieve the desired density. During the calibration procedure 20mm height (h) between particles was chosen as suitable for the model. It was noted that the system exhibited dense behavior at the (h < 20mm).

The following equation is used to calculate the average unit weight (γ) of a dry backfill soil with a specific gravity (G_s) and a porosity of (n):

$$\gamma = G_s \rho_w g (1 - n) \tag{5.1}$$

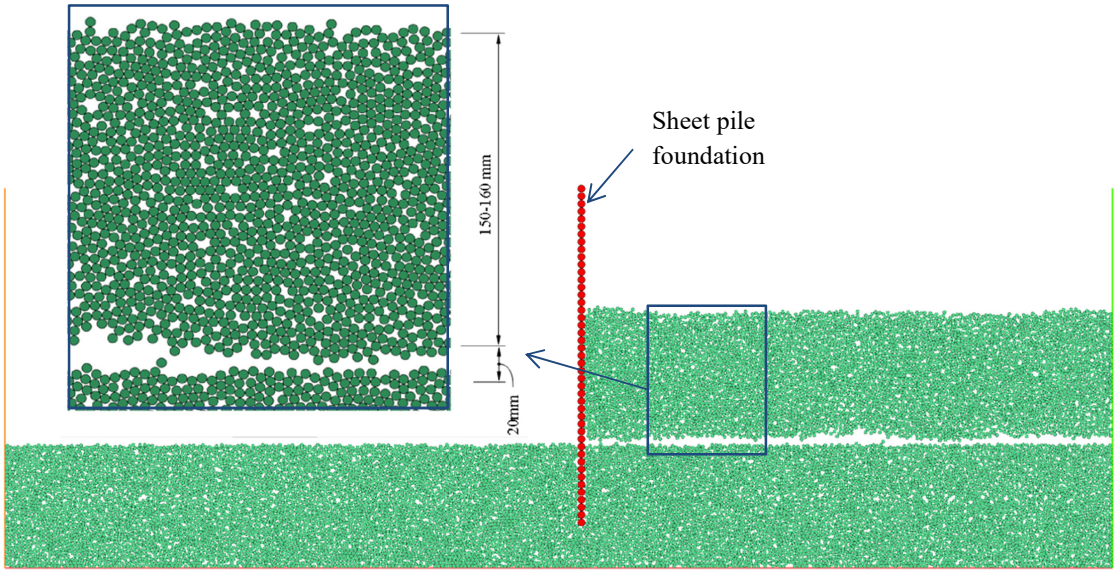

Figure 5.2. Soil preparation in PFC2D

The microparameters of the soil and contact properties (k_n, k_s, μ) obtained from DEM simulation of the direct shear test (Chapter 4) have been used in this study stage.
The contact parameters between the soil and sheet pile particles were considered the same as the contact parameters with the container walls. Hence, the contact types were the ball-ball for the soil-sheet pile interaction and the ball-facet for the soil-container interaction, which parameters were calibrated during the calibration procedure.

In previous studies, sheet piles and retaining walls were modelled using a wall mechanism (Fukumoto et al., 2021, Yang and Deng, 2019, Chen et al., 2018, Zhang et al., 2011). However, wall mechanism was not able to replicate a physical model of sheet pile foundation under static loading. Wall logic provided motionless behavior, and the sheet pile could be deformed only by applying kinematics to it.

Hence, the sheet pile foundation in PFC2D, is created by connecting 45 rigid discs (balls) of an equal radius is 5mm with parallel bonds (ITASCA, 2019). This method was used to model geogrids (Han et al., 2012, Wang et al., 2012). The numerical parameters of the simulated sheet pile are determined based on the physical parameters of Plexiglas. The parallel bonds' normal and shear stiffnesses were considered to resemble the actual sheet pile.

The initial model simulation started with sheet pile generation before the soil generation. However, whenever the soil particles touched the sheet pile, the particles of the sheet pile were getting scattered. To prevent this mechanism the sheet pile insertion stage was required to produce a contact between the sheet pile particles as well as the initial interaction between the embedded sheet pile and the soil particles.

In order to perform this stage, FISH functions were used to insert the sheet pile into a specified location. We decided to install the sheet pile by driving it into the dry sand without previously removing any soil. The foundation part is considered to be completed after inserting the sheet pile into dry soil. Figure 5.3 shows the sheet pile insertion and the soil particles displacement distribution around the sheet pile.

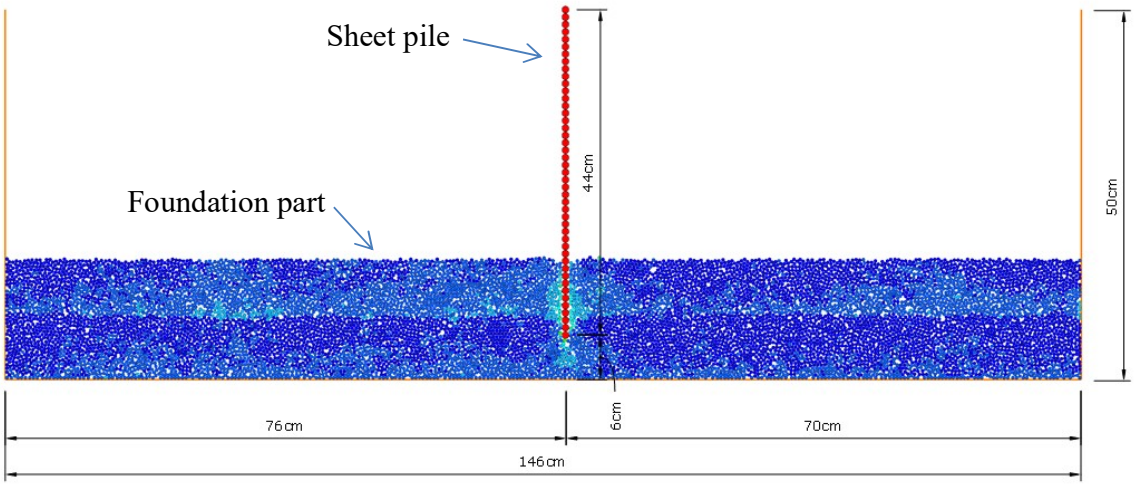

Figure 5.3. Sheet pile and foundation part

The mechanical time-step was established during the soil preparation stage. The critical time-step, t_{crit} for the mass-spring system was determined using Equation (3.10) in the Chapter 3.

For the model particle with a diameter of 4.9mm, which mass is 0.05034kg, and normal spring stiffness is $8 \cdot 10^5$ N/m, t_{crit} is equal to $6.29 \cdot 10^{-5}$s. The time-scale approach is implemented at the soil preparation step to accomplish rapid convergence to an equilibrium configuration.

The list of numeric parameters of the soil particles, wall boundaries, and sheet pile particles of the DEM model is given in Table 5.1.

Table 5.1. Input parameters for sheet pile simulations

Sand particles	
Diameter of the disk (mm)	0.49
Density, ρ (kg/m^3)	2670
Normal stiffness, k_n (N/m)	$8 \cdot 10^5$
Tangent stiffness, k_s (N/m)	$4 \cdot 10^5$
Friction coefficient, μ	0.7
Granulated rubber particles	
Diameter of the disk (mm)	2.8
Density, ρ (kg/m^3)	1120
Normal stiffness, k_n (N/m)	$6 \cdot 10^4$
Tangent stiffness, k_s (N/m)	$3 \cdot 10^4$
Friction coefficient, μ	1.5
Sheet pile particles	
Young's modulus (Pa)	$3 \cdot 10^9$
Shear Modulus (Pa)	$1.7 \cdot 10^9$
Diameter of the disk (mm)	10
Density, ρ (kg/m^3)	1190
Normal stiffness, $\overline{k_n}$ (N/m)	$3 \cdot 10^{10}$
Tangent stiffness, $\overline{k_s}$ (N/m)	$1.7 \cdot 10^{10}$
Normal strength, $\overline{\sigma_c}$ (Pa)	$8 \cdot 10^7$
Wall-boundaries	
Normal stiffness, k_n (N/m)	$1.6 \cdot 10^6$
Tangent stiffness, k_s (N/m)	$8 \cdot 10^5$
Friction coefficient, μ	0.0

5.2.2 Loading Process

Four cases of sheet pile response under applied vertical load were simulated. The hydraulic jack with a circular bearing plate was represented using wall logic to replicate the loading process. Wall generate command was used to create the box. The box had a width of 26cm and a height of 5cm, which corresponded to the bearing plate diameter as in the experimental model. They generated in group 'load' in PFC2D. Figure 5.4 shows a schematic view of the DEM model in PFC2D.

In this study, we decided to apply vertical load using servo-mechanism with the desired force-contact to the walls ('load' in PFC2D). Walls were placed slightly above the soil level to avoid instability in force contact between the wall and the soil particles.

First, a velocity was applied to place the walls onto the soil surface. In the first simulation, the sheet pile started to bend under the mass of the soil. A function to control the fixity of the sheet pile was required. To do this, a FISH function is defined, and callback events are registered, and given in Appendix B. It means that the sheet pile particles were fixed until the loading process was started to prevent deflections.

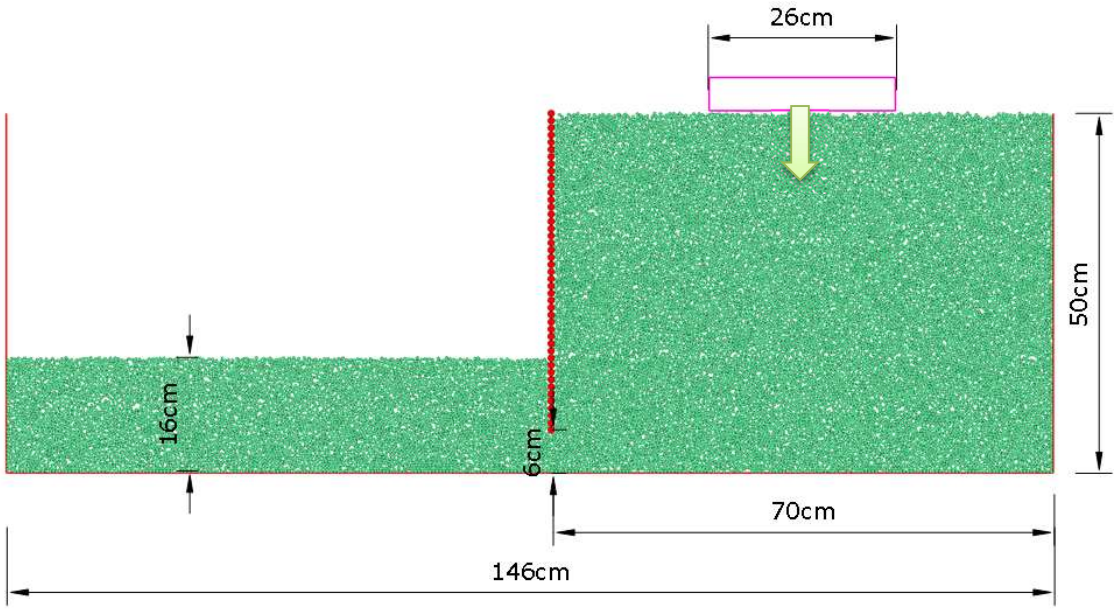

Figure 5.4. The schematic view of the DEM model in PFC2D

Since the bottom wall of the ‘load’ box made contact with the soil's surface, the pile fixity was modified, and the loading process began.

In the beginning, velocity to the ‘load’ box was assigned as 0.1m/ timestep. During the loading process, it was discovered that the initial assigned velocity of 0.15 m/ timestep was quite quick, resulting the force-contact between the bearing platen and the soil to achieve the target force before the sheet pile reached the desired horizontal displacement. More stable results were obtained at the velocity 0.05m/timestep.

Figure 5.5 represents horizontal displacements of the sheet pile at the various values of the applied load. It is obvious that at high values of the applied load velocity, the contact force reached the target force before the sheet pile had been deformed.

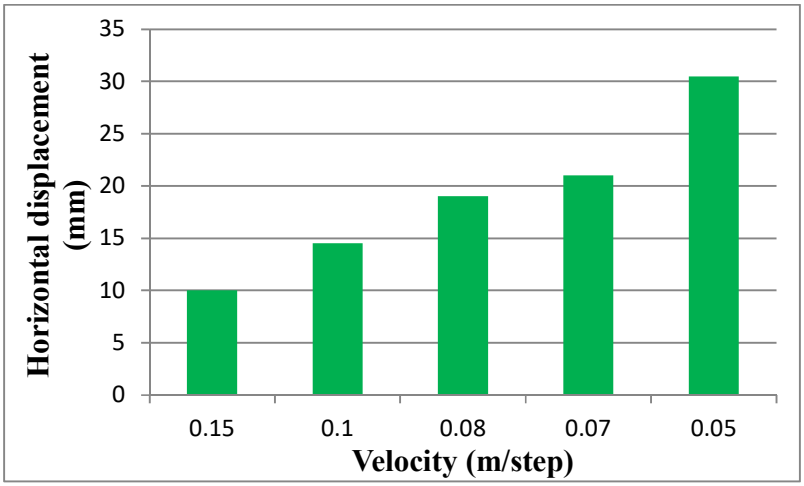

Figure 5.5. Horizontal displacement of the sheet pile at the different velocities of the applied load

5.2.3 Monitoring the loading stage

At the initial soil preparation part, the specimen's porosity was monitored using measure logic, which used a measuring circle (MC) placed into the backfill center. PFC documentation Itasca describes theoretical ideas concerning measurement logic in PFC2D and its limitations (2019). The location of the measurement circle is presented in Figure 5.6. The measurement circle is placed at the location of (1.11; 0.25), and its radius is 15cm.

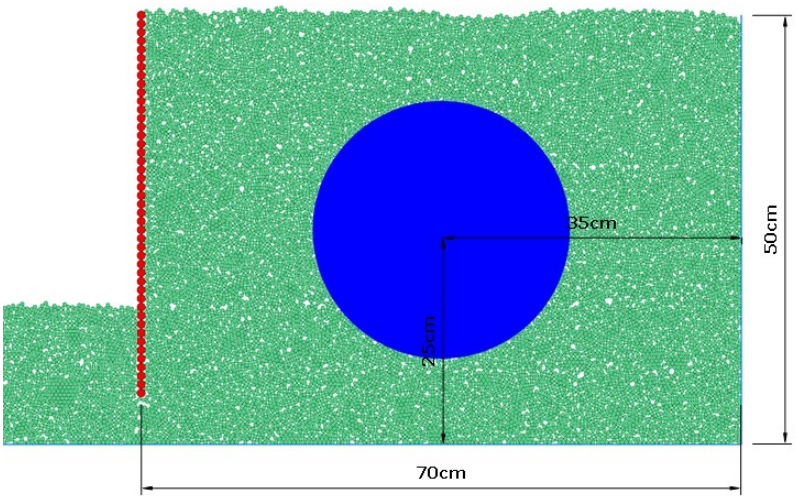

Figure 5.6. Measurement circle location

The soil sample behaved as dense soil at a porosity of n < 0.125, resulting in an early accomplishment of the target force before the target displacement of the sheet pile. The calibrated value of the n that assigned to the whole sample was 0.145. The calibrated porosity value corresponds to the system porosity (n=0.3, a medium soil state).

It was observed that the porosities of the DEM models were decreasing during the loading process, as shown in Figure 5.7. The initial porosity of the systems before loading is represented by the blue column. As recorded by the measuring circle, the porosity after the load application is shown in the green column.

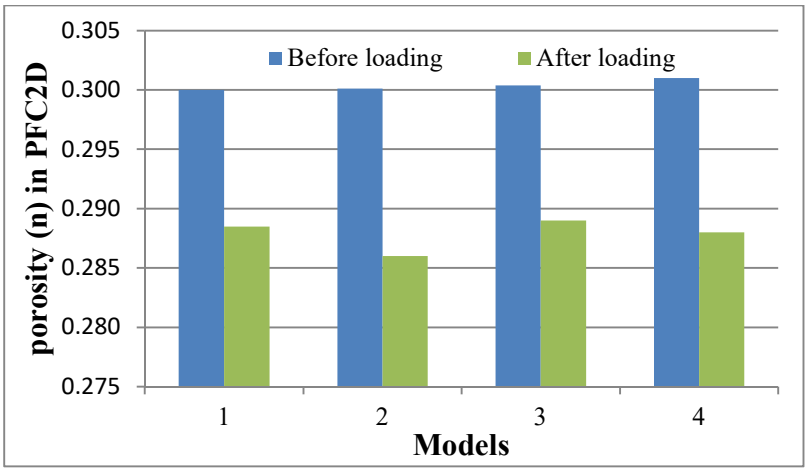

Figure 5.7. The porosity of the backfill before and after the loading process

At the loading stage, the lateral pressure on the sheet pile initially measured using the particles within the sheet pile, which was in contact with the soil, as shown in Figure 5.8. The horizontal pressure was recorded during DEM simulation.

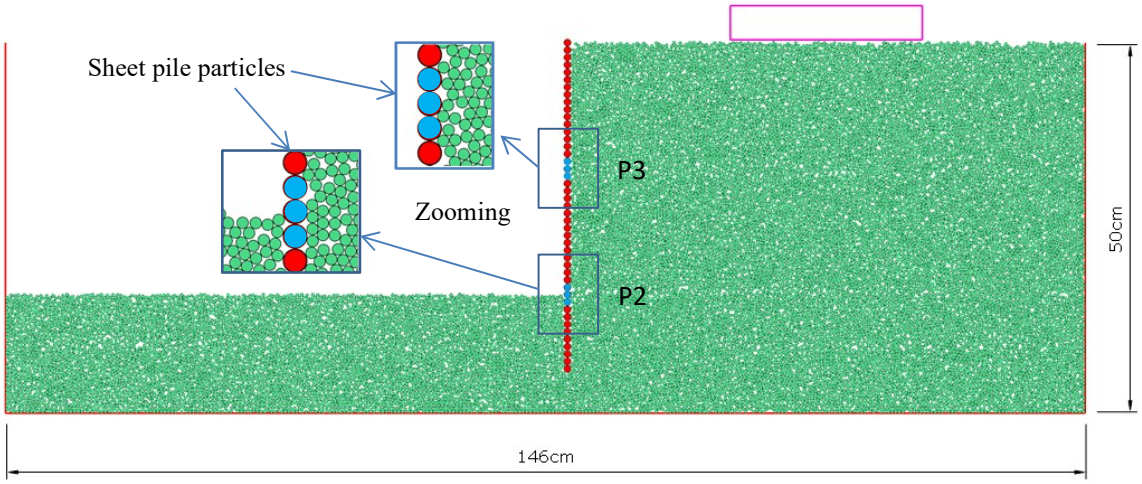

Figure 5.8. Lateral pressure measurement using measuring particles

The lateral pressure was calculated as the average of the pressures on each of the three particles generated by all the contacts acting on the balls using FISH functions. Contact force distribution within sheet pile particles was recorded during the tests. Figure 5.9(a) shows the values of the measured contact forces on the monitoring particles of the sheet pile, when the model is at rest (immediately after backfilling soil in the box) condition. Figure 5.9(b) shows the values of the measured contact forces on the monitoring particles of the sheet pile, when the model is under the vertical load.

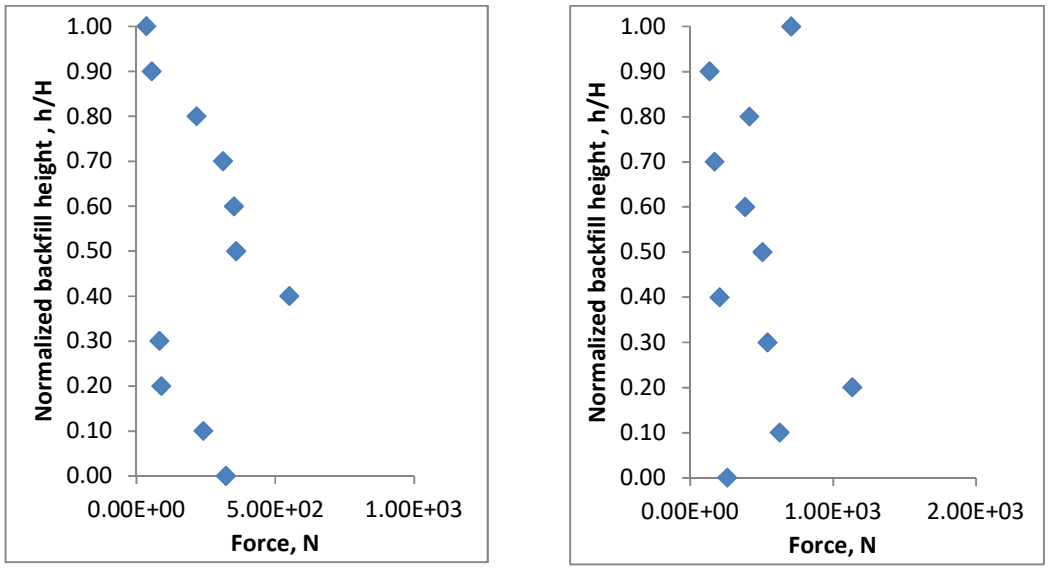

(a) At rest condition (b) During loading

Figure 5.9. Force-contact recorded by measuring particles at rest and during loading process

It is obvious that the contact forces recorded by measuring particles have no reasonable pattern and that the forces are distributed randomly. This behavior is because the sheet pile particles are not all well-connected to soil particles during backfill soil preparation and during the loading process, as we can see in Figure 5.10.

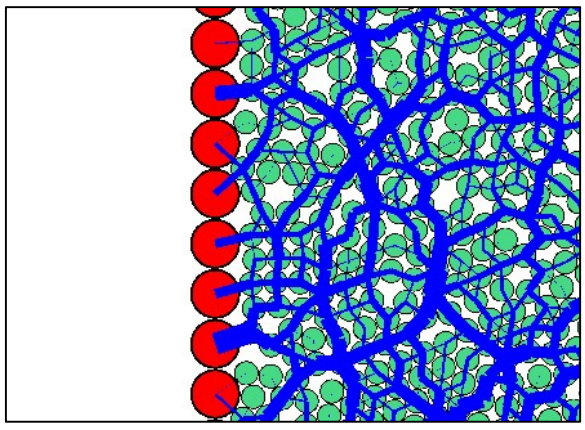

Figure 5.10. Contact forces between sheet pile and soil particles

As a result, monitoring lateral pressure using specified particles of the sheet pile will not provide accurate results.

To overcome this issue, measurement circles with a radius of 1cm were placed at the specified location, as shown in Figure 5.10. According to (Yang and Deng, 2019), measurement circles could be used to measure lateral pressure in the DEM model. During loading, the measuring circles moved as the sheet pile was deformed. The FISH function was required to implement this process.

Each of these measuring circles acts as a pressure cell in which the lateral pressure acting in all the balls inside the measuring circle is recorded, as presented in Figure 5.11. To measure lateral pressure inside the measurement circle, average stress-xx was used. The average stress σ_{xx} in a volume V measuring region is calculated as follows (Christoffersen et al., 1981):

$$\overline{\sigma_{xx}} = -\frac{1}{V}\sum_{N_c} F^{(c)} L^{(c)} \tag{5.2}$$

where N_c is the number of the contacts inside the measurement circle, $F^{(c)}$ is the contact vector, and the branch vector $L^{(c)}$ connects the centroids of the two balls in contact.

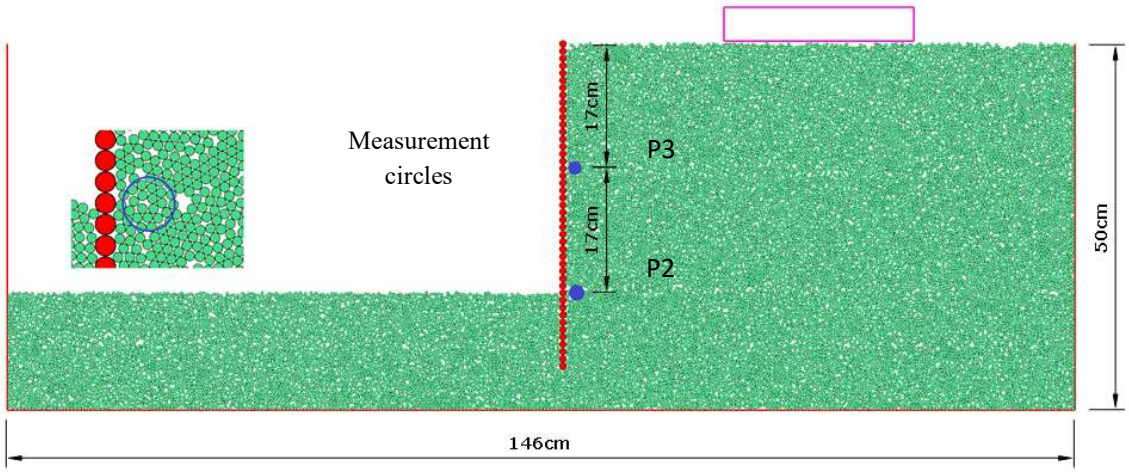

Figure 5.11. Measure circles location

Measuring the lateral pressure using measure particles indicates low lateral pressure values at the beginning of the loading process, according to the results from the first model's loading stage. Because the sheet pile began to bend at the beginning of the loading phase, causing a break in contact with the soil particles, as shown in Figure 5.12 between $0.73x10^5$ and $0.78x10^5$ step.

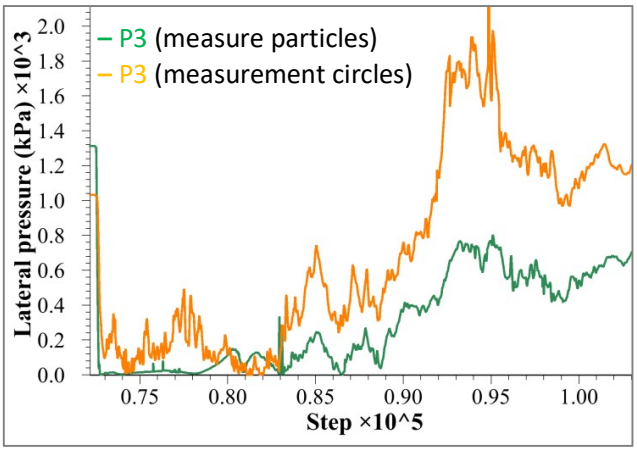

Figure 5.12. Lateral pressure data (P3) recorded from the first model dry condition

Therefore, it was decided to implement measurement logic as a monitoring tool, which involved measurement circles. The final sheet pile displacement monitoring was conducted using horizontal displacement of the top ball of the sheet pile using FISH functions.

5.3 Comparison of the DEM model and physical model

The lateral pressures-displacement curves were obtained from DEM simulations, and the Model results have been compared to the experimental model observations and results.

Contact properties with sheet pile, loading process velocity, and particle sizes were all calibrated in a series of numeric experiments in PFC2D. Two simulation models were calibrated first, and afterward the calibrated parameters were applied to the remaining two models.

5.3.1 First Model – Clean Sand Backfill Model

The final state of the loading process in the dry clean sand model is shown in Figure 5.13, which includes the particle displacement distribution. The particle displacement distribution shows the area that is affected by the applied force.

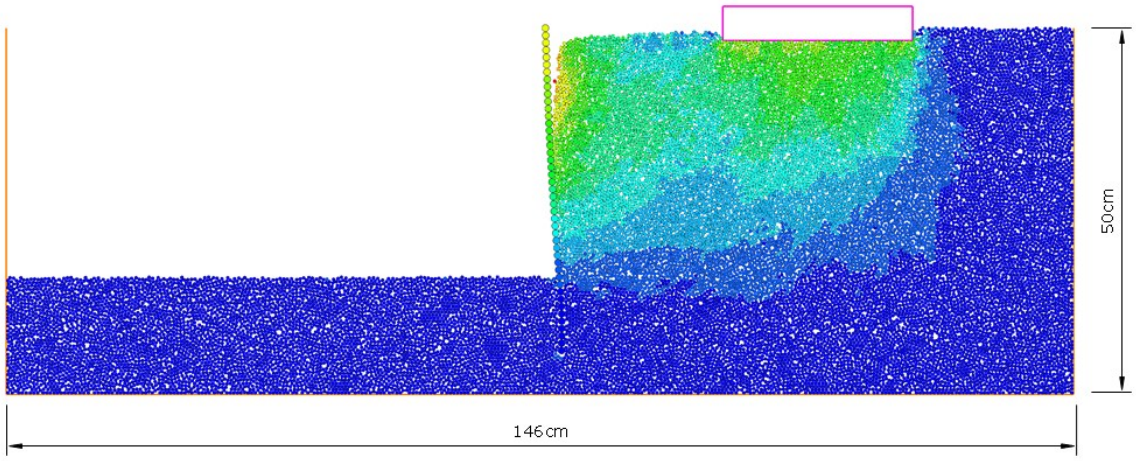

Figure 5.13. The particle displacement distribution of the First Model in PFC2D

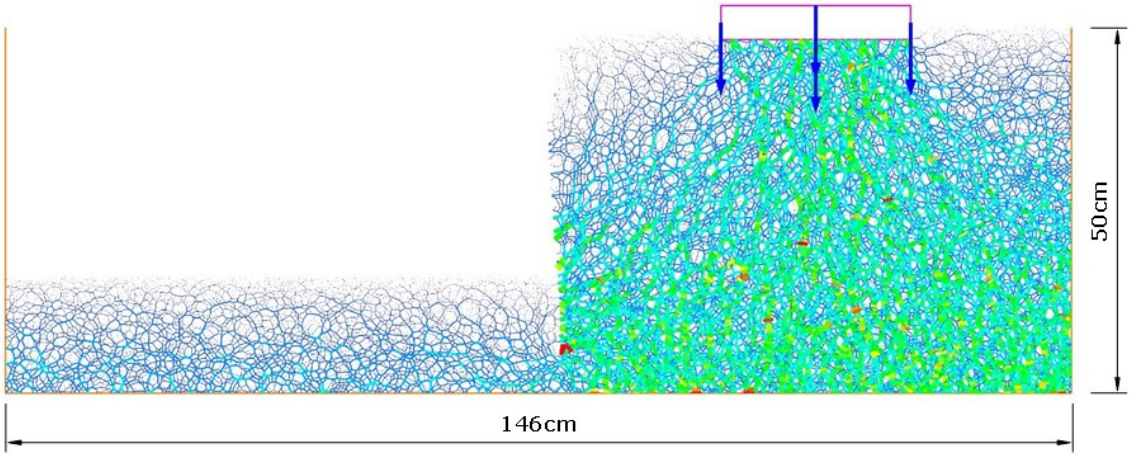

Figure 5.14. Force chains within the soil particles of the First Model

Figure 5.14 depicts the force chains that arise within the soil particles. The force chains are colored according to the value of the contact force. The contact force is immediately under bearing plate and is distributed throughout the backfill. Also, we can observe the intensity of the forces at the base of the model, which shows increase in stress.

Figure 5.15 represents the comparison of the results of the load cell recorded during a laboratory experiment and DEM simulation. As indicated in the figure, a peak implies soil failure until the maximum applied pressure of 33kPa is reached.

The sheet pile bent up to 1 cm under vertical load and soil mass, while the applied force only increased until 12.34 and slightly increased to 14.05kPa. At the maximum load of 171kg, the sheet pile horizontal deformation was 30.5mm; on the other hand in the laboratory experiment, the maximum horizontal displacement was 32.5cm under the vertical load of 133kg.

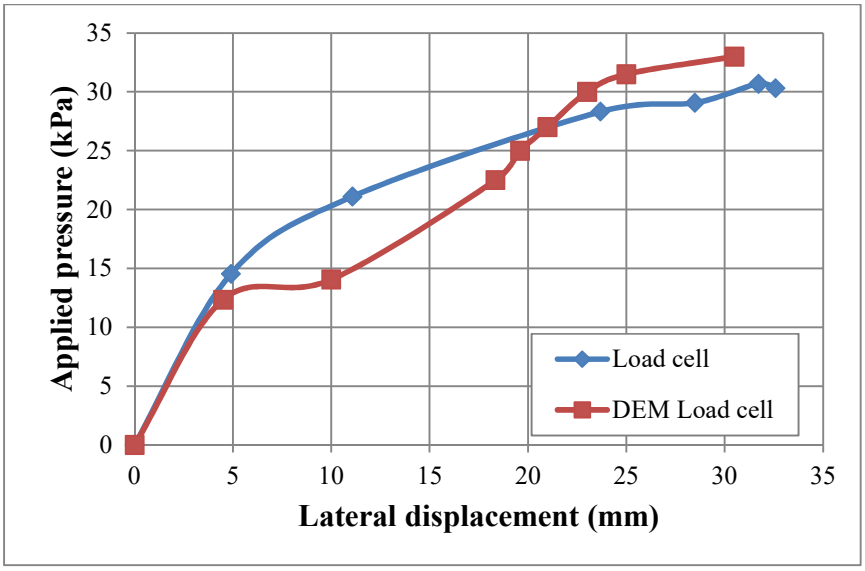

Figure 5.15. Applied pressure development with the lateral displacement in the first model

According to Figure 5.16, the initial displacement of the sheet pile to 1 cm caused a reduction in the force contact between the particles, leading to decline in the level of lateral pressure (P2) and (P3). After that, both (P2) and (P3) began to increase. Peak lateral pressure at (P2) was at the lateral displacement of 17mm, which occurred later than in the

laboratory experiment. The peak lateral pressure of 2.64kPa at (P2) of numeric model was the same as in the experimental model. At (P3), the peak lateral pressure was 2.71kPa, which was bigger by 24% from the experimental value.

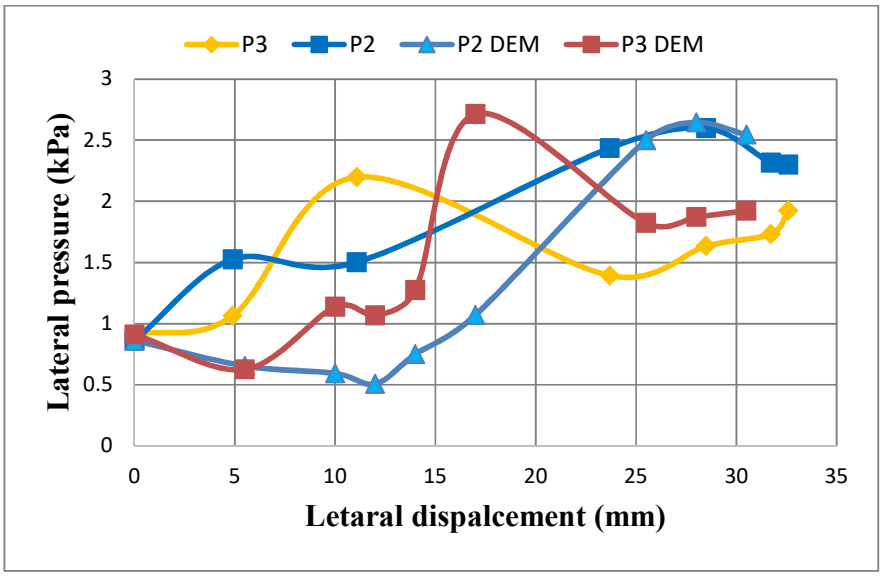

Figure 5.16. Lateral pressure development with the lateral displacement in the first model

5.3.2 Second Model

A numerical model with reinforced backfilling with fine-grained rubber was examined in PFC2D, following the model with clean sand. Figure 5.17 shows the final state of the loading process of the second model, where the particle displacement distribution is represented.

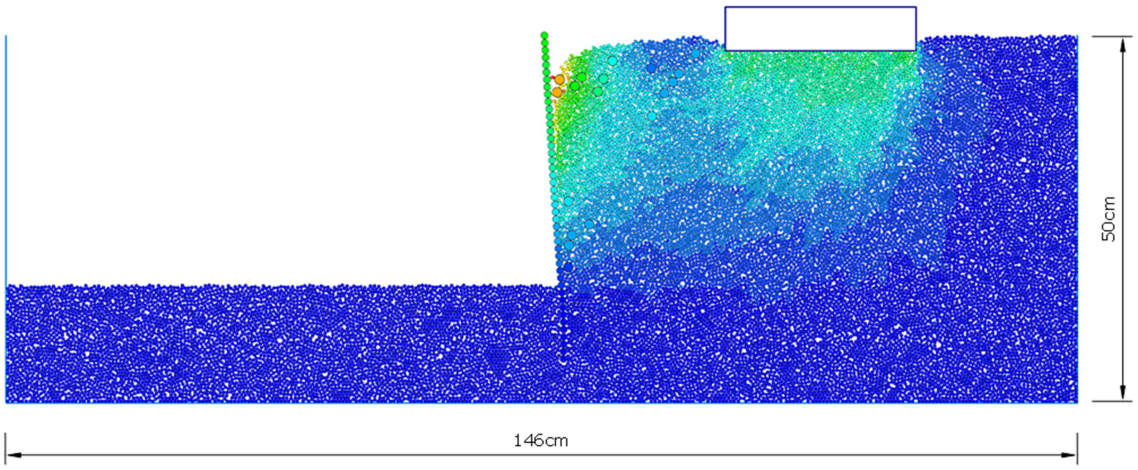

Figure 5. 17. The particles displacement distribution of the Second Model in PFC2D

The force chains that arise within the soil particles under vertical load are illustrated in Figure 5.18. The thickness and the color of the force chains show the intensity of the forces within soil particles. The force chain intensity is growing directly behind the sheet pile, near the base.

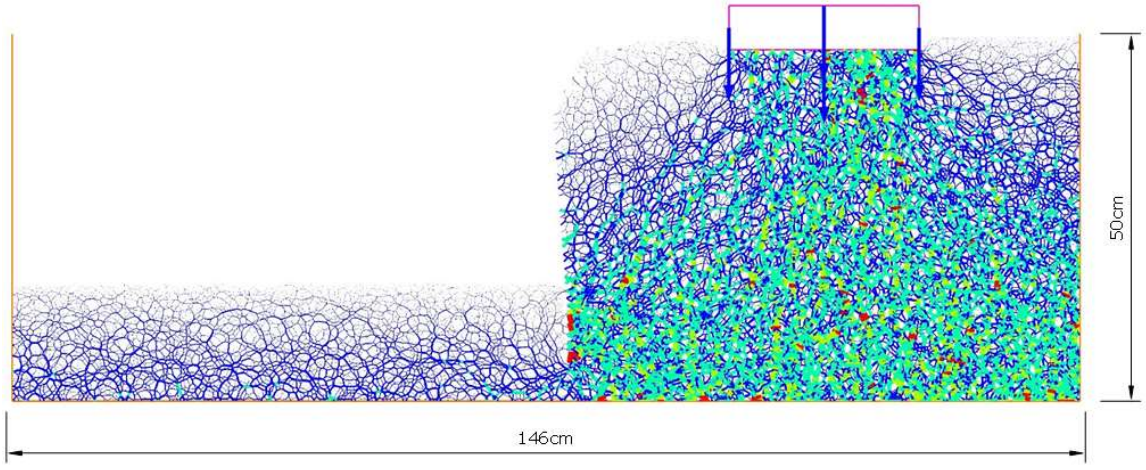

Figure 5. 18. Force chains within the soil particles of the Second Model

The comparisons of the histories of the applied pressure against the lateral displacement in the sheet pile are shown in Figure 5.19. There were two peaks at 10.95kPa and 19.74kPa before the maximum loading level of 29.19kPa. The maximum applied load

of 155kg was indicated in DEM simulation, close to the maximum applied of 154.2kg in the experimental model.

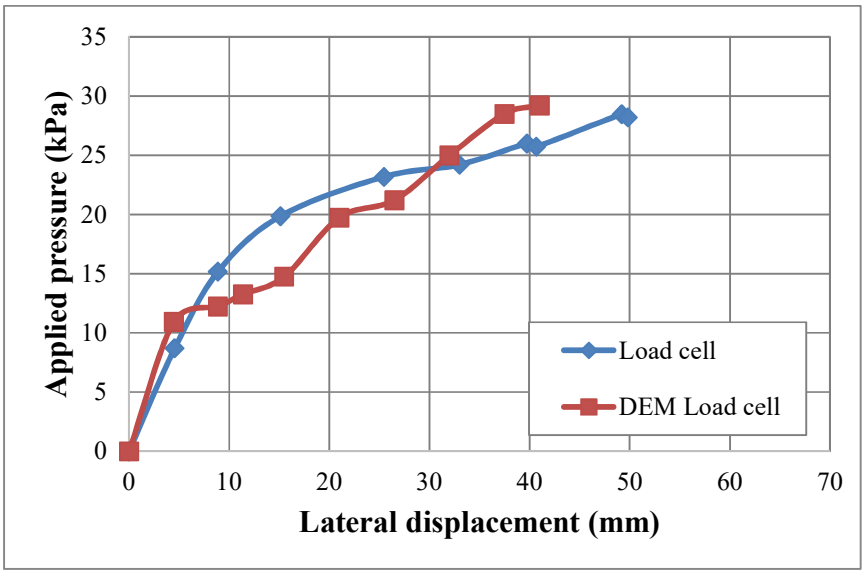

Figure 5.19. Applied pressure development with the lateral displacement in the second model

The results of the lateral pressures at (P2) and (P3) were compared with the results from laboratory experiments, which are represented in Figure 5.20. The maximum pressure (P2) of numeric model was 1kPa at 41mm displacement. The peak value of the lateral pressure of (P3) was 0.7kPa at 37.5mm displacement. At the first 10mm displacement of the sheet pile the lateral pressure levels at both (P2) and (P3) were decreasing. The pressure level at (P3) reached minimum values between the applied pressures of 19.74 and 21.21kPa. At (P2) pressure level, an uptrend was noticed after reaching 21.21kPa. The increase in pressure at (P3) is detected after reaching 25kPa applied pressure.

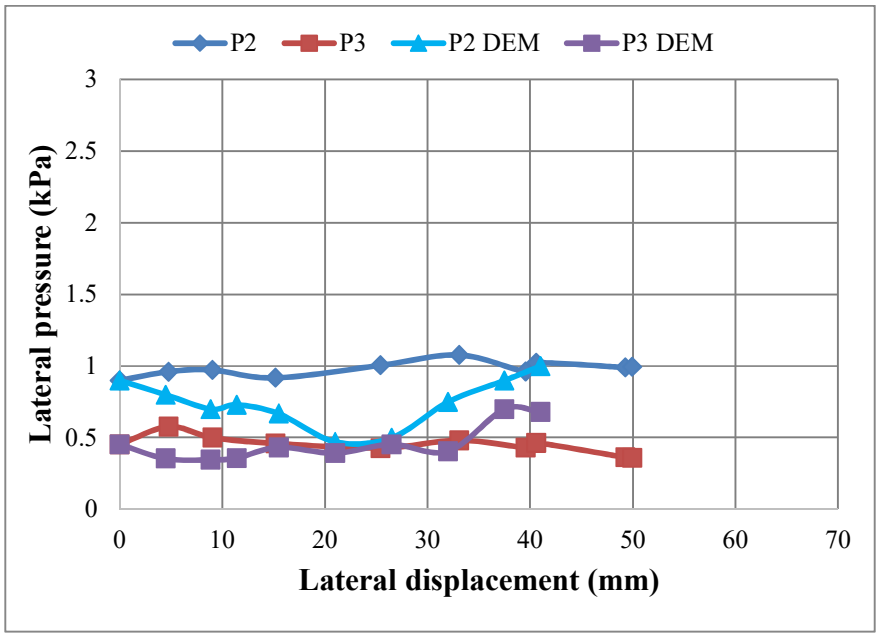

Figure 5.20. Lateral pressure development with the lateral displacement in the second model

5.3.3 Third Model

The simulation of the third model has been performed in PFC2D. The backfill was reinforced with a sand-rubber mix that was placed inside the 32cm base and 30cm height triangular area. The particle displacement distribution obtained as a result of the loading process is shown in Figure 5.21.

Figure 5.22 illustrates the distribution of the contact forces within the soil particles under vertical loading. As shown in previous DEM models, we can observe the analogous intensity of the force chains at the base.

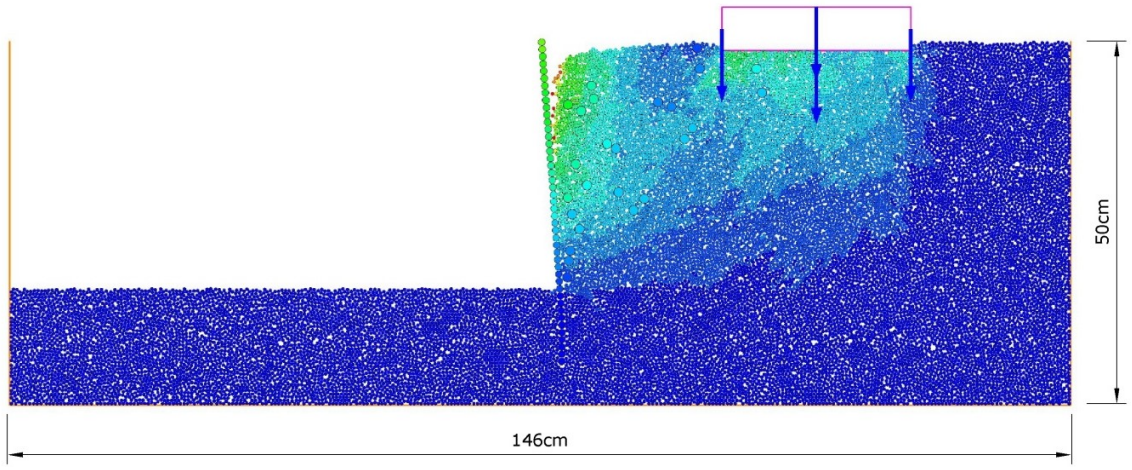

Figure 5.21. The particles displacement distribution of the Third Model in PFC2D

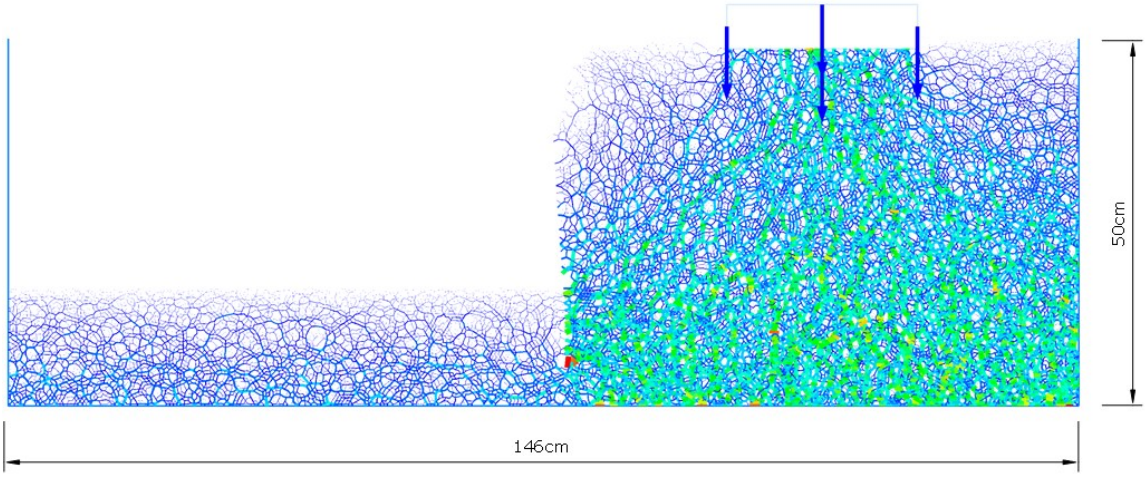

Figure 5. 22. Force chains within the soil particles of the Third Model

Recorded applied load history of the DEM model was compared with the results of the experimental model. Figure 5.23 shows histories of applied pressures against lateral displacement of the sheet pile of both DEM and experimental models. The maximum applied load in DEM simulation was 145kg, and the maximum sheet pile displacement was 55.5mm. Compared with experimental model results, in which the maximum applied load was 139.98kg at 64.8mm, the results from DEM simulation were higher.

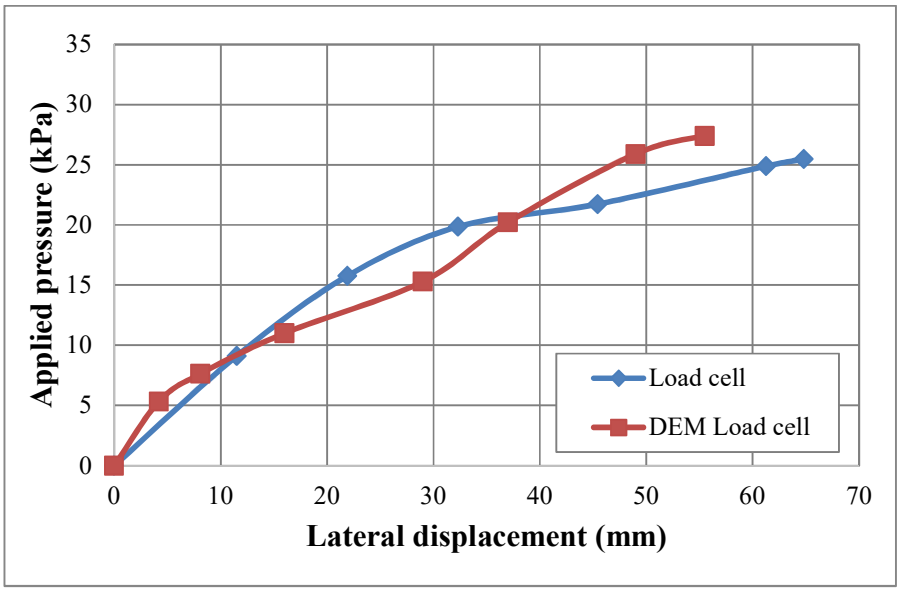

Figure 5.23. Applied pressure development with the lateral displacement in the third model

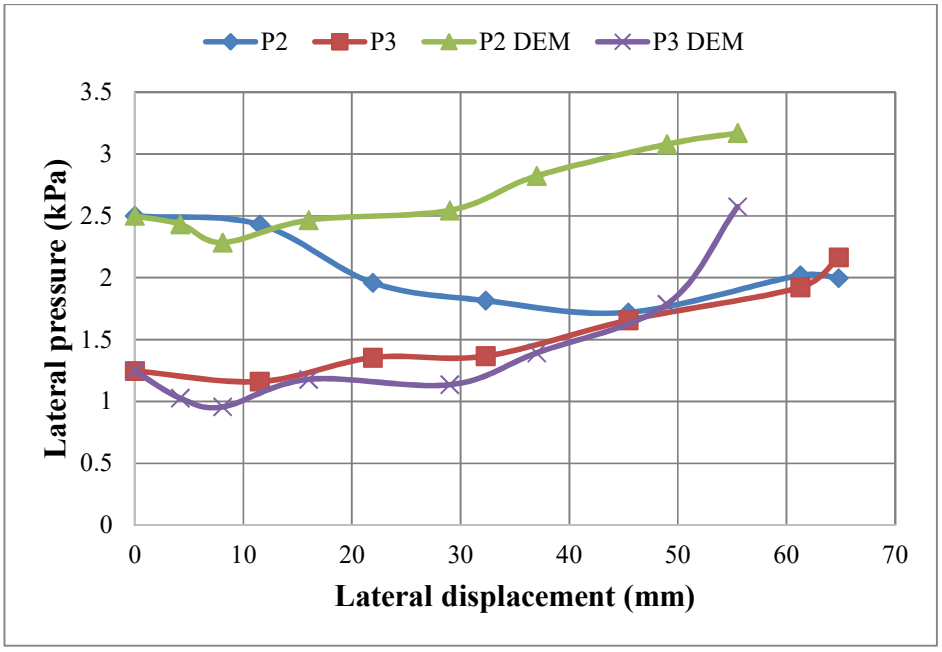

Figure 5.24. Lateral pressure development with the lateral displacement in the third model

Figure 5.24 compares the pressure-displacement curves of the DEM simulations and the experimental model. Initial displacement of the sheet pile of 8.1mm until reaching 7.64kPa applied pressure led to the breakage of the contact forces between sheet pile and

soil particles; the lateral pressure at (P2) met its minimum. The sheet pile moved. The soil began to reform, forcing the pressure to rise, as seen at (P2) and (P3).

5.3.4 Fourth Model

The backfill was reinforced with a sand-rubber mixture that was placed inside the 48cm base and 30cm height triangle region in the fourth model, which was simulated in PFC2D. The final state of the fourth numeric model is represented in Figure 5.25. The analysis of the sheet pile deformation under applied load has been done, and the results are shown below.

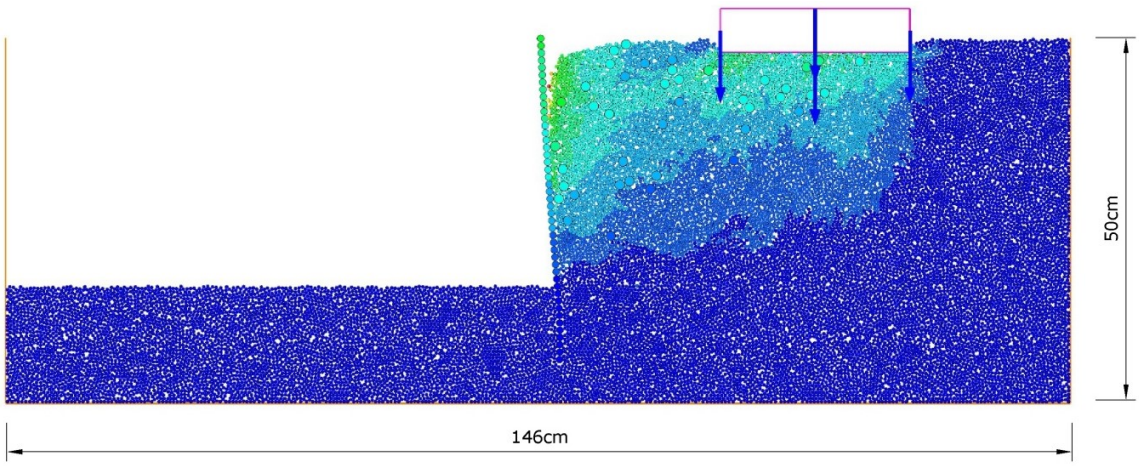

Figure 5. 25. The particles displacement distribution of the Fourth Model in PFC2D

As shown in Figure 5.26 we can observe the force distribution within the soil particles affected by the applied load. Furthermore, the DEM model can detect the contact between the sheet pile and the soil particles at the end of the loading process.

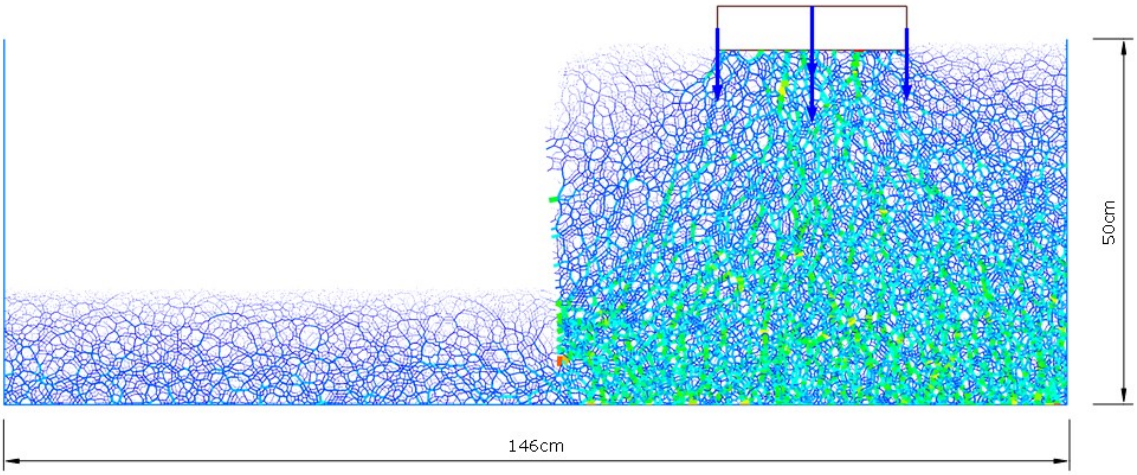

Figure 5. 26. Force chains within particles of the Fourth Model

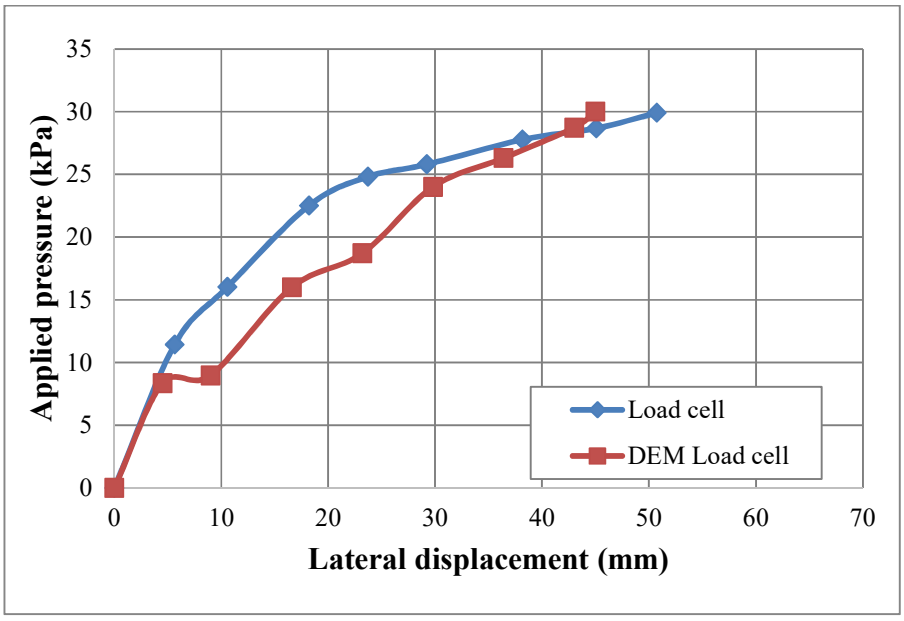

Figure 5.27. Applied pressure development with the lateral displacement in the fourth model

Figure 5.27 represents the recorded values of applied pressure of DEM simulation and experimental model. When applied load reached 8.34kPa sheet pile head started to decline and reached 4.5mm. Until 9mm of sheet pile head displacement the applied pressure stayed constant. During this period soil mass started to fall onto the sheet pile

surface. Following increase in pressure at (P2) and (P3) between 5mm and 15 mm of lateral displacement showed this response in numeric model.

The maximum applied load in the fourth model in PFC2D was 160.1kg; meanwhile, the maximum applied load in the laboratory experiment was 163kg. However, the maximum displacement of the sheet pile in the numeric model was 45mm, which is less than in the experimental model (maximum horizontal displacement was 50.7mm). The fourth model sheet pile showed analogous behavior at the beginning of the loading stage, where the first failure occurred at the applied load of 47.6kg.

Figure 5.28 compares the lateral displacement against the lateral pressure of the DEM simulations and the experimental model. The lateral pressure at the depth of 17cm below the soil surface at the displacement 4.5mm reached its minimum of 1.166kPa. Then it started to increase, reaching a maximum value of 1.79kPa. The lateral pressure at the depth of 34cm had a peak of 1.54kPa at the 9mm displacement, decreased until 0.872kPa at the 29.8mm, and started to increase again.

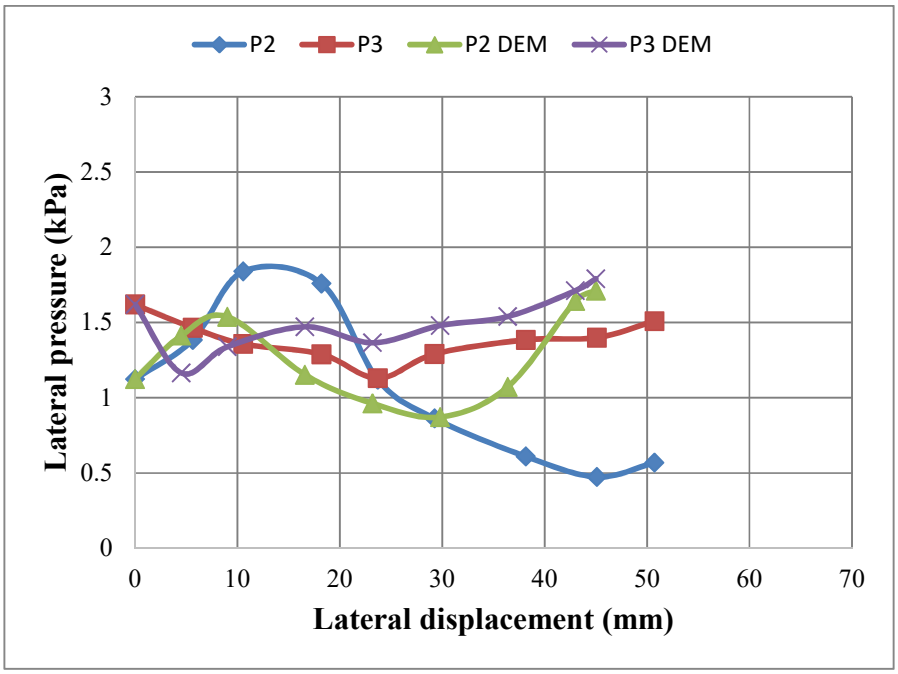

Figure 5.28. Lateral pressure development with the lateral displacement in the fourth model

CHAPTER 6

CONCLUSION

The purpose of this study was to understand more about how clean sand and a sand-rubber mixture behave in backfill when vertical loads are applied. Accordingly, the DEM software Particle Flow Code 2-Dimensional is used to model experimental tests in the DEM environment (ITASCA, 2019).

First, the experimental direct shear test was used to determine the strength and stress-strain properties of the two types of soil. The laboratory studies employed clean sand and sand mixed with 10% granulated rubber as soil samples (Khlaif, 2021). Hence, numerical model of direct shear test has been done to calibrate the micromechanical parameters of the granular materials, such as sand and rubber particles. The particle sizes, density, interparticle friction coefficient, and contact stiffness of the sand and rubber discrete elements were determined. The unique set of the micromechanical properties which correspond to macromechanical strength parameters have been obtained. Based on the DEM model of the direct shear test, the inclusion of granulated rubber improved the shear strength of sand by 5.5%, while in the laboratory experiment it was 3.6%.

Then, calibrated microparameters were used for the DEM simulation of sheet pile foundation. The numeric model of the sheet pile foundation with the 10% fine granulated rubber-sand mix backfilling in dry condition were performed in PFC2D environment. During the calibration process, we observed that loading process speed, contact stiffnesses, and porosity of the system had a significant impact on the deformation parameters of the sheet pile and lateral pressure distribution of the granulated rubber-sand mix backfill. Previous papers suggested various measurement methods. In this study two measurement methods were investigated. In the first approach, the measuring particles of the sheet pile were taken into account, whereas in the second, the measuring circles were placed behind the sheet pile foundation. The measurement circles proposed by (ITASCA, 2019) were considered suitable for the DEM model.

Figure 6.1 shows the results from the numerical model of the sheet pile foundation with the 10% fine granulated rubber-sand mix backfilling under vertical loading. Model 1

curve in the Figure 6.1 represents the results obtained from the numerical model with clean sand backfilling. Model 2 to 4 are the models with different filling zones made of sand-rubber mixture. Model 2 load-displacement curve showed similar response as in the third model under the vertical loading. The vertical load is applied to the initial soil and then distributed throughout the mixture in the second model, decreasing the lateral pressure on the sheet pile. Among the soil models studied, Model 3 demonstrated the weakest response. Since the vertical load was applied to the weakest zone between the backfill and the initial soil. Model 4 represents the fourth model with the largest volume of the sand-rubber mixture (48cm base and 30cm height triangle region), showed that a large lateral displacement obtained under lower force. Under active loading upper part of the sheet pile foundation showed good results in DEM models. On the other hand, the lower part did not show the predicted deformations. Additionally, due to the uniform particle of the DEM model, lesser density from the experimental model was observed. All this phenomena led to a decrease in the intensity of stresses in the lower part. As can be shown in Chapter 5, the complexity in modelling sheet piles resulted in a difference between DEM and the results of laboratory experiments.

Numerical results from DEM simulations showed a relative agreement with the results of the physical model. Finally, the ability of the PFC2D code as a discrete element approach in modelling of cohesionless granular material and sheet pile foundation provided with insights into contact force and stress distribution under vertical loads.

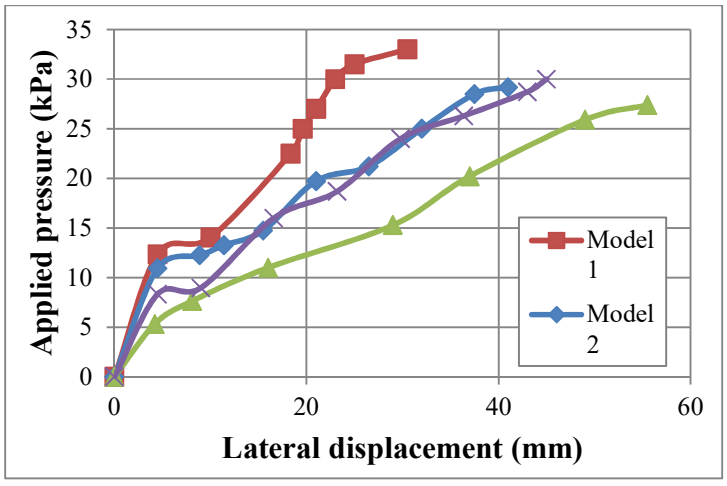

Figure 6.1. Applied load with the lateral displacement in dry soil models

6.1 Recommendations for Future Research

Since nobody studied the micro interaction between the soil and the sheet pile foundation under static vertical load. At the present work the sheet pile foundation was modelled as bounded circular disks to investigate the force-displacement response at active vertical loading. However, there are still some issues related to the sheet pile foundation modelling.

Overall, the sheet pile simulation could represent force-displacement behavior of actual model. Under active loading upper part of the sheet pile foundation showed good results in DEM models. On other hand, lower part didn't show predicted deformations.

Additional study employing the ITASCA PFC2D software is required:

1. Implementation of clump logic in the soil and rubber chip particle generation
2. Random distribution of soil particles by size in specimen generation stage
3. Different methods of sheet pile modelling
4. Complex parametric studies of sand and rubber chips particles in DEM simulations
5. Simulations of the sheet pile foundation with sand-rubber mixture backfilling in saturated condition
6. Simulations of the sheet pile foundation with sand-rubber mixture backfilling in three-dimensional environment by PFC3D
7. Comparison of the results of the DEM model in PFC3D with the results of the model in PFC2D.

REFERENCES

Achmus M., Abdel-Rahman K. (2002).”The influence of “up-scaling” on the results of particle method calculations of non-cohesive soils”. Numerical Modeling in Micromechanics via Particle Methods, 183-187.

Asadi, M., Mahboubi, A., Thoeni, K., (2018). “Discrete modeling of sand–tire mixture considering grain-scale deformability”. Granular Matter, 20(2).

Aksenov V.V., Lavrikov S.V., Revuzhenko A.F., (2014). “Numerical modeling of deformation processes in rock pillars”. Applied Mechanics and Materials, vol. 682, 203–205.

Ashmawy A., McDonald R., Carreon D., Atalay F., (2006). “Stabilization of Marginal Soils using Recycled Materials”. Final Report, Florida Department of Transportation.

Bagi, K. (2005). “An algorithm to generate random dense arrangements for discrete element simulations of granular assemblies”. Granular Matter, 7(1), 31–43.

Bathe, K. J., Wilson, E. L., (1976). “Numerical Methods in Finite Element Analysis”. Englewood Cliffs: Prentice-Hall.

Bosscher P.J., Edil T.B., and Eldin N., (1993). “Construction and Performance of Shredded Waste Tire Test Embankment. Transportation Research”. no. 1345, Transport Research Board, Washington, D.C., 44–52.

Bosscher, P.J., Edġl., T.B., Kuraoka, S. (1997). “Design of Highway Embankments Using Tire Chips”. Journal of Geotechnical and Geoenvironmental Engineering, ASCE, 123 (4), 295-304.

Calvetti. F. (2003). “Limitations and perspectives of the micromechanical modelling of granular materials”. Mathematical and Computer Modelling 37,485-495.

Cao W., (2007). “Study on properties of recycled tire rubber modified asphalt mixtures using dry process”. Construction and Building Materials, 21, 1011–1015.

Cao, P., Zhong, Y. F., Li, Y. J., Liu, J. (2014). “Investigations on Direct Shear Tests and PFC2D Numerical Simulations of Rock-Like Materials with a Hole and Prefabricated Cracks”. Key Engineering Materials, 627, 477–480.

Chang N. B., (2008). “Economic and policy instrument analyses in support of the scrap tire recycling program in Taiwan”. Journal of Environmental Management, 86, 435–450.

Chen, Y., Deng, A., Wang, A., Sun, H., (2018). “Performance of screw–shaft pile in sand: Model test and DEM simulation”. Computers and Geotechnics, 104, 118–130.

Cheung, Geraldine, and O'Sullivan C., (2008). “Effective simulation of flexible lateral boundaries in two-and three-dimensional DEM simulations”. Particuology 6 (6), 483-500.

Christoffersen, J., Mehrabadi M. M., Nemat-Nasser S., (1981). “A micromechanical description of granular material behavior”. J. Appl. Mech., 48, 339-344.

Coetzee, C. J., and Els, D. N. J. (2009). “Calibration of granular material parameters for DEM modelling and numerical verification by blade–granular material interaction”. Journal of Terramechanics, 46(1), 15–26.

Corriveau, D., Savage, S.B., Oger, L. (1997). “Internal Friction Angles: Characterization Using Biaxial Test Simulations”. IUTAM Symposium on Mechanics of Granular and Porous Materials. Solid Mechanics and its Applications, vol 53, 313-324

Cui, L., O'Sullivan C., (2006). “Exploring the macro- and micro-scale response of an idealised granular material in the direct shear apparatus”. Geotechnique. 56. 455-468.

Cui, L., O'Sullivan C., and O'Neill S. (2007). “An analysis of the triaxial apparatus using a mixed boundary three-dimensional discrete element model”. Geotechnique 57 (10), 831-844.

Cundall, P.A. (1971). “A Computer Model for Simulating Progressive Large Scale Movements in Blocky Rock Systems.” Proceedings of the Symposium of the International Society for Rock Mechanics, Society for Rock Mechanics (ISRM), France, II-8.

Cundall, P. A. (1974). “Rational Design of Tunnel Supports (A Computer Model for Rock Mass Behavior Using Interactive Graphics for the Input and Output of Geometrical Data).” Technical Report MRD-2-74, Missouri River division, U. S. Army Corps of Engineers.

Cundall, P. A. (1978). “BALL–A Program to Model Granular media Using the Distinct Element Method”. London, United Kingdom: Dames & Moore. Advanced Technology Group". Technical Note No. TN-LN.

Cundall, P.A., and Strack, O.D.L. (1979). “Discrete numerical model for granular assemblies”. Ge´otechnique, 29: 47–65.

Demir, T. (2020). “Araç lastiklerinin geri dönüşümü üzerine bir derleme”.

Eidgahee, D. R., Hosseininia, E. S. (2013). “Mechanical behavior modeling of sand-rubber chips mixtures using discrete element method (DEM)”.

Forrest, M. (2014). “Recycling and Re-use of Waste Rubber”.

Fukumoto, Y., Yang, H., Hosoyamada, T., Ohtsuka, S. (2021). “2-D coupled fluid-particle numerical analysis of seepage failure of saturated granular soils around an embedded sheet pile with no macroscopic assumptions”. Computers and Geotechnics, 136, 104234.

Gong, H., Song, W., Huang, B., Shu, X., Han, B., Wu, H., & Zou, J. (2019). “Direct shear properties of railway ballast mixed with tire derived aggregates: Experimental and numerical investigations”. Construction and Building Materials, 200, 465–473.

Gotteland, P., Lambert, S., Salot, Ch. (2008). “Investigating the strength characteristics of tyre chips - Sand mixtures for geo-cellular structure engineering”. 351-361.

Han, J., Bhandari, A., and Wang, F. (2012). “DEM Analysis of Stresses and Deformations of Geogrid-Reinforced Embankments over Piles”. International Journal of Geomechanics, 12(4), 340–350.

Hong Y., Yang Z. and Orense R. P. (2015). “Investigation of Sand-Tire Mixtures as Liquefaction Remedial Measure”. Proceedings of the 10th Pacific Conference on Earthquake Engineering Building an Earthquake-Resilient. Sydney, Australia, 1-8.

ECOsight. (n.d.). Tire Waste & Recycling. http://www.ecosight.com/tire-waste-and-recycling

Indraratna, B., Qi, Y., Ngo, T., Rujikiatkamjorn, C., Neville, T., Ferreira, F., and Shahkolahi, A. (2019). “Use of Geogrids and Recycled Rubber in Railroad Infrastructure for Enhanced Performance”. Geosciences, 9(1), 30.

Itasca. (2019). User's manual for PFC3D. In. Minneapolis, USA: Itasca Consulting Group, Inc.

Jamshidi, R., Towhata, I., Ghiassian, H., and Tabarsa, A. R. (2010). "Experimental evaluation of dynamic deformation characteristics of sheet pile retaining walls with fiber reinforced backfill". Soil Dynamics and Earthquake Engineering, 30(6), 438–446.

Jeong, S.W., Kighuta, K.,Lee, D.E., Park, S.S. (2021). "Numerical Analysis of Shear and Particle Crushing Characteristics in Ring Shear System Using the PFC2D". Materials, 14, 229.

Jiang, M. J., Konrad, J. M., and Leroueil, S. (2003). "An efficient technique for generating homogeneous specimens for DEM studies". Computers and Geotechnics, 30(7), 579–597.

Kruyt, N. P. (1993). "Towards micro-mechanical constitutive re-lations for granular materials". Proc. Modern approaches to Plasticity. Balkema, 147-178.

Khlaif, A. H., (2021). "Experimental study of sheet pile retaining walls with granulated rubber reinforced backfill". Master's Thesis, İzmir Institute Of Technology.

Khosravi, M., Hamedi Azad, F., Bahaaddini, M., Pipatpongsa, T., (2017). "DEM Analysis of Backfilled Walls Subjected to Active Translation Mode". International Journal of Mining and Geo-Engineering, 51(2), 191-197.

Lee S. J., Akisetty C. K., Amirkhanian S. N., (2008). "Recycling of laboratory-prepared long-term aged binders containing crumb rubber modifier", Construction and Building Materials, 22, 1906–1913.

Liang, J., Mourelatos, Z. P., Tu, J. (2004). “A Single-Loop Method for Reliability-Based Design Optimization”. Volume 1: 30th Design Automation Conference.

Lo Presti, D., (2013). “Recycled Tyre Rubber Modified Bitumens for road asphalt mixtures: A literature review”. Construction and Building Materials, 49, 863–881.

Lobo-Guerrero, S., and Vallejo, L. E. (2005). “Discrete Element Method Evaluation of Granular Crushing Under Direct Shear Test Conditions”. Journal of Geotechnical and Geoenvironmental Engineering, 131(10), 1295–1300.

Lu, Y., Frost, D., (2010). “Three-Dimensional DEM Modeling of Triaxial Compression of Sands”. Soil Behavior and Geo-Micromechanics.

Mashiri, M.S., Vinod, J.S., Sheikh, M.N., Tsang, H.-H. (2015). “Shear strength and dilatancy behaviour of sand–tyre chip mixtures”. Soils Found. 55, 517–528.

Mindlin, R. D., and Deresiewicz, H., (1953). “Elastic Spheres in Contact Under Varying Oblique Forces.” ASME. J. Appl. Mech. 20(3), 327–344.

Nadukuru, S. S., Michalowski, R. L. (2012). “Arching in Distribution of Active Load on Retaining Walls”. Journal of Geotechnical and Geoenvironmental Engineering, 138(5), 575–584.

Nadukuru, S., Michalowski, R. (2012). “Arching in distribution of active load on retaining walls”. Journal of Geotechnical and Geoenvironmental Engineering, 138(5), 575-84.

Noonan, D. K. J., Nixon, J. F. (1972). “The Determination of Young’s Modulus from the Direct Shear Test”. Canadian Geotechnical Journal, 9(4), 504–507.

O'Sullivan, C. (2011). "Particle-Based Discrete Element Modeling: Geomechanics Perspective". International Journal of Geomechanics, 11(6), 449–464.

Oetomo, J. J., Vincens, E., Dedecker, F., and Morel, J.-C. (2015). "Modeling the 2D behavior of dry-stone retaining walls by a fully discrete element method". International Journal for Numerical and Analytical Methods in Geomechanics, 40(7), 1099–1120.

Oikonomou, N., Mavridou, S. (2009). "The Use Of Waste Tire Rubber In Civil Engineering Works in Sustainability of Construction Materials". Edited by Jamal Khatib, Chapter 9, 213-238.

Onay O., Koca H., (2015). "Determination of synergetic effect in co-pyrolysis of lignite and waste tyre". Fuel, 150, 169–174.

O'Sullivan, C., Bray, J. D. (2004). "Selecting a suitable time step for discrete element simulations that use the central difference time integration scheme". Engineering Computations, 21(2/3/4), 278–303.

O'Sullivan C, (2015). "Advancing geomechanics using DEM". 3rd International Symposium on Geomechanics from Micro to Macro, Publisher: CRC PRESS-TAYLOR and FRANCIS GROUP, 21-32.

Quezada, J.-C., Vincens, E., Mouterde, R., Morel, J.-C. (2016). "3D failure of a scale-down dry stone retaining wall: A DEM modelling". Engineering Structures, 117, 506–517.

Potyondy, D.O. and Cundall, P.A. (2004). "A Bonded-Particle Model for Rock". International Journal of Rock Mechanics & Mining Sciences, 41, 1329-1364.

Powrie, W., Ni, Q., Harkness, R. M., Zhang, X., (2005). “Numerical modelling of plane strain tests on sands using a particulate approach”. Géotechnique, 55(4), 297–306.

Pöschel, T., Schwager, T., Salueña, C. (2000). “Onset of fluidization in vertically shaken granular material”. Physical Review E, 62(1), 1361–1367.

Ratnam A.V., Prasad D. S., Raju G. V. and Ratna P. S., (2016). “Influence of Waste Tyre Rubber Chips on Strength and Settlements of Soils”. International Journal of Engineering Innovation and Research Vol. 5, Issue 4, 282-287.

RevuzhenkoA.Ph., Klishin S.V. (2013). “Numerical Method for Constructing a Continual Deformation Model Equivalent to a Specified Discrete Element Model”. Physical Mesomechanics, Volume 16, Issue 2, 152–161.

Schallamach, A. (1958). “Friction and abrasion of rubber”. Wear, 1(5), 384–417.

Shi, D., Xue, J., Zhao, Z., and Shi, J. (2015). “A DEM investigation on simple shear behavior of dense granular assemblies”. Journal of Central South University, 22(12), 4844–4855.

Shu, X., Huang, B. (2014). “Recycling of waste tire rubber in asphalt and portland cement concrete: An overview”. Constr. Build. Mater. 67 (Part B), 217–224.

Singh B., Vinot V., (2011). “Influence of Waste Tire Chips on Strength Characteristics of Soils”. Journal of Civil Engineering and Architecture, Vol.5, No.5, 819-827.

Sitharam, T. G., Dwivedi, R., Maji, V. B., (2005). “Numerical modeling of tri-axial testing of jointed rock mass using FLAC-3D.”J. Rock Mech. Tunneling Tech., 11(2), 67–82.

Starfield, A. M., Cundall P. A. (1988). “Towards a Methodology for Rock Mechanics Modeling,” Int. J. Rock Mech. Min. Sci. and Geomech. Abstr., 25(3), 99-106.

Takano D., Chevalier B. J. , Otani J. (2014). “Experimental and numerical simulation of shear behavior on sand and tire chips”. 14th IACMAG International Conference, Kyoto, Japan.

Thay, S., Kitakata, S., Pipatpongsa, T., and Takahashi, A. (2012). “Measurements of vertical pressure profile beneath a planar valley of loose sand and its estimation based on self-similar solution of elliptic equation system”. Journal of Japan Society of Civil Engineers. Ser. A2 (Applied Mechanics), 68(2), I21-32.

Thornton, C. (2000). “Numerical simulations of deviatoric shear deformation of granular media”. Géotechnique, 50(1), 43–53.

Umar J., Sonthwal V. K, Duggal A. K., Rattan J.S., Mohd I., (2015). “Soil Stabilization Using Shredded Rubber Tyre: A Review”. International Journal of Civil and Structural Engineering Research, Vol. 02 Issue: 09, 57-60.

Valdes, J. R., and Evans, T. M. (2008). “Sand–rubber mixtures: Experiments and numerical simulations”. Canadian Geotechnical Journal, 45(4), 588–595.

Vignali, V., Mazzotta, F., Sangiorgi, C., Simone, A., Lantieri, C., & Dondi, G. (2016). “Incorporation of Rubber Powder as Filler in a New Dry-Hybrid Technology: Rheological and 3D DEM Mastic Performances Evaluation”. Materials, 9(10), 842.

Walton, O. R., Braun, R. L. (1986). “Viscosity, granular-temperature, and stress calculations for shearing assemblies of inelastic, frictional disks”. Journal of Rheology, 30(5), 949–980.

Wang, Z., Jacobs, F., Ziegler, M. (2014). “Visualization of load transfer behaviour between geogrid and sand using PFC2D”. Geotextiles and Geomembranes, 42(2), 83–90.

Wang, Z., Miao, L., Wang, F. (2012). “Theoretical and Numerical Analysis of Jacked Pile in Sand”. GeoCongress.

Wenmin Y., Bin H., Lichen L., Xiaolong C., Chenxi R. (2016). “Particle Flow Simulation of the Direct Shear Tests on the Weak Structural Surface”. Electronic Journal of Geotechnical Engineering, (21.26), 10349-10363.

Wu, K., Sun, W., Liu, S., and Zhang, X. (2021). “Study of shear behavior of granular materials by 3D DEM simulation of the triaxial test in the membrane boundary condition”. Advanced Powder Technology, 32(4), 1145–1156.

Yang, M., and Deng, B. (2019). “Simplified Method for Calculating the Active Earth Pressure on Retaining Walls of Narrow Backfill Width Based on DEM Analysis”. Advances in Civil Engineering, 2019, 1–12.

Yoon Y. W., Heo S. B., Kim K. S., (2008). “Geotechnical performance of waste tires for soil reinforcement from chamber tests”. Geotextiles and Geomembranes, 26, 100-107.

Youwai S., (2003). “Strength and Deformation Characteristics of Shredded Rubber Tire-Sand Mixtures”. Canadian Geotechnical Journal, Vol. 40, No. 2, 254-264.

Zhang S. L., Xin Z. X., Zhang Z. X., Kim J. K., (2009). “Characterization of the properties of thermoplastic elastomers containing waste rubber tire powder”, Waste Management, 29, 1480–1485.

Zhang, L., Zhang, F., Hua, M., (2011). “Application of Sheet Pile Wall in a Channel to Upgrade Waterways”. Slope Stability and Earth Retaining Walls.

Zhang, J., Chen, X., Zhang, J., Jitsangiam, P., Wang, X. (2020). “DEM investigation of macro- and micro-mechanical properties of rigid-grain and soft-chip mixtures”. Particuology.

Zhu, H. P., Zhou, Z. Y., Yang, R. Y., and Yu, A. B. (2007). “Discrete particle simulation of particulate systems: Theoretical developments”. Chemical Engineering Science, 62(13), 3378–3396.

Zornberg, J.G., Alexandre, R.C and Viratjandr, C., (2004). ”Behaviour of Tire Shred-Sand Mixtures”. Canadian Geotechnical Journal, 41(2), 227-241.

APPENDICES

APPENDIX A

FISH Functions to determine stress, displacement values.

```
[wb_left  = wall.find('botLeft')]
[wt_right = wall.find('topRight')]
[wb_right = wall.find('botRight')]
[wb_bot   = wall.find('botBottom')]
[wt_top   = wall.find('topTop')]
; FISH functions to get box dimensions
fish define wlx;
  wlx  = wall.pos.x(wb_right) - wall.pos.x(wb_left)
end
fish define wly
  wly  = wall.pos.y(wt_top)   - wall.pos.y(wb_bot)
end
;stresses
fish define wsxx
  wsxF = math.abs(wall.force.contact.x(wb_right))
  wsxx = wsxF / (wly *0.5)
end
fish define wsyy
  wsyF = math.abs(wall.force.contact.y(wt_top))
  wsyy = wsyF/ (wlx*0.5)
end
;strains
fish define xstrain
    disply = wall.pos.x(wt_top) - comp.y(B)
    displx = wall.pos.x(wt_right) - comp.x(B)
    ystrain = (wall.pos.x(wt_top) - comp.y(B))/wly
    xstrain = (wall.pos.x(wt_right) - comp.x(B))/wlx
end
```

APPENDIX B

FISH Function was used in loading stage in order to check loading platen – soil particles contact.

```
;check for loading platen – soil particles contact
fish define checkwall(arr)
   ct=arr(1)
   if type.pointer(ct) # 'ball-facet' then
   exit
   endif
   ;in case of ball-facet contacts, contact.end1 refers to the ball,
   ;contact.end2 refers to the facet
   if wall.group(wall.facet.wall(contact.end2(ct)),"Default") == "load"
   command
     ball free velocity-x spin range  group 'sheet pile' id 11005 not
     measure modify id 3 position [0.78 - displxP2]  0.32 radius 0.01
     measure modify id 2 position [0.78 - displxP3]  0.16 radius 0.01
   end_command
   endif
end
```